Application of Geophysical Methods for Characterizing a Selected Solid Waste Disposal Site in Songkhla Province

Thirat Sommai

A Thesis Submitted in Partial Fulfillment of the Requirements for the Degree of Master of Science in Geophysics

Prince of Songkla University

2015

Thesis Title	Application of geophysical methods for characterizing a selected solid waste disposal site in Songkhla province
Author	Mr.Thirat Sommai
Major Program	Geophysics

Major Advisor

……

(Dr. Kamhaeng Wattanasen)

Co-advisor

……

(Asst.Dr. Sawasdee Yordkayhun)

Examining Committee :

……Chairperson

(Assoc.Prof.Dr.Tanit Chalermyanont)

……Committee

(Assoc.Prof.Dr. Boonlua Phongdara)

……Committee

(Asst.Prof. Dr. Sawasdee Yordkayhun)

……Committee

(Dr. Kamhaeng Wattanasen)

The Graduate School, Prince of Songkla University, has approved this thesis as partial fulfillment of the requirements for the Master of Science Degree in Geophysics

……..……..

(Assoc. Prof. Dr. Teerapol Srichana)

Dean of Graduate School

This is to certify that the work here submitted is the result of the candidate's own investigations. Due acknowledgement has been made of any assistance received.

…….Signature

(Dr. Kamhaeng Wattanasen)

Major Advisor

…….Signature

(Mr. Thirat Sommai)

Candidate

I hereby certify that this work has not been accepted in substance for any degree, and is not being currently submitted in candidature for any degree.

…….Signature

(Mr. Thirat Sommai)

Candidate

ชื่อวิทยานิพนธ์ การประยุกต์ใช้วิธีการทางธรณีฟิสิกส์เพื่อแสดงลักษณะของพื้นที่ที่เลือกใช้สำหรับการฝังกลบขยะมูลฝอย ในจังหวัดสงขลา

ผู้เขียน นายธีรัตม์ สมหมาย

สาขาวิชา ธรณีฟิสิกส์

ปีการศึกษา 2557

บทคัดย่อ

งานวิจัยนี้ได้ประยุกต์ใช้วิธีธรณีฟิสิกส์ได้แก่ วิธีการวัดค่าสภาพต้านทานไฟฟ้า วิธีการวัดการเหนี่ยวนำโพราไรเซชั่น วิธีวัดคลื่นไหวสะเทือนแบบหักเห และวิธีวัดศักย์ไฟฟ้าธรรมชาติ เพื่อแสดงลักษณะโครงสร้างใต้ผิวดินบริเวณพื้นที่ฝังกลบขยะในจังหวัดสงขลา โดยทำการศึกษาในพื้นที่(1) พื้นที่ทางด้านทิศเหนือของหลุมฝังกลบขยะของเทศบาลนครหาดใหญ่ ต.ควนลัง อ.หาดใหญ่ และ (2) พื้นที่โรงเรียนบ้านหน้าวัดโพธิ์ ต.คลองหอยโข่ง อ.คลองหอยโข่ง ซึ่งเป็นหนึ่งในห้าพื้นที่ฝังกลบขยะที่เหมาะสมในจังหวัดสงขลาที่ได้จากการศึกษาด้วยวิธีระบบสารสนเทศภูมิศาสตร์ ผลการศึกษาด้วยวิธีธรณีฟิสิกส์พบว่า ในพื้นที่แรกโครงสร้างชั้นดินมี3 ชั้น ได้แก่ ดินชั้นบน รองรับด้วยชั้นที่สองที่ค่าสภาพความต้านทานไฟฟ้าประมาณ 100 โอห์ม-เมตร มีค่าการเหนี่ยวนำโพลาไรเซชั่นต่ำและมีค่าความเร็วคลื่นพีประมาณ 1,900 เมตรต่อวินาที มีความหนาประมาณ 10 เมตร ซึ่งน่าจะเป็นชั้นดินโคลนแห้งหรือชั้นดินเหนียวปนทราย โดยมีชั้นดินเหนียวปนดินตะกอนที่อิ่มตัวด้วยน้ำ มีค่าสภาพต้านทานไฟฟ้า< 40 โอห์ม-เมตร วางตัวอยู่ด้านล่าง นอกจากนี้ยังพบบริเวณมีค่าการเหนี่ยวนำโพลาไรเซชั่นสูง(> 300 มิลลิวินาที) คาดว่าอาจจะเป็นบริเวณที่มีการปนเปื้อนของของเสียจากการรั่วไหลและถูกพัดพาโดยน้ำใต้ดินผ่านช่องทางที่ชั้นดินเหนียวมีความไม่ต่อเนื่อง พื้นที่ที่สองพบโครงสร้างชั้นดินมี2 ชั้น ชั้นแรกเป็นดินชั้นบนหนาประมาณ 3 เมตร รองรับด้วยชั้นที่มีค่าสภาพต้านทานไฟฟ้าต่ำ(4 – 100 โอห์ม-เมตร) มีค่าการเหนี่ยวนำโพลาไรเซชั่นต่ำ และมีค่าความเร็วคลื่นพีประมาณ1,960 เมตรต่อวินาที มีความหนา > 20 เมตร ซึ่งน่าจะเป็นชั้นดินเหนียวปนทรายหรือชั้นดินเหนียวปนดินตะกอนที่อิ่มตัวด้วยน้ำ พื้นที่นี้พบความไม่ต่อเนื่องทางด้านข้างของค่าสภาพต้านทานไฟฟ้าซึ่งเป็นตัวบ่งชี้ความแตกต่างกันขององค์ประกอบของชั้นดินการศึกษาครั้งนี้แสดงให้เห็นว่าวิธีธรณีฟิสิกส์สามารถตรวจสอบธรณีวิทยาของชั้นกักเก็บตามเกณฑ์มาตรฐานสภาพธรณีวิทยาของพื้นที่ฝังกลบ ได้แก่ ชั้นดินเหนียวได้ในขณะเดียวกันยังสามารถระบุพื้นที่ที่อาจจะเกิดการปนเปื้อนได้ด้วยดังนั้นวิธีธรณีฟิสิกส์จึงเป็นวิธีการที่สำคัญและควรจะนำมาใช้ร่วมกับวิธีการอื่น เช่น วิธีระบบสารสนเทศภูมิศาสตร์ ในงานสำรวจเพื่อคัดเลือกพื้นที่สำหรับฝังกลบขยะ

Thesis Title	Application of geophysical methods for characterizing a selected solid waste disposal site in Songkhla province
Author	Mr.Thirat Sommai
Major Program	Geophysics
Academic Year	2014

ABSTRACT

This research has been applied four geophysical methods; electrical resistivity, induce polarization, refraction seismic, and self-potential with the aim to characterize the subsurface structures of an active solid waste disposal and a selected high potential area for solid waste disposal sites in Songkhla province. The study has been carried out in two areas: 1) the surrounding area is in the north of the active landfill of HatYai municipality, Kuanlang sub-district, HatYai district and 2) the area is at Ban Na Wat Pho School, Klong Hoi Khong district, where it has been recommended by previous GIS study for a highly suitable area from five areas for waste disposal site in Songkhla province. The geophysical results in Kuanlang site found that the subsurface model consists of 3 layers; top soil layer underlain by a layer of about 10 meters thick with resistivity about 100 ohm-m, low IP, and P-wave velocity about 1,900 m/s, interpreted as dry mud or sandy clay. The third layer of low resistivity (< 40 ohm-m) is possibly wet clay or saturated some contents of clay found at a depth of >10 meters. The high IP zones (chargeability > 300 msec) may be the contaminated areas that caused by the wastes leaked from landfill and have been transported by groundwater through the channel of discontinuous clay layer were found. In Ban Na Wat Pho School site, 2 main layers of top soil layer and a thick layer (> 20 m) of low IP, P-wave velocity about 1,960 m/s, and low resistivity of 4 -100 ohm-m interpreted as sandy clay, wet clay and/or some contents of clay layer were found. The resistivity pseudo-section here showed lateral resistivity variation. With according to the standard criteria for the subsurface geological structure of landfill site, the subsurface geological barrier such as clay layer can be obtained by 2D – IP & resistivity imaging and seismic refraction data. In addition, the subsurface contaminated area can probably be provided by IP and resistivity data. This study showed that geophysical methods can be an importance tools for characterizing the subsurface geological structure of selected landfill site after roughly selected by e.g. GIS method.

ACKNOWLEGEMENT

This work never has been completed without helping and supporting from people who I would like to acknowledge during my studies in Master Degree of Science in Geophysics program.

First of all, I would like to express my deep gratitude to my advisor, Dr. Kamhaeng Wattanasen, for his guidance in the discussion, suggestions, valuable discussion; critical reading and correcting the manuscript, that have more improved the quality of this thesis. Without his enthusiasm and expert coaching, this thesis would not have been possible.

I would like to express my sincere thanks to my co-advisor, Dr. Sawasdee Yordkayhun, for his suggestions and invaluable discussions during the seismic refraction investigation and processing, which is an important part in the final understanding. Without his generous guidance to the right way this thesis would not have been completed.

My thanks go to the Graduate School, Prince of Songkla University for a supporting research grants, also to the Department of Physics, Faculty of Science, PSU. Thanks also to International Program in the Physical Science of Uppsala University, Sweden, for supporting research equipment. Thanks further to the Department of Groundwater Resources (DGR), Songkhla province, Thailand, for their generosity in providing the borehole information, which is an important part of this work.

The important part of helping that I would never forget is my field work team, which I have to say "***special thanks***". There are my "brothers" and my "sister" in Geophysics Group as they always went with me in the field and also to all my lovely friends in the Physics Group, who are cheering up me always.

Finally, my deepest gratitude is to my family who always stood beside me. My parents, who always encourage me, believe in me and give me the encouragement to keep walking.

Thirat Sommai

CONTENTS

		Page
ABSTRACT		v
CONTENTS		vii
LIST OF TABLES		x
LIST OF FIGURES		xi
CHAPTER 1	INTRODUCTION	1
1.1	Wastes and disposal of wastes	2
	1.1.1 Wastes classification	2
	1.1.2 Effect of wastes	3
	1.1.3 Solid wastes management	4
	1.1.4 Principle of selected solid waste disposal by landfill	6
1.2	Literature review	8
1.3	Objectives	12
CHAPTER 2	RESEARCH METHODOGY	13
2.1	Study area	13
	2.1.1 General physiography	15
	2.1.2 Administrative division	15
	2.1.3 Population	16
	2.1.4 Meteorology	16
	2.1.5 Geology	17
	2.1.6 Groundwater resources	20
2.2	Geophysical investigation plan	23
2.3	Methodology	26
	2.3.1 Resistivity method	26
	2.3.2 Induced Polarization method	36
	2.3.3 Self-potential survey	41

CONTENTS (CONTINUED)

		Page
	2.3.4 Seismic refraction method	46
CHAPTER 3	RESULTS AND DISCUSSION	56
3.1	Geophysical investigation	56
	3.1.1 Resistivity imaging subsurface characterization	58
	3.1.2 IP imaging subsurface characterization	69
	3.1.3 Seismic refraction	71
	3.1.4 SP interpretation	80
3.2	Integrated interpretation of geophysical results	82
3.3	Discussion	83
CHAPTER 4	CONCLUSION AND RECOMMENDATION	85
BIBLIOGRAPHY		87
VITAE		90
SCHOLARLY PUBLISHING		91

LIST OF TABLES

		Page
2.1	Resistivity of various rocks and sediments (Telford, 1990) (Milsom, 2003)	27
2.2	The median depth of investigation (Z_e) for the different array (Loke, 1997).	33
2.3	The pattern of data file format for the IP measurement (Geotomo Software, 2009).	40
2.4	The compressional wave velocity of various materials (Reynolds, 1997).	47
3.1	Geological information of borehole H0853SKL372.	63

LIST OF FIGURES

		Page
1.1	Type of sanitary landfill (Pollution Control Department, 2009).	7
1.2	Inverted section by Res2dinv (version 3.50t) software(Dahlin et al., 2002).	8
1.3	(a) 2D – resistivity section of the plume, (b) 2D – chargeability section cutting through the plume that correlate with contaminant concentration anomalies from GMW (Sogade et al., 2006).	11
1.4	2D – geoelectric section along E – W section of Igando landfill (Oladap et al., 2013).	12
2.1	The location map of the study area in Songkhla province.	14
2.2	Population – year curve of Songkhla province in 2002 to 2012.	16
2.3	The geological map of the study area in Songkhla province (Modified from Department of Mineral Resources, 2007).	19
2.4	Hydrogeological cross section; a) $C - C'$ line and b) $B - B'$ line (this two lines are in in Hat Yai basin) (Modified: Arun Lookjan,2009).	22
2.5	Map of study area showing geophysical measurement line on Kuan Lang sub district, Hat Yai district, Songkhla province.	24
2.6	Map of study area showing geophysical measurement line on Ban Na Wat Pho School, Klong Hoi Khong district, Songkhla province.	25
2.7	The generalized form of the electrode configuration in the resistivity measurements (Modified: Telford,1990).	30
2.8	Common electrode configurations that are used in resistivity investigations.	31
2.9	Dipole – dipole configuration (Modified: Telford, 1990)	32
2.10	Pseudo plotted data for the double – dipole array (Modified: Loke, 1997).	34
2.11	Schlumberger array (Modified: Telford, 1990).	35
2.12	Induced polarization phenomenon (Kearey, 1984).	36
2.13	Non – polarizing electrode(Modified; Telford, 1990).	38

LIST OF FIGURES (CONTINUED)

		Page
2.14	Datum point for resistivity and IP survey in G5 line	39
2.15	fixed – base configuration for SP data collection (Modified: Allred, 2008).	45
2.16	Travel-time versus distance curve for the direct, reflection and refraction waves at a horizontal interface between two layers with seismic velocities V_1 and V_2 ($V_2 > V_1$) (Lowrie, 2007).	48
2.17	Position of wavefronts associated with the direct and refracted waves (Kearey, 1984).	49
2.18	Travel-time curves for the direct wave and refracted wave (Kearey, 1984).	50
2.19	(a) Ray path geometry for dipping refractor and (b) Travel-time of refraction profile from dipping refractor in the forward and reverse directions (Kearey, 1984).	52
3.1	Study area at landfill site, Kuan Lang subdistrict	56
3.2	Example of study area; a) G1 profile of northern active landfill, b) Ban Na Wat Pho school site.	57
3.3	Preparing Cu-$CuSO_4$ electrodes for IP& resistivity and SP surveys	58
3.4	Inversion resistivity model section; a) G1 profile, b) G2 profile, c) G3 profile, d) G4(AB) profile, e) G4(C) profile, f) G5 (AB) profile, g) G5(C) profile, h) G6(AB) profile, and i) G6 (C) profile.	60
3.5	Inversion resistivity model section of KH01 profile.	61
3.6	The sounding curve of measurement point borehole H0853SKL373	62
3.7	The sounding curve of measurement point; a) G1 point, b) G2 point	65
3.8	The sounding curve of measurement point; a) G3 point, b) G4 point	66
3.9	The sounding curve of measurement point; a) G5 point, and b) G6 point.	67
3.10	The sounding curve of measurement point KH01	68
3.11	Inversion IP model section; a) G1 profile, b) G2 profile, c) G3 profile, d) G4(AB) profile, e) G4(C) profile, f) G5 (AB) profile, g) G5(C) profile, h) G6(AB) profile, and i) G6 (C) profile.	70

LIST OF FIGURES (CONTINUED)

		Page
3.12	Inversion IP model section of KH01 profile.	71
3.13	Subsurface structure from refraction interpretation of G1 profile; Velocity computation in layer 2 by regression and the Hobson-Overton method is represented by red and blue number, respectively. And Weighted average of velocity is represented by black number.	72
3.14	Subsurface structure from refraction interpretation of G2 profile; Velocity computation in layer 2 by regression and the Hobson-Overton method is represented by red and blue number, respectively. And Weighted average of velocity is represented by black number.	73
3.15	Subsurface structure from refraction interpretation of G3 profile; Velocity computation in layer 2 by regression and the Hobson-Overton method is represented by red and blue number, respectively. And Weighted average of velocity is represented by black number.	75
3.16	Subsurface structure from refraction interpretation of G4 profile; Velocity computation in layer 2 by regression and the Hobson-Overton method is represented by red and blue number, respectively. And Weighted average of velocity is represented by black number.	76
3.17	Subsurface structure from refraction interpretation of G5 profile; Velocity computation in layer 2 by regression and the Hobson-Overton method is represented by red and blue number, respectively. And Weighted average of velocity is represented by black number.	77
3.18	Subsurface structure from refraction interpretation of G6 profile; Velocity computation in layer 2 by regression and the Hobson-Overton method is represented by red and blue number, respectively. And Weighted average of velocity is represented by black number.	78

LIST OF FIGURES (CONTINUED)

		Page
3.19	Subsurface structure from refraction interpretation of KH01 profile; Velocity computation in layer 2 by regression and the Hobson-Overton method is represented by red and blue number, respectively. And Weighted average of velocity is represented by black number.	79
3.20	SP value after drift corrected of measurement profile; (a) G1 profile, (b) G2 profile, and (c) G5 profile.	80
3.21	SP value after drift corrected of measurement KH01 profile	81

CHAPTER 1

INTRODUCTION

Demand of using several resources is very high because of continuously increase in population of the world. Several goods or products are constructed to response each human's demand. Some pieces of goods or products are thrown away after using and they become the solid wastes. These solid wastes can be managed by several methods that were under the control of economics, society, the availability of personnel and organization, and landscape.

The solid waste problem is currently the several important problems that affects the environment and people's lives from these wastes such as bad scenery, water contaminates, air pollution, etc. To reduce affection, the good management has to be performed. Many methods such as reuse, recycle, incineration, open dump, and sanitary landfill can be used for global solid wastes management. In Thailand, the sanitary landfill is the suitable method of solid waste disposal (Pollution Control Department, 2009). However, the leakage waste from the landfill site will be a serious issue to environment if the subsurface structure of the landfill site has a defect of natural barrier e.g. clay layer etc. The leakage was in form of solid or solution will be transported by water to contaminate in soil, surface water, and groundwater.

The groundwater is one of the most important natural resource for every life on the earth. Thus, groundwater pollution is firstly considered before selecting the area and the method for solid waste management.

Songkhla province is a center of education, industrial, and commercial in southern part of Thailand. Its basically has abundance of natural resources, which support the Songkhla province to dominant in tourist industrial as well. The result of population and economics grow cause an increasing of the solid waste. A landfill method has been selected for the solid waste disposal in this province. The interesting study for area selection for solid waste disposal in Songkhla province was studied by GIS method (Rottana, 2002), the five biggest zone of high suitability areas for disposal site that have been recommended are in Klong Hoi Khong, Thung Mhor, and Samnak Kham sub-district.

Department of Mineral Resources (2001) presented the new way for selecting the landfill site in Thailand, by finding out areas with a suitable geological barrier. The standard

criteria for suitable subsurface geological structure for landfill site should have character as below;

- Low permeability : $k_f < 10^{-7} m/s$ i.e. (in unconsolidated sediment) mainly clay
- Homogeneous structure and no gaps of higher permeability
- Large thickness (> 5 meters)
- Low effective porosity
- High natural retention capacity for hazardous substances
- Wide lateral extension
- High depth to groundwater
- Thin coverage with other sediments (<2 m)

However, there is no drilling test which was performa in those five selective areas in Songkhla province. Thus, the ageement between the subsurface geological structure and the standard criteria for subsurface geological structure for landfill site still is not confirmed.

Geophysical methods that can find the model of subsurface geological structure and can give the coninueous image of subsurface have been introduced to test a reccommended area from GIS studied. Geophysics methods will also be used to test an active landfill site of Hat Yai municipality for examining the agreement of subsuface geological structure and standard criteria for selecting landfill site. Moreover, the results from geophysical models and the distribution of physical properties in the subsurface can identify the possible cotaminated area that the wastes may leak from the landfill site.

1.1 Wastes and disposal of waste

1.1.1 Wastes classification

Waste is unwanted material, substance, thing that has been left over from some process. The wastes were separated to be five types by the wastes classification from composition of them (Thongchai, 1988). The five types of the wastes were explained as following;

I) Solid wastes are unwanted materials, substances, things that are in the solid form. They are wastes resulting from human activities, agriculture, horticulture, food preparation and processing, forestry, industries, dormitory, municipality, and urban community. Pollution Control

Department (2004) given definition that “Solid waste is garbage or waste resulting from activities in urban community excepting hazardous waste and infectious waste.” Nowadays, quantity of solid waste increase highly when it was compared with its quantity in the past.

The Public Health Act (1992) defined that “ solid waste is unwanted thing that is solid or soft form and it has moisture such as rags, plastic, dung, waste paper, garbage, ashes, dead animals.”

II) Liquid wastes are unwanted substances, water that has been left over from some process. They were called “sewage”. They are sewage resulting from waste management facilities, off-site waste water treatment plants and the preparation of water intended for human consumption and water for industries, waste from oil regeneration.

III) Gaseous wastes or air pollution is waste resulting from industries, combustion process of petroleum, gas and lignite.

IV) Radioactive wastes are garbage resulting from nuclear industries. they are hazardous wastes.

V) Mining wastes are the unwanted materials resulting from exploration, mining, quarrying, physical and chemical treatment of minerals e.g. wastes from mineral excavation, wastes from ore dressing, riprap, wastes from physical and chemical processing of mineral, drilling mud and other drilling wastes.

1.1.2 Effect of the waste

Nowadays, quantity of the waste increase more than its quantity in the past. If disposal of the waste is bad disposal or unsuitable method, it’ll impact to environment and human by direct and indirect way as following;

1.1.2.1 Soil Pollution

The waste is on the surface along time, it’ll changes soil into alkaline / acid and changes physical properties of the soil such as Sodium make the soil to be crumbly etc. If the soil is contaminated, it’ll impact to human’s health.

1.1.2.2 Water Pollution

If water is contaminated without water treatment, it’ll become sewage. And sewage impact to drinking water and human’s health.

1.1.2.3 Air Pollution

The smell emitted interference from waste if disposal of the waste is bad system. It makes air pollution that impact to human's health.

1.1.2.4 Visual Pollution

Disposal of waste is non-organized, it make squalor. Moreover, that area is scenery bad for visitor.

1.1.2.5 Breeding Place

Scavenger receives ailment/disease from the waste especially from infectious waste from hospital that mixes with general waste. Open dumping is breeding place of infectious insects such as rat, fly, etc.

1.1.2.6 Nuisance

Nuisance is resulting from visual pollution, stink, and poison gas because food wastes or garbage makes hydrogen sulfide (H_2S) and ammonia (NH_3) that are stink gas. Sometime, open dumping on land and burning have nuisance from smoke and hazard from toxic gas that is resulting from incomplete combustion.

1.1.3 Solid Wastes Management

From increasing of wastes problem, U.S. Environmental Protection Agency (U.S. EPA) prefer four process (or in other name called Integrated Solid Waste Management (ISWM)) for wastes management such as source reduction, recycling, waste combustion, and landfill. Each step of the integrated solid waste management has detail as following;

1.1.3.1 Source Reduction

Source reduction decreased the quantity of the solid waste in urban and it reduced quantity of chemical/ hazardous chemical that contaminated in solid waste. Population, customer, and producer can reduce source of the solid waste by using seven ways such as refusing or rejecting, refilling, returning, repairing, reusing, recycling (separating useful solid waste e.g. plastic product, glass, can etc.), and reducing.

1.1.3.2 Recycling

Recycling is a process that separated some solid waste for using these waste again. This process will increase efficiency of waste disposal. The solid waste was separated for using again such as paper, old newspaper, glass, plastic, iron, Aluminum, Copper, and Lead etc.

1.1.3.3 Waste Transformation

Meaning of waste transformation covered about materials — can be recycling — to produce again that it makes to get new product. Moreover, waste transformation mean transformation of waste by biochemical and chemical process.

1) Composting

Composting is degradation of organic matter by biochemical process. Organic matter was degraded by microorganism. Composting process was carried out under the aerobic condition. Microorganism has reaction of organic matter degradation as following:

$$Organic\ matter + O_2 \xrightarrow{aerobic\ \ bacteria} new\ cells + CO_2 + H_2O + NH_3 + SO_4$$

2) Combustion or Incineration

Combustion or incineration is the waste transformation by chemical process. Temperature in the incineration varied between $850^\circ C$ and $1{,}200^\circ C$. Moreover, incineration is complete combustion by its result is water (H_2O), Carbon dioxide (CO_2), and other gas that contaminated in air pollution.

1.1.3.4 Landfill

Landfill is a last step of the integrated solid waste management (ISWM). The sanitary landfill is waste disposal by using engineering principles for protection environment and human health. The solid waste in the sanitary landfill is layers and it is covered by soil. Organic matter was degraded by microorganism in anaerobic decomposition process. Therefore, the sanitary landfill should have methane (CH_4) drainage and wastewater treatment system.

There are three methods of landfill separated by the area characteristic or the topography (Pollution Control Department, 2009).

1) Area Method

Area method is landfill without digging (Figure 1.1a). This method, the waste is compacted to be layering. Thus, this method needs embankment or berm to sustain waste layering and to prevent sewage (wastewater) to leak into outside. The area that has groundwater level

lower than surface a little bit (less than 1 meter) (lowland) is a suitability area for the area method.

2) Trench Method

Trench method is landfill that dig lower than normal level (Figure 1.1b). After the waste is compacted to be thin layering. The waste layer is overlapped each other. Normally, the depth of trenching is limited by groundwater level at the bottom of pit. This method, its wall is used for sustaining solid waste layer.

3) Canyon Method

Canyon method is landfill managed on large basin area (Figure 1.1c) that is formed by nature or/and human made such as mine, valley, creek etc. Form of landfill and compaction of waste is different, which depends on topography.

Hat Yai municipality landfill is the integrated landfill that mixed between the area method and trench method. The solid waste here is firstly managed by trench method and area method is later applied for supporting the solid waste.

1.1.4 Principle of selected solid waste disposal by landfill

The sanitary landfill for good efficiency of the solid waste disposal should have suitability area characteristic as following (Pollution Control Department, 2009);

1) It should be far more than 5,000 meters from airport.

2) It should be far more than 1,000 meters from archaeological site, clean river, community, reservation, and natural resource that be conserved.

3) It should be far more than 700 meters from drinking resource and water supplied industries.

4) It should be far more than 100 meters from public water resource.

(a)

(b)

(c)

Figure 1.1 Type of sanitary landfill, (a) Area method, (b) Trench method, and (c) Canyon method

(Pollution Control Department, 2009)

Moreover, the main important factor for landfill is geology of the area. The geological area has suitable for sanitary landfill as following;

1) It should be far more than 100 meters from fracture, fault, cavity, and the unstable area.

2) It should have subsurface structure that has low permeability of water. Permeability property is less than and/or equal to $1\times10^{-5} cm/s$ (or $8.9\times10^{8} mDarcy$) through 3 meters thickness. And width of landfill is more than 50 meters.

3) It should have subsurface structure that can supported quantity of waste according engineering principle.

1.2 Literature Review

Dahlin et al. (2002) used resistivity and induced polarization (IP) surveys to identified location of landfill at Dalby Östra Möla in the southern part of Sweden. Previous research shown that the location of landfill in Dalby village had low resistivity. Resistivity and induced polarization (IP) data were inverted by Res2dinv (version 3.50t) software which inversion program. Invertion model in Figure 1.2 shown the zone of low resistivity and high chargeability was consistency with the location of landfill. Thus, waste can be charactered by high chargeability.

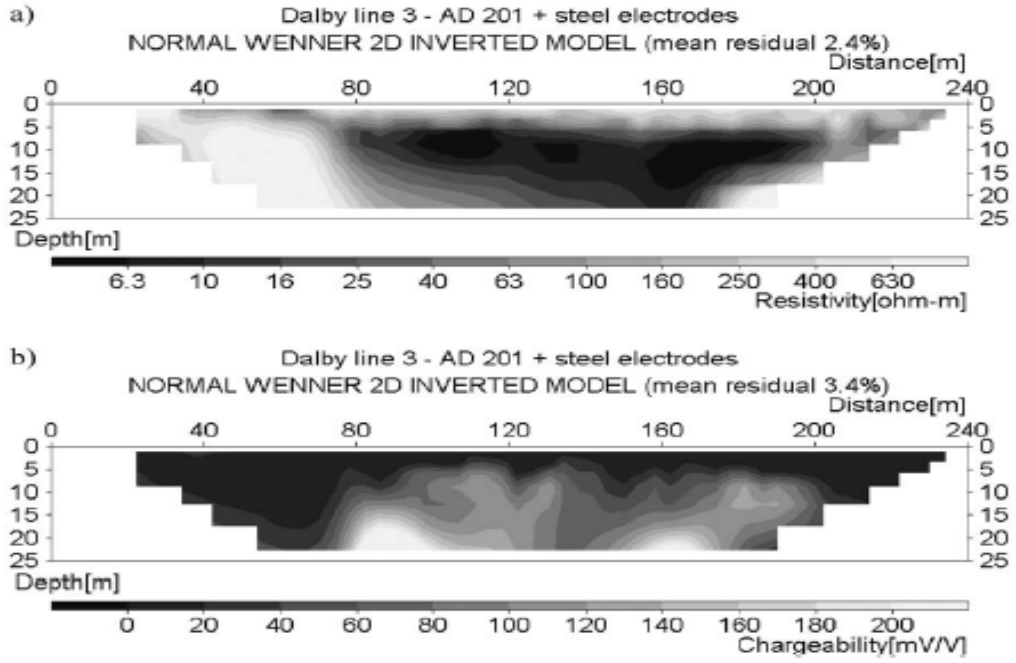

Figure 1.2 Inverted section of resistivity and IP data by Res2dinv (version 3.50t) software.

(Dahlin et al., 2002)

Aristodomou et al. (2000) used resistivity and induced polarization methods to monitor the spread of contamination in underlying aquifer due to a landfill site. Application of resistivity and induced polarization (IP) investigation has been found the suitability method for monitoring contaminant related to landfill site. Geology of study area consists of sand and clay layer. Four objectives for this investigation were (1) to monitor landfill characteristic in resistivity and chargeability term, (2) to determine the base of landfill, (3) to identify a spread of contamination, (4) to identify clay layer. Clay layer is normally behaved as a natural barrier for protection contamination from the leachate due to landfill site. Inverted chargeability data can separate groundwater zone that underlies beneath the landfill site. Moreover, resistivity investigation in L1 and W1 profile shown that area near borehole was contaminated by inorganic matter. The contaminated areas can be identified clearly from the inverted IP data.

Grissemann et al. (2004) used geophysics surveys to investigate geological barrier around the landfill site at Ban Mae Hia and Ban Nong Han, Chiang Mai province. 2D – resistivity, Electromagnetic, Seismic, Gravity, and Magnetic method were carried out for detail survey of geological structure, distribution of sand and clay layers, groundwater table, direction of groundwater flow, and physical characteristic of waste. The interpretation of geophysics data were supported by borehole, hydrogeological data and chemical investigation. The result of reflection seismic shown geological structure under the sediment layer of Chiang Mai – Lamphun basin. Resistivity survey showed dry clay layer that has a few resistivities. 2D – resistivity and electromagnetic surveys showed detail about spatial distribution of clay – rich colluvial sediments and sandy alluvial sediments that were important of geological barrier at landfill site. Magnetic and gravity surveys identified materials with high iron content in community of landfill site.

Mota, R. et al. (2004) used geoelectric survey in granite region of Northern Portugal, to detect the possible spread of contamination leakage from an active landfill. The investigation was complemented with Self-potential (SP), Dipole-Dipole profile and Azimuthal Vertical Electrical Sounding methods. Significant groundwater circulation was detected by low resistivity (less than 400 Ohm-meters). Anomalous zone has been identified by very low resistivity (less than 200 Ohm-meters) that might be the groundwater contamination due to landfill. Result of Azimuthal Vertical Electrical Sounding shown a direction of granite fracture. Self – potential (SP) survey shown a direction of groundwater flow with according with topography.

Jaime A. Reyes Lopez et al. (2008) used geophysics investigation, chemical analysis and hydrological methods for detection a spread of contamination in Guadalupe Victonia landfill, Mexica, where the groundwater table is shallow (approximate 1 meters depth). Vertical Electrical Sounding (VES) and Ground Penetrating Radar (GPR) have been applied and their results showed the contaminating area expanded in South-Eastern and North-Western of landfill site. Contamination in groundwater was supported by chemical data of groundwater.

Reinhard K. Frohlic et al. (2008) used Schlumberger depth sounding at the Picillo Farm, in western Rhode Island, where there is an unauthorized disposal site of hazard organic wastes. The aim of the study is to compare between contamination and non-contamination zone. The result showed that in south – eastern part of area, the formation factor value was between 12 and 45. The zone, where there was no contamination found the formation factor value between 2.5 and 7.7. This normal zone or zone of non-contamination, vertical electrical anisotropy in range of 2-3 was found. For the contaminated area, the vertical electrical anisotropy was found higher than 5. Investigated results detected the contamination was concentrated in the north – western (NW) more than in the south – western (SW) of study area.

Ehirim, C.N. and Ofor, W (2009) used 2D – resistivity imaging and Vertical Electrical Sounding (VES) surveys for study of the aquifer vulnerability to surface pollutants near two landfill site in Port Harcourt municipality, Nigeria. The objectives of the study was characterizing a typical Niger Delta coastal aquifer and assessing its potential risk to pollutant seepage. The studied result showed that there were two anomalous areas; the high resistivity area of between 725 and 4,419 Ohm-meters, which suspected to be landfill gases at depths deeper than 31.4 meters, and low resistive leachate contaminant plumes of resistivity between 15.6 and 179 Ohm – meters at depth of 1.25 meters to more than 31.3 meters implying that the aquifer was contaminated by leakage waste from landfill site.

Sogade et al. (2006) used induced polarization (IP) survey for detecting and mapping of contaminant plumes at the Massachusetts Military Reservation (MMR) that located in Cape Cod, Massachusetts. Result of 2D – resistivity in Figure 1.3a shown a zone of 300 Ohm – meters that may be represent of clay or sandy clay as refer to the geology map. 2D – chargeability shown three distinct anomalous zones (130 mV/V located 20 – 80 meters laterally, 15 – 60 meters vertically; 50 mV/V located 200 – 240 meters laterally, 40 – 80 meters vertically; and 80 mV/V

located 300 – 340 meters laterally, 30 – 60 meters vertically). 2D – chargeability section cutting through the both plumes as shown in Figure 1.3b. A distribution of chargeability anomalies from can be confirmed by GMW (Groundwater monitoring wells) data and in a contaminant-free zone, the high chargeability was found.

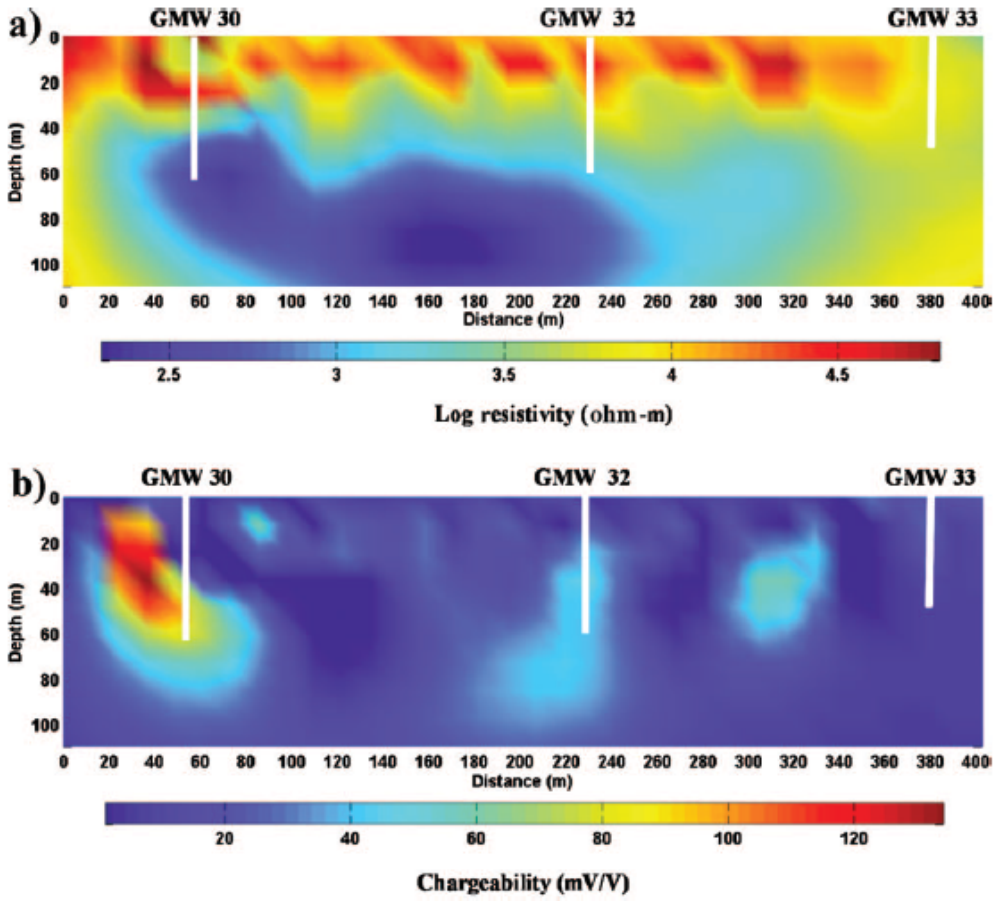

Figure 1.3 (a) 2D – resistivity section across of the plume, (b) 2D – chargeability section cutting through the plume that correlate with contaminant concentration anomalies from GMW. (Sogade et al., 2006)

Martinho, E. and Almeida, F. (2006) used resistivity and induced polarization (IP) surveys to investigate contamination plumes in vicinity of two municipal landfills (Ovar and Ilhavo) in Portugal. 2D – resistivity and IP surveys can map shape and dimension of contamination associated with landfill site. Shallow layer was identified to be dry sand dune that has resistivity more than 2,600 Ohm-meters. Low resistivity ($\rho < 100\ \Omega m$) are associated with

the known polluted area. Induced polarization (IP) measurement showed high chargeability which was associated with contaminated areas and the zones of high clay content as well. Inverted resistivity and induced polarization data were supported by local boreholes. This study shows that the method can be a good investigation tool in combination with resistivity and other geophysics methods.

Oladap et al. (2013) used Vertical Electrical Sounding (VES) utilizing Schlumberger electrode array to determine hydrogeology implications due to landfill site in Lagos municipality, Southwestern Nigeria. Igando landfill is one of three major landfill in Lagos, the study showed that the resistivity value of between 2.5 Ohm-meters stage and 26.1 Ohm – meters the decomposed stage and fairly decomposed/dry stage areas. The surrounding lithology is defined by low resistivity values that are indicative of clay. 2D-geoelectric section in Figure 1.4 shows that the landfill is underlain by thick an impermeable laterite/clay layer.

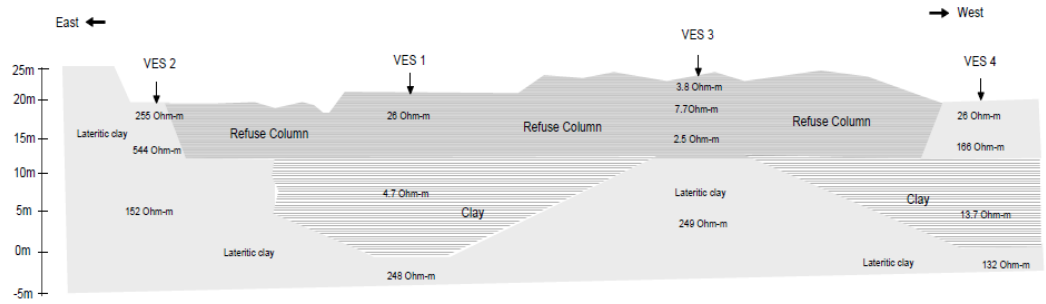

Figure 1.4 2D – geoelectric section of Igando landfill along E – W.

(Oladap et al., 2013)

1.3 Objectives

The aims of this study are (1) to characterize the subsurface structure around an active landfill site of Hat Yai municipality and to characterize the subsurface structure in a selected solid waste disposal site (Klong Hoi Khong). Studied by GIS method, (2) to test the agreement between the subsurface geological structure of both studied areas and the subsurface geological structure from standard criteria for selecting landfill site.

CHAPTER 2

RESEARCH METHODOLOGY

2.1 Study area

Two study areas were choosen, where there are interests in characterizing the subsurface geological structure with reference to the standard criteria for selecting landfill site, and there are borehole data that may be used for a geological and hydrogeological reference. The study area was divided to be two sites that are in Songkhla province (Figure 2.1). The first study area is located at longitude 655500 – 656750 E and latitude 770250 – 770750 N in the plain area of Khuan Lang sub district, Hat Yai district. It is 8 km far from Hat Yai town and it is about 3 km to the NW, where the Hat Yai international airport is located. This area is an active landfill site that has been managed by Hat Yai city municipality. The waste here has been collected from Hat Yai city municipality, Klong Hae municipality, Tha Chang municipal district, and Chalung Administrative organization sub-district, with totally more than 100 tons per day. Here the possible contamination into the environment of waste leakage from landfill should be determined.

The second study area is located at longitude 652600 – 652900 E and latitude 762400-762500 N in Klong Khong sub-district, Klong Hoi khong district. This area is recommended by GIS study (Rottana, 2002) to be a suitably potential area (one from five areas) for the landfill site in Songkhla province.

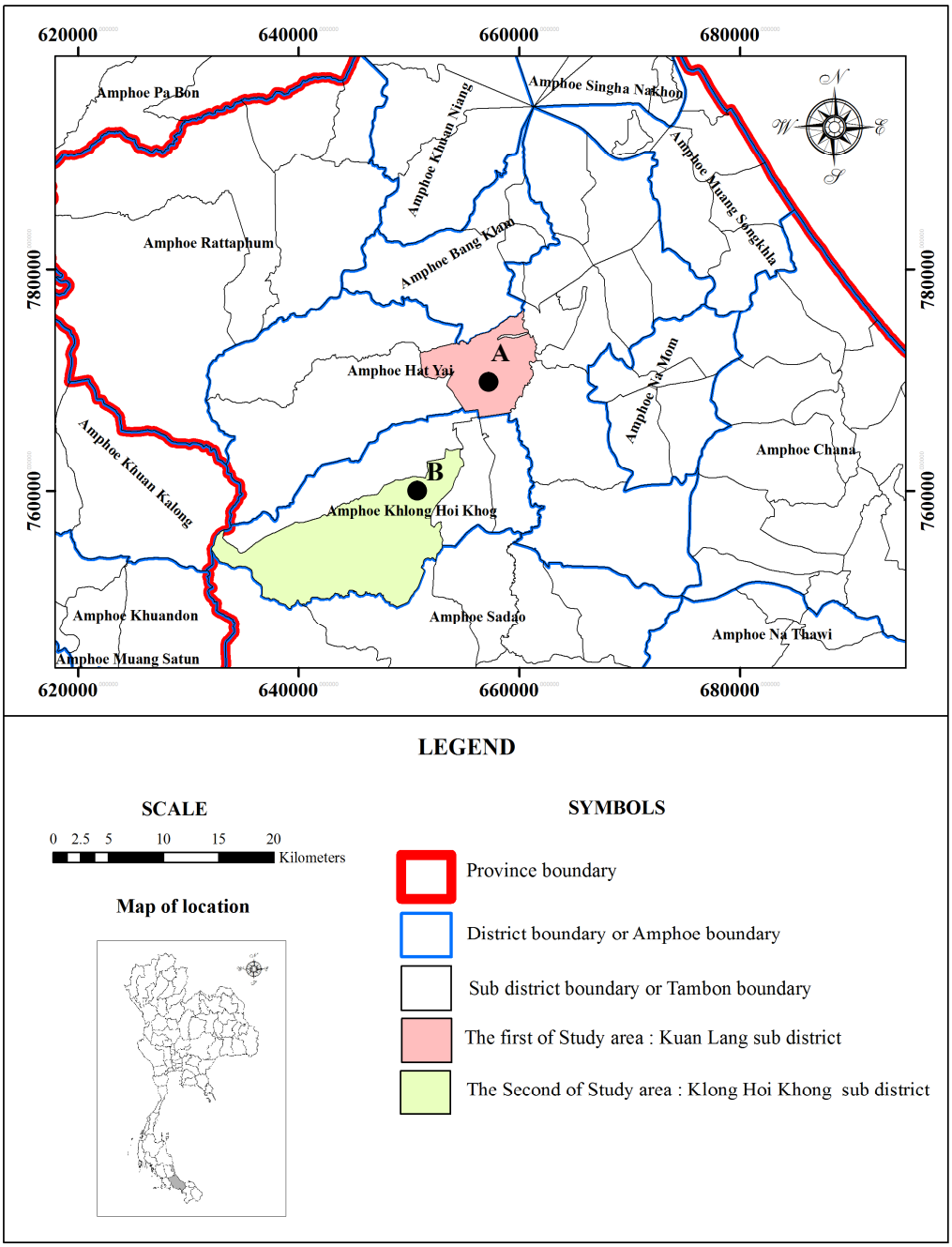

Figure 2.1 The location map of the study area in Songkhla province, Site A is an active landfill at Kuan Lang subdistrict and site B is at Ban Na Wat Pho School, Klong Hoi Khong sub-district.

2.1.1 General physiography

Songkhla province is located in the Peninsular Thailand, on the eastern coast of the Gulf of Thailand. In the northern part of the province is mostly low land where there is the largest nature lake in Thailand, Songkhla Lake is located. The eastern area is coastal plains. In addition, the southern and the western areas are mountains and plateau which are main recharge areas for the Songkhla Lake watershed. Songkhla province is bounded by latitudes 6° 17′ to 7° 56′ N and longitude 100° 01′ to 101° 06′ E. The shape of the province is long narrow peninsular along the south to north into the sea. Its elevation is approximately 4 meters above mean sea level (MSL). The province is approximately 950 kilometers from Bangkok by highway and about 947 kilometers by rail. Total area of the province is 7,393.889 square kilometers. Its territory is shown as below;

North: Nakhon Si Thammarat and Phatthalung

East: The Gulf of Thailand

South: Yala, Pattani, State of Kedah and Perlis of Malaysia

West: Phatthalung and Satun

2.1.2 Administrative division

Songkhla province is subdivided into 16 districts which are further subdivided into 127 subdistricts and 987 villages. All districts are shown as below;

1. Mueang Songkhla
2. Sathing Phra
3 Chana
4. Na Thawi
5. Thepha
6. Saba Yoi
7. Ranot
8. Krasae Sin
9. Rattaphum
10. Sadao
11. Hat Yai
12. Na Mom
13. Khuan Niang
14. Bang Klam
15. Singhanakhon
16. Klong Hoi Khong

2.1.3 Population

The total number of population of Songkhla province is 1,378,574 people in December 2012. It was ranked 10th of Thailand and 2nd of southern Thailand, with an average population density of about 186.45 people per square kilometers (Department of Provincial Administration, Ministry of Interior). Population statistic of Songkhla province from 2002 to 2012 shows a steadily increased every year as linear increasing form (see Figure 2.2).

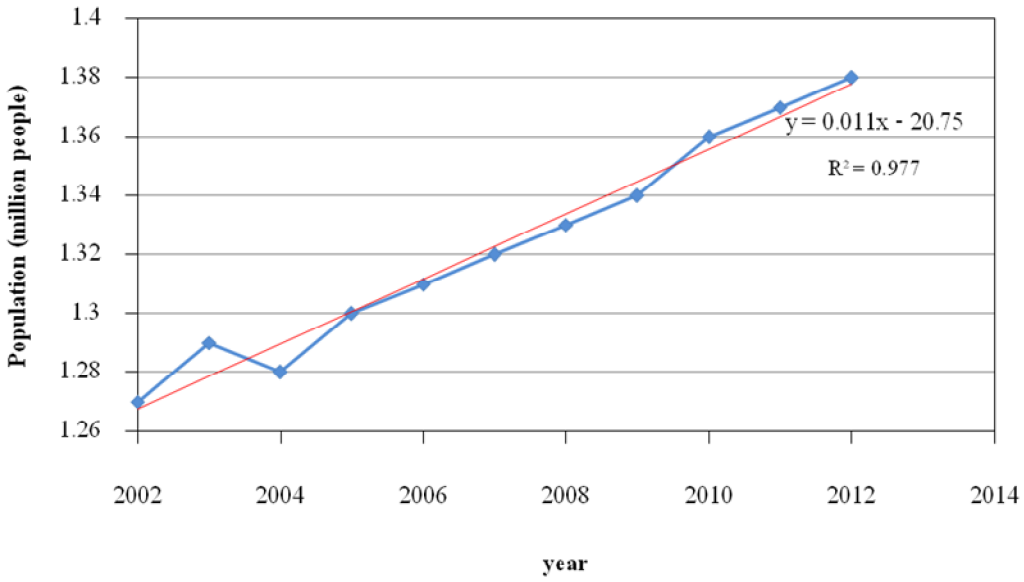

Figure 2.2 Population – year curve of Songkhla province from 2002 to 2012.

2.1.4 Meteorology

There are two meteorological seasons in the southern Thailand, a rainy and dry seasons. The meteorological season is considered by monsoon type. The rainy season lasts for nine months from May to January. The area is under the influence of SW monsoon during May to September, and under the NE monsoon during October to January. This season is characterized by heavy rainfall under these two monsoons. The dry season begins in February until April, and it is characterized by the high temperature with little rainfall under the influence of the SE monsoon.

2.1.5 Geology

Department of Mineral Resources (2007) presented the geological map of Songkhla province (Figure 2.3). Songkhla province is underlain stratigraphically by a variety of rocks ranging in age from the oldest rock of Cambrian to the youngest Quanternary beach/alluvial deposits.

Cambrain rocks are compose predominantly of brownish gray, brown, yellowish brown sandstone, shale, quartzite, and phyllite, locally red sandstone, siltstone, and shale. This rock is also lithostratigraphically designated as the Tarutao Group. This sequence is exposed in the western part of province.

Ordovician rocks comprise predominantly of light to dark gray, bluish gray, massive to thin bedded limestone and argillaceous layers. The sequences are commonly designated as the Thung Song Group. Usually, the sequence expose in the southwestern of Rattaphum district.

Silurian-Devonian rocks are currently classified under the lithostratigraphic system as the Thong Pha Phum Group. This rock unit expose in the western part of Rattaphum district. The rocks consist mainly of sandstone, shale, chert, metatuff, schist, quartzite, black shale and mudstone with limestone lenses.

Carboniferous rocks are characterized by mudstone, sandstone, shale, bedded chert, and cross-bedded quartz sandstone with fossils of brachiopods, pelecypods, trilobites and conodonts. Mostly, these rocks are exposed in the western province and also distributed around Hat Yai, Khuan Niang, and Muang Songkhla district.

Permian rocks comprise predominantly of bedded to massive limestone with partly dolomitic limestones, chert nodules, as lenticular beds are common, and occasionally intercalated with shale and siltstone. The sequence is currently classified as Ratburi Group, and are only limited in the western part of Songkhla area.

Triassic rocks are mainly marine deposits of red-bed sequences. The sequence comprise of thick-bedded to massive cross-bedded sandstones, siltstones, and locally dolomitic limestone. The sequences are exposed continuously in the eastern province with the regional trend in the N-S direction.

Jurassic-Cretaceous rocks are characterized as non-marine deposits, consisting mainly of deep red, red brown, cross-bedded sandstone, siltstone, shale, conglomeratic sandstone, and basal conglomerate; intercalated with gray shale, limestone, dolomitic limestone and dolomite. The sequence expose at Krasae Sin district.

Quaternary deposits comprise all of the younger unconsolidated deposits, terrace/colluvial and beach/alluvial deposits. Terraces, alluvial fans, colluvials of unconsolidated gravels, sands, silts and clays characterize the former sequence. The later sequence is composed mainly of unconsolidated beach deposits, consisting of beach sands, silts, and clays. However, alluvial gravel, clayey estuarine and tidal flat deposits are also common. The sequence is extensively distributions, especially in the intermountain basins, undulated terrains, as well as along the minor and major stream courses in the area.

Cretaceous-Tertiary granitic rock consists of porphyritic biotite granite, granodiorite, hornblende adamellite and fine-grain muscovite-tourmaline granite. These rocks expose at central to the western of area, and at the western of Saba Yoi district.

Jurassic-Triassic granitic rock is medium- to course- grained porphyritic biotite granite, adamellite, and granodiorite. The rocks mainly distributed at the southern of Muang Songkhla area and in Nakhon Si Thammarat range from Phatthalung.

With reference to the geology map in Figure 2.3, the geology in both study areas is in age of Quaternary, the areas are underlain by Quaternary deposits comprise of the younger unconsolidated deposits, terrace deposits of gravels, sands, silts, clay and laterite, fluvial deposits of gravels, sands, silts and clay characterize the former sequence.

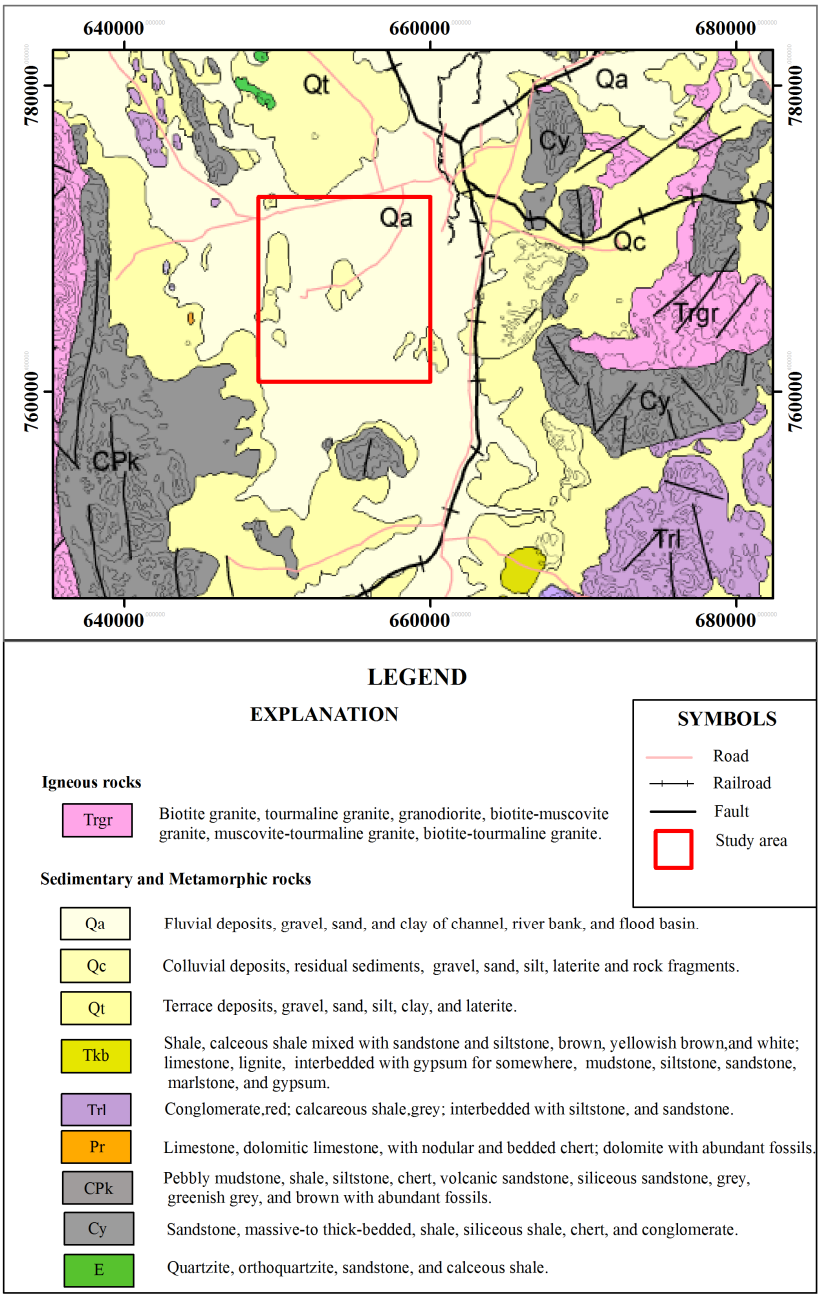

Figure 2.3 The geological map of the study area in Songkhla province.

(Modified from Department of Mineral Resources ,2007)

2.1.6 Groundwater resources

The study area is located in area of Hat Yai basin. Department of Groundwater Resources (1996) divided groundwater layer into 3 layers as following;

I) Hat Yai aquifer

Hat Yai aquifer is a top aquifer which is hosted by sand and gravel at a depth of about 20-50 meters from the surface. The thickness of sand and gravel layer is an average of 10-20 meters. In Hat Yai district, this layer has thickness of about 20-40 meters. It is covered with clay or sandy clay in which water can permeate through a little bit. This aquifer is unconfined aquifer or semi-confined aquifer.

II) Ku Tao aquifer

Ku Tao aquifer is at depth of about 60 – 100 meters with an average thickness about 30 meters. This aquifer is separated from Hat Yai aquifer by clay layer. Ku Tao aquifer is confined aquifer and it consists of multi-layer aquifer and clayey sand.

III) Kor Hong Aquifer

Kor Hong aquifer is laying under Ku Tao aquifer. These two deeper aquifer are separated by clay layer. A depth of this aquifer is more than 100 meters. It's a confined aquifer hosted by sand and gravel.

Arun Lookjan (2009) presented five hydrogeological cross section that covered Hat Yai basin, with reference to lithologic study and data of borehole in Hat Yai basin. There are two hydrogeological cross section that they pass through the study areas as following;

The fist hydrogeological cross section is $C - C'$ line (Figure 2.4a) that is across the first study area (Kuan Lang sub district, Hat Yai district). It showed that there are three aquifers;

I) Hat Yai aquifer is under the clay layer. Thickness of the aquifer is average about 20 meters. It's between 0 to -30 meters (MSL) average depth and consists of gravel and clayey sand.

II) Ku Tao aquifer has depth between -55 to -90 meters (MSL). It does consist of gravel and clayey sand.

III) Kor Hong aquifer has depth between -100 to -125 meters (MSL) and average thickness about 30 meters. It does consist of gravel and sand.

The second hydrogeological cross section is $B - B'$ line (Figure 2.4b) that is across the second study area (Ban Na Wat Pho School, Klong Hoi Khong subdistrict). It showed that there are three aquifers as below;

I) Hat Yai aquifer is under the clay layer. Thickness of the aquifer is average about 20 meters. It's between +5 to -15 meters (MSL) average depth and consists of gravel and clayey sand.

II) Ku Tao aquifer has depth between -35 to -60 meters (MSL). It does consist of gravel and clayey sand.

III) Kor Hong aquifer has depth between -80 to -120 meters (MSL) and average thickness about 30 meters. It does consist of gravel and sand.

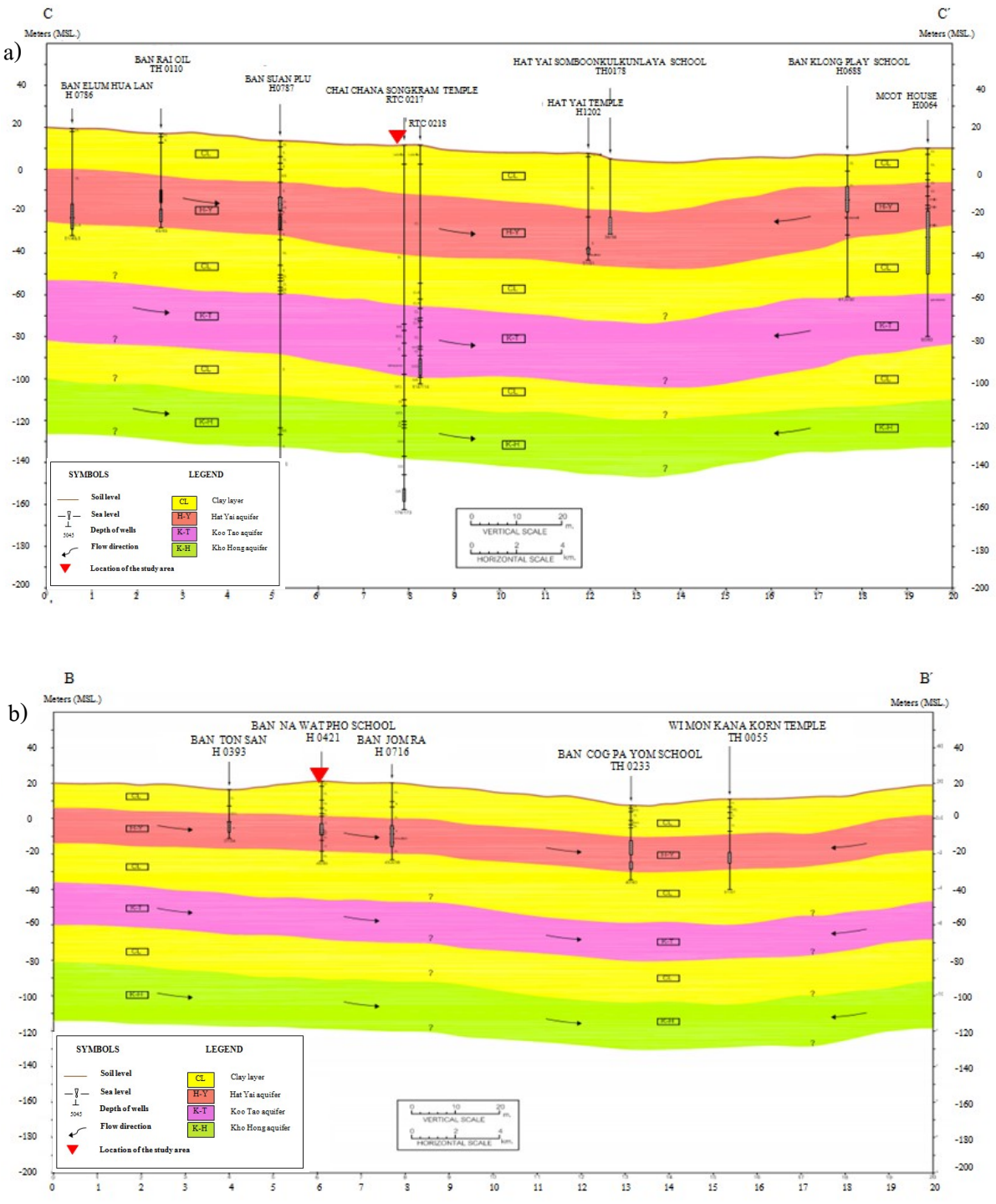

Figure 2.4 Hydrogeological cross section in Hat Yai basin; a) $C - C'$ line and b) $B - B'$ line

(Modified: Arun Lookjan,2009)

2.2 Geophysical investigation

Subsurface geological characterization in two study areas have been conducted by geophysics methods, 2D-Induceed polarization & resistivity imaging, Vertical Electrical Sounding (VES), Self-potential (SP), and Seismic refraction in active landfill of Hat Yai municipality (Kuan Lang area). The six profiles were investigated in northern part of the active landfill with reference to the direction of groundwater flow in the area that flows from the southwest to the northeast (Tanit, 2008: Amornrat, 2009) (Figure 2.5). G1, G2, and G3 profiles are paralleled by G4, G5 and G6 profiles respectively with the aim to check the change of subsurface geological structure among the paralled profiles and to determine the leakaged wastes from landfill site. The profiles, length of G1, G2, and G3 are 650, 300, and 400 meters respectively and 650, 300, 400 meters for G4, G5, and G6 respectively. Partial of G4 and G6 profiles are flooding zone which it is impossible to do geophysical measurements.

The second site, Ban Na Wat Pho School which is located in Klong Hoi Khong sub-district, Klong Hoi Khong district. This site is one in five biggest areas of high suitability areas for waste disposal which it is recommended by Rottana Ladachart (2002). One geophysical investigation profile was carried out on Ban Na Wat Pho School with the aim to prove the Rottana's work by geophysics method, which there is a borehole data (H0421) in the inviciny area used for constraining the interpretation (Figure 2.6). 2D-Induceed polarization & resistivity imaging, Vertical Electrical Sounding (VES), Self-potential (SP), and Seismic refraction have been employed in all measuring profiles. The direction of groundwater flow in the area that flows from the southwest to the northeast (Amornrat, 2009).

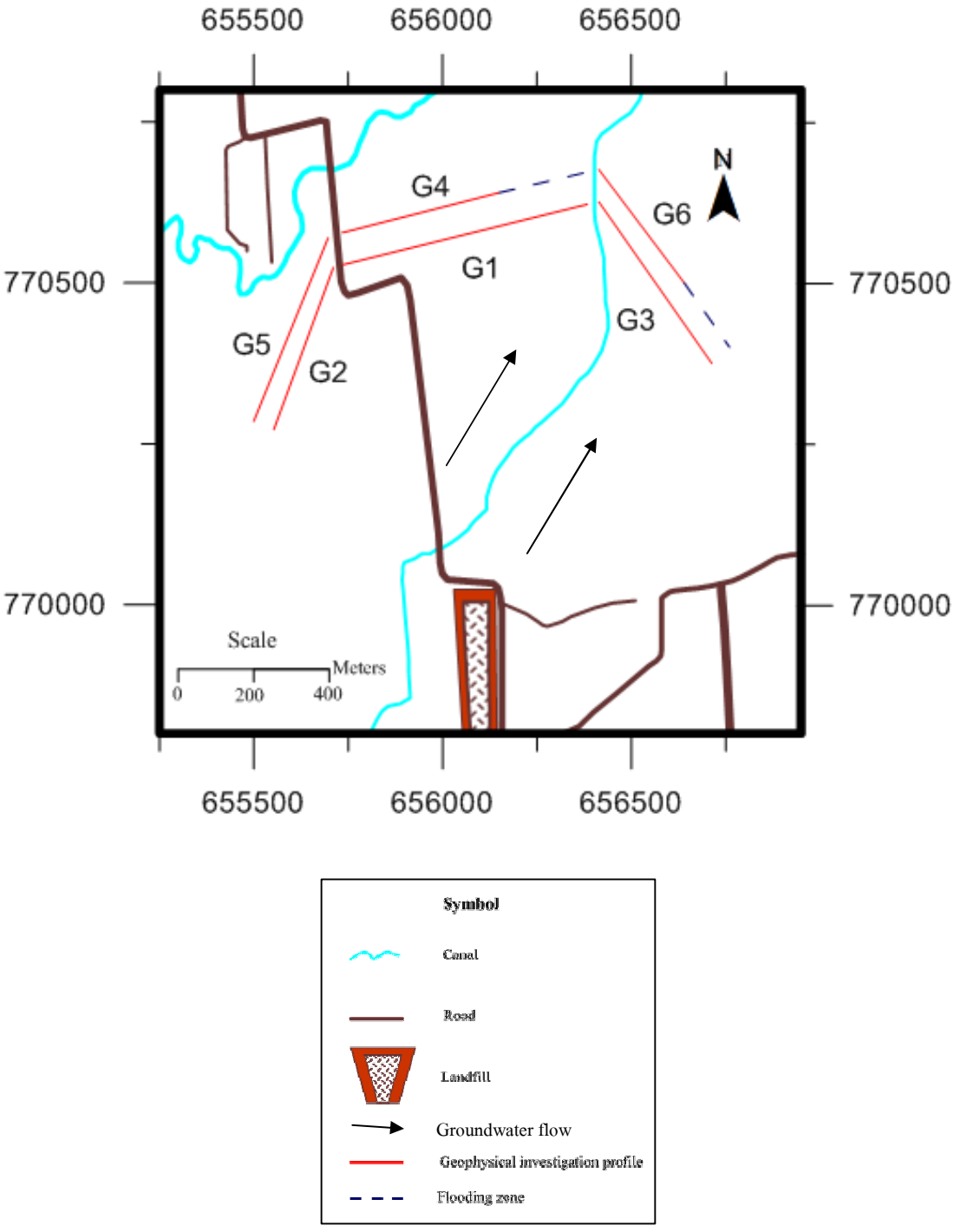

Figure 2.5 Map of study area showing geophysical measurement line on Kuan Lang sub district, Hat Yai district, Songkhla province.

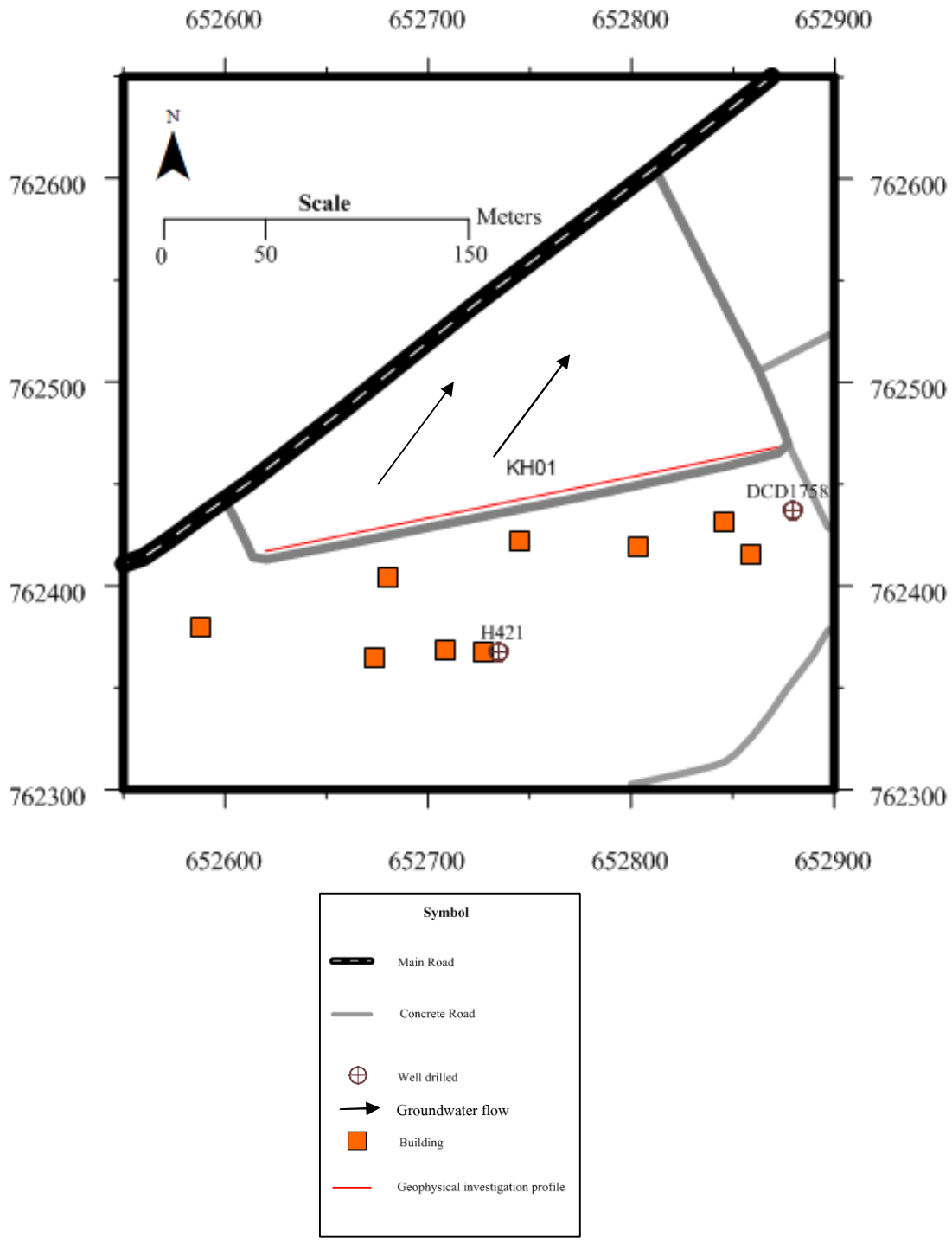

Figure 2.6 Map of study area showing geophysical measurement line on Ban Na Wat Pho School, Klong Hoi Khong district, Songkhla province.

2.3 Theoritical Background

2.3.1 Resistivity method

Resistivity method is electrical investigation which artificially – generated electric currents are introduced into the ground and the resulting potential differences are measured at the surface. The pattern of potential differences expected from homogeneous ground provides information on the form and electrical properties of subsurface heterogeneities.

2.3.1.1 Electrical properties of rock

Contrasts in electrical conductivities are expected like e.g. between soil and rocks, or soil above and beneath the groundwater surface. The inability of a medium to conduct an electric current is termed electrical resistivity ρ (Ωm) and its inverse the electrical conductivity σ (S/m) is sometimes used. When a static electric field E (V/m) is applied, a current density J (A/m^2) is established. Ohm's law in the case of a linear isotopic medium state that

$$E = \rho J = \frac{J}{\sigma} \tag{2.1}$$

Earth bulk materials are comprised of a solid phase (soils and rocks) and a space phase (pores, cracks, microfissures, fractures, etc.) that occupy the space between the solid materials. Thus, the bulk resistivity of Earth materials is associated with the resistivity of the solid phase (rock matrix) and resistivity of materials that fill the open space which may be air, oil or any liquid. The resistivity of an electrolyte in rock spaces dominates the formation resistivity in most cases. This means that the resistivity of rock matrix is negligible, except for media with metallic resistivity (e.g. pyrrhorite, pyrite, etc.) and clays. The oldest empirically determined and the most widely used relationship between the porosity (ϕ), water saturation (S_w), resistivity of the electrolyte (ρ_w) and bulk resistivity (ρ) can be written:

$$\rho = \rho_w S_w^{-n} \phi^{-m} \qquad \text{(Archie's law)} \tag{2.2}$$

When m and n are empirical constant. The exponent m is the cementation factor that increases with compaction, cementation and consolidation varies between about 1.3 and 1.5. The exponent n is the saturation exponent, which is in general given a value of n = 2.

The rock matrix cannot be assumed to be an insulator when clay minerals are present. In fact, clay minerals are very good conductors due to the presence of mobile ion inside the grains and they have an ability to absorb and retain ions. At the interface between the grains of clay minerals and the electrolyte, the ions in the electrolyte will be attracted or repelled from

the clay surface and produce an electric double layer. The resistivity of an electric double layer is the surface resistivity $\rho_s \left(= 1/\sigma_s \right)$, expressed in ohm-meter. The bulk conductivity, when the surface conductivity is present, is expressed by a modification of Archie's law:

$$\sigma = \sigma_w S_w^n \phi^m + \sigma_s \tag{2.3}$$

Another factor that influences the bulk resistivity is the temperature. Both in the rock matrix and in the electrolyte the resistivity decreases when the temperature increases.

Table 2.1 Resistivity of various rocks and sediments (Telford, 1990) (Milsom, 2003)

	Resistivity range (Ωm)
Top soil	50-500
Loose sand	500-5,000
Gravel	100-600
Slates (various)	$6\times10^2 - 4\times10^7$
Gabbro	$10^3 - 10^6$
Basalt (dry)	$10 - 1.3\times10^7$
Graphite schist	10-100
Consolidated shale	20-2,000
sandstone	200-8,000
Limestone	500-10,000
Unconsolidated wet clay	20
clay	1-100
Dolomite	350-5,000
Conglomerates	$2\times10^3 - 10^4$
Quartzite (various)	$10 - 2\times10^8$

2.3.1.2 Resistivity measurements

The electrical resistivity of a homogeneous cylindrical solid of length L and cross section A, having resistance R between the end faces, is given by

$$\rho = R\frac{A}{L} \tag{2.4}$$

If A is in square meters, L is in meters, and R is in ohms, the resistivity unit is the ohm-meters (Ωm). The resistance R is given in term of the voltage V applied across the ends of the cylinder and the resultant current I flowing through it, by Ohm's law:

$$R = \frac{V}{I} \tag{2.5}$$

Where R is in ohms and V and I are in the units of volts and amperes, respectively.

The basis of electrical resistivity method is to introduce a known current into the ground and measure potential differences on the surface to estimate the resistivity of the subsurface. Assume that a current electrode is placed on a homogeneous ground; the current flows radially out through a hemisphere of radius r, with a surface area $2\pi r^2$ and the current density J at distance r is then,

$$J_r = \frac{I}{2\pi r^2} \tag{2.6}$$

That will be

$$E_r = \rho J_r = \frac{I\rho}{2\pi r^2} \tag{2.7}$$

The potential V at distance r from the current electrode is derived by the integral of E_r between r and infinity assuming the potential at infinity to be zero.

$$V_r = \int_r^\infty E_r dr = \frac{I\rho}{2\pi r} \tag{2.8}$$

For heterogeneous (non-homogeneous) subsurface, the electrical anomalies, which are measured, depend up on the resistivity difference between difference rocks/sediments (Table 2.1)

Normally, the four electrode spreads are used in resistivity field work. When the distance between the two current electrodes are finite (Figure 2.7), the potential at any nearby surface point will be affected by the both current electrodes. As before, the potential due to C_1 at P_1 is

$$V_1 = -\frac{A_1}{r_1} \quad \text{Where } A_1 = -\frac{I\rho}{2\pi} \tag{2.9}$$

Because the currents at the two electrodes are equal and opposite in direction, the potential due to C_2 at P_1 is

$$V_2 = -\frac{A_2}{r_2} \quad \text{Where } A_2 = \frac{I\rho}{2\pi} = -A_1 \tag{2.10}$$

The potential V_C at an internal electrode P_1 is the sum of the potential contributions V_1 and V_2 from the current source at C_1 and the sink at C_2. From equation (2.9) and (2.10), this will be:

$$V_C = \frac{I\rho}{2\pi}\left(\frac{1}{r_1} - \frac{1}{r_2}\right) \tag{2.11}$$

similarly, the potential V_D at an internal electrode P_2 is the sum of the potential contributions V_3 and V_4 from the current source at C_1 and the sink at C_2. From equation (2.9) and (2.10), this will be:

$$V_D = \frac{I\rho}{2\pi}\left(\frac{1}{r_3} - \frac{1}{r_4}\right) \tag{2.12}$$

So, the potential difference ΔV between electrodes P_1 and P_2 is measured as equation below

$$\Delta V = V_C - V_D = \frac{I\rho}{2\pi}\left\{\left(\frac{1}{r_1} - \frac{1}{r_2}\right) - \left(\frac{1}{r_3} - \frac{1}{r_4}\right)\right\} \tag{2.13}$$

Thus,

$$\rho = \frac{2\pi\Delta V}{\left\{\frac{1}{r_1} - \frac{1}{r_2} - \frac{1}{r_3} + \frac{1}{r_4}\right\} I} \tag{2.14}$$

Where ρ is the resistivity in ohm-meters, ΔV is the potential difference in volts, I is the current in ampere, and r_1, r_2, r_3, r_4 are positions of electrodes in meters. However, the resistivity will vary with the relative position of the electrodes. Any computed value is then known as the "apparent resistivity" ρ_a and will be function of the form of the heterogeneity. Equation (2.14) can rewritten that

$$\rho_a = G\frac{\Delta V}{I} \tag{2.15}$$

That will be

$$G = \frac{2\pi}{\left\{\frac{1}{r_1} - \frac{1}{r_2} - \frac{1}{r_3} + \frac{1}{r_4}\right\}} \tag{2.16}$$

Where ρ_a the apparent resistivity in ohm-meters is, $\Delta V / I$ is the resistance in ohms, and G is geometric factor which depend on the arrangement of four electrodes. Equation (2.15) is the basic equation for calculating the apparent resistivity for any electrode configuration.

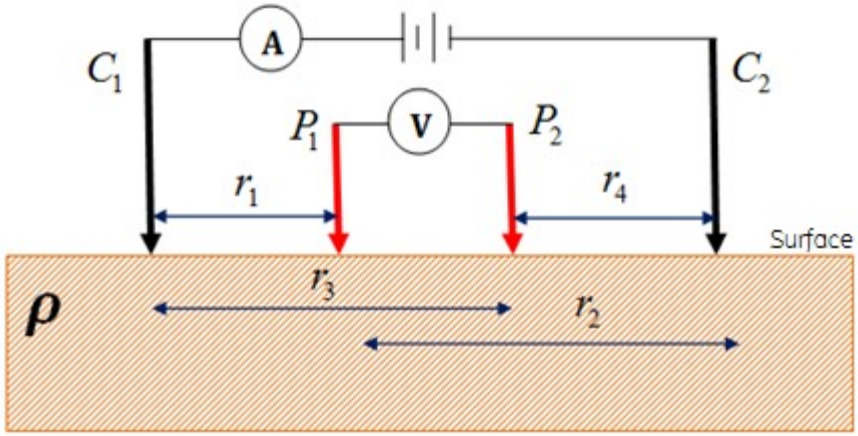

Figure 2.7 The generalized form of the electrode configuration in the resistivity measurements. (Modified: Telford,1990)

2.3.1.3 Configurations

The arrays that are most commonly used for two dimensions resistivity imaging investigations are Wenner, Dipole-Dipole, Wenner – Schlumberger, Pole –Pole and Pole – Dipole (Figure 2.8). The best array to use generally depends on the type of structure to be mapped, the sensitive of the resistivity meter, the background noise level and manpower.

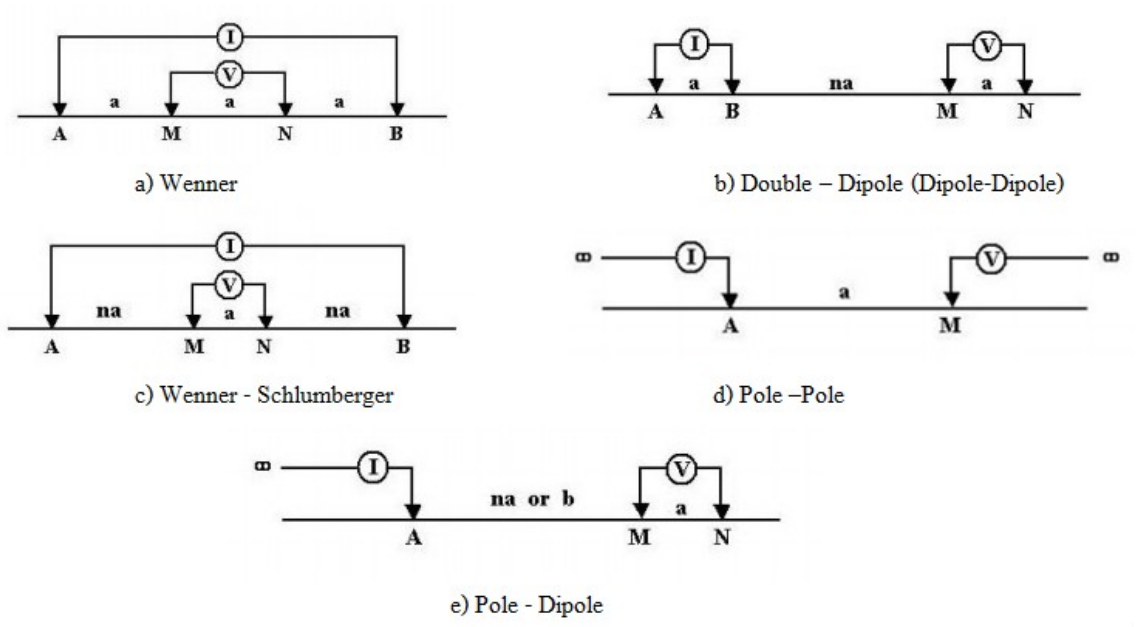

Figure 2.8 Common electrode configurations that are used in resistivity investigations.

The most important factors for choosing the appropriate array are:

1) The sensitivity of the array to vertical and horizontal changes in the subsurface resistivity

2) The depth of investigation

3) The horizontal data coverage

4) The signal strength

The sensitivity of the array is estimated from the potential difference that can be measured from a specific change in resistivity. Normally, the highest sensitivity can be obtained closest to the electrode. For example, the Double-Dipole (Dipole - Dipole) array is also good in mapping vertical changes but poor in mapping horizontal changes. For estimation of resolution towards depth in pseudosection Edwards (1977) used the median depth of penetration for various methods in a homogeneous media. These values will tell how deep the ground can be mapped by a particular array and it is a good guide when designing a field investigation. For Double –Dipole array, the depth of penetration will be shallower when compared to the Wenner array. The greatest depths are reached when using a Pole-Pole array. Double-Dipole array gives wider horizontal data coverage than the Wenner and the Pole-Pole array gives the widest horizontal data coverage. The signal strength of the arrays can be determined from the inverse value of the

geometric factor, G, of a particular array (Loke, 1999). The array, which has the greatest signal strength, is the most appropriate to use in areas with high background noise.

2.3.1.4 Dipole-Dipole array

Dipole-dipole array is used for the resistivity measurement in this research work. For dipole-dipole configuration, the position of four electrodes is shown in Figure 2.2.

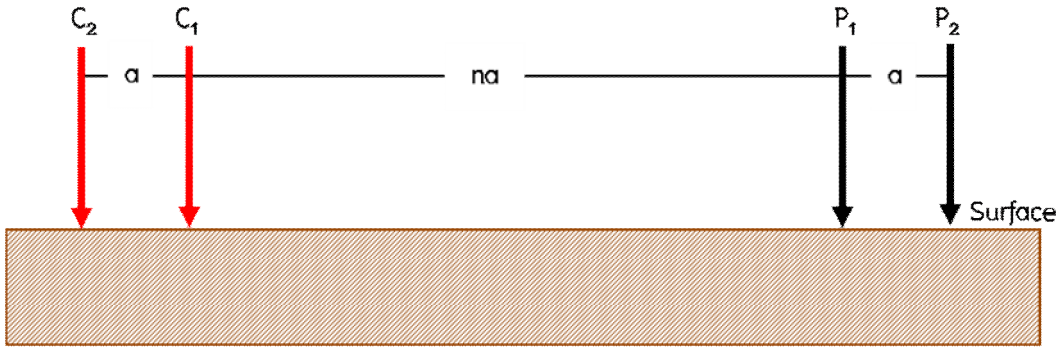

Figure 2.9 Dipole – dipole configuration.

(Modified: Telford, 1990)

The geometric factor for double-dipole configuration is defined as below

$$G = \pi na(n+1)(n+2) \tag{2.17}$$

Where 'a' is the dipole separation in meters, and 'n' is factor that is ratio of the distance between C_1 and P_1 electrode to dipole separation ($C_2 - C_1$ *or* $P_1 - P_2$). The 'a' spacing is initially kept fixed and the 'n' factor is increased from 1 to 2 to 3 until up to about 6 in order to increase the depth for investigation. The median depth of investigation also depends on the 'n' factor, as well as the 'a' factor (see in Table 2.2).

Table 2.2 The median depth of investigation (Z_e) for the different array (Loke, 1997).

Array type	Z_e/a
Wenner alpha	0.519
Wenner beta	0.416
Wnner gamma	0.594
Dipole-dipole n =1	0.416
n = 2	0.697
n = 3	0.962
n = 4	1.220
n = 5	1.476
n = 6	1.730
n = 7	1.983
n = 8	2.236
Equatorial dipole-dipole	
n = 1	0.451
n = 2	0.809
n = 3	1.180
n = 4	1.556
Wenner-Schlumberger	
n = 1	0.512
n = 2	0.925
n = 3	1.318
n = 4	1.706
n = 5	2.093
n = 6	2.478
n = 7	2.863
n = 8	3.247
n = 9	3.632
n = 10	4.015

There are generally three basic procedures in resistivity work. The particular procedure to be used depends on whether one is interested in the resistivity variations with lateral extent or with depth. The first procedure is vertical electrical sounding (VES) that is resistivity variations with depth. The second procedure is interested in lateral resistivity variations which is called profiling or mapping. The combination of the two procedures is the third one, which it can produce the resistivity pseudosection showing vertical and lateral or horizontal resistivity variation. Two types of resistivity measurement have been conducted in this study area.

(a) Dipole-dipole resistivity pseudosection

Dipole-dipole configuration has been widely used in resistivity and IP surveys due to a low electromagnetic coupling between current and potential circuit. This array is most sensitive to horizontal change in resistivity, thus the discontinueity layer is suitable to be mapped by this array. The arrray has a relatively poor resolution of the horizontal structures like sill or sedimentary layers (Loke, 1999), however, it has a good horizontal data coverage for 2D survey and can give a high resolution with overlapping data levels by combining measurements with different 'a' and 'n' values, where 'n' must be an integer (1,2,3,…,etc.).

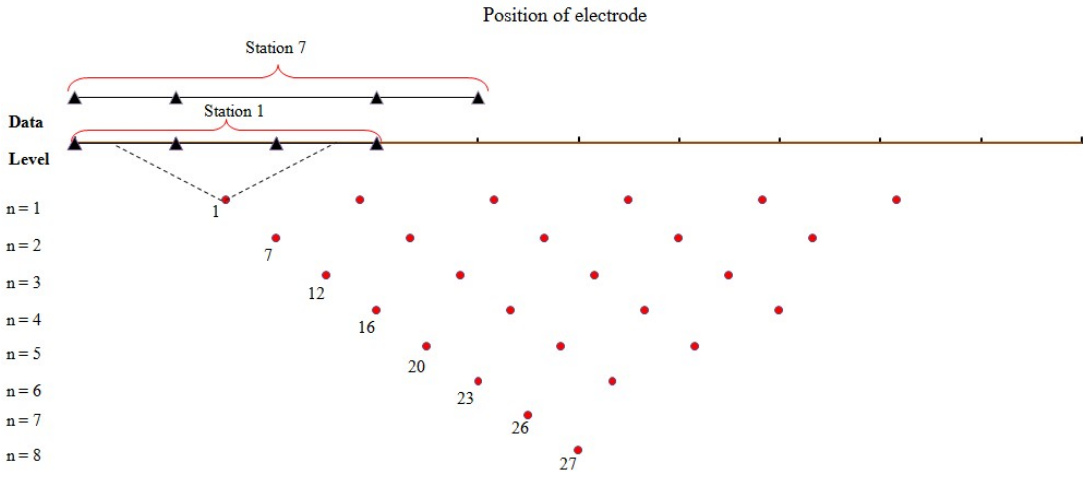

Figure 2.10 Pseudo plotted data for the dipole – dipole array.

(Modified: Loke, 1997)

For data processing, 2D-resistivity model were calculated by the RES2DINV program (Loke, 1999). In this inversion program, the subsurface is divided into small rectangular blocks. Each block represents the data point of apparent resistivity. The depth of the bottom row of blocks is equal to the median depth of investigation (Edwards, 1977). Because of the inversion program gives model of the subsurface resistivity, it was not ready to be used for interpretation due to the different setting parameter of each model, such as color scale. Thus, the model files were saved and then the Surfer9 program (Golden Software, Inc. 1999) was used to make more sophisticated contouring before interpretation.

(b) Schlumberger Vertical Electrical Sounding (SVES)

This procedure, also known as 'electrical drilling' or 'expanding probe', is used mainly in the study of horizontal or near – horizontal interfaces. The field procedure is to use a fixed center with an expanding spread. In this research work, the resistivity measurement utilizing Schlumberger array is used for vertical sounding investigation. For Schlumberger (gradient) array, the current electrodes are spaced much further apart than the potential electrodes. Four electrodes for the Schlumberger array is shown as Figure 2.11

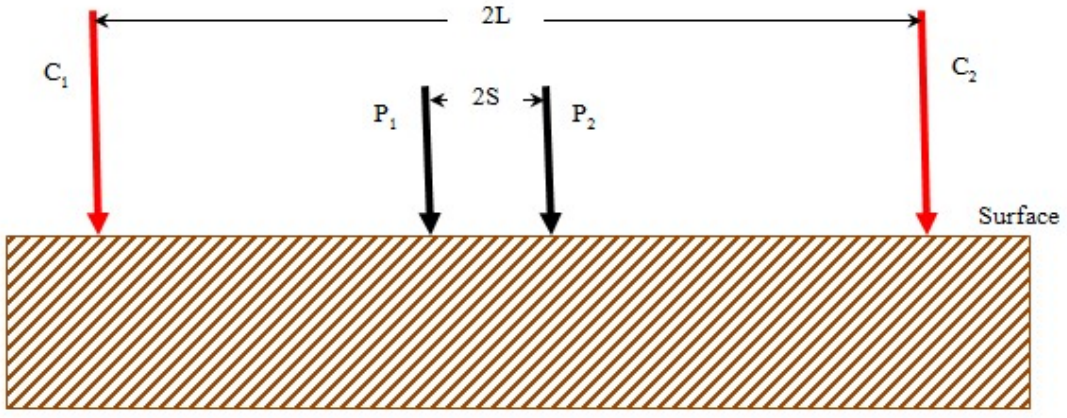

Figure 2.11 Schlumberger array.

(Modified: Telford, 1990)

The geometric factor for Schlumberger (gradient) array is defined as below

$$G = \frac{\pi}{2}\left[\frac{L^2 - S^2}{S}\right] \tag{2.18}$$

Where 'L' is half distance of the current electrodes spacing. And 'S' is half distance of the potential electrodes spacing. For data processing, the apparent resistivity is plotted against the current electrode spacing in log-log scale. These results are sounding curve which is the base of data inversion to obtain the resistivity and depth of the subsurface structure.

2.3.2 Induced Polarization method

2.3.2.1 Induced Polarization measurements

Induced polarization (IP) is obtained with a standard four electrode DC resistivity spread by interrupting the current abruptly. The voltage across the potential electrodes generally does not drop to zero instantaneously, but decays rather slowly, after an initial large decrease from the original steady – state value (Figure 2.12). The decay time is in the order of second or even minutes.

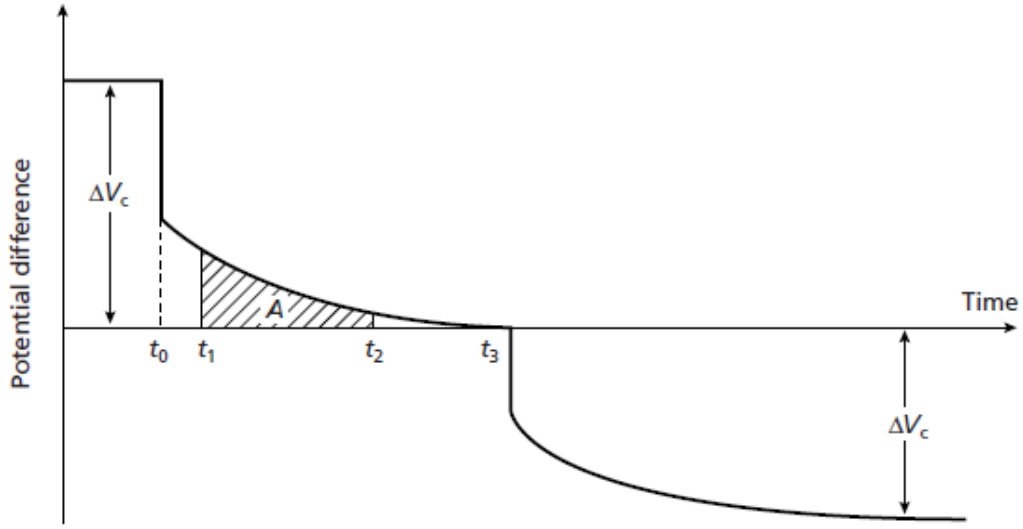

Figure 2.12 Induced polarization phenomenon.

(Kearey, 1984)

There are really only two types of induced polarization (IP) detector. Measurements of IP may be made either in the time or the frequency. Induced polarization is measured in function of time that is known as "*Time – domain*". And induced polarization is measured in function of frequency that is called "*Frequency – domain*". For this research work, time – domain IP is interested in the investigation. So, there are three types of time – domain IP measurement as following;

(a) Millivolts per volt (IP percent)

The simplest way IP effect measurement with the time – domain equipment is comparison the residual voltage $V(t)$ exist a time t after the current is cut off with the steady voltage V_C during the current – flow interval. It is not possible to measure potential at the instant of cut off because of large transients caused by breaking the current circuit. The $V(t)$ is measured before the residual has decayed to noise level. Because of $V(t)$ is much smaller than V_C. So, the ratio $V(t)/V_C$ is expressed as millivolts per volt, or as a percent.

(b) Decay – time integral

Commercial IP sets generally measure potential integrated over a definite time interval of the transient decay. If this integration time is very short and if the decay curve is sampled at several points, the values of the integral are effectively a measurement of the potential existing at different times, that is V (t_1), V (t_2),…, V (t_n). This is an extension of the measurement in mV/V (or percent) from which one also obtains the decay curve shape.

(c) Chargeability

Chargeability is one type of time – domain IP that is defined as

$$M = \frac{1}{V_C}\int_{t_1}^{t_2} V(t)dt \qquad (2.19)$$

which V (t) and V_C have the same unit. So, the chargeability (M) is in milliseconds. On the other hand, the chargeability is the most generally used in time – domain IP measurement.

For the induced polarization (IP) measurement, steel electrodes are usually used for current electrodes. And non – polarizing electrodes are used for potential electrodes. Metal immersed in a saturated solution of its own salt, such as Copper in Copper Sulphate (Cu-$CuSO_4$) or Silver in Silver Chloride (Ag-AgCl), is used for the non – polarizing electrodes (Figure 2.13). In this work, Copper in a saturated solution of Copper Sulphate is used for the non – polarizing

electrodes. The solution is contained in a porous pot which allows slowly solution leakage into the ground for reducing the contact resistance. The non – polarizing electrodes will be buried in shallow holes, approximate 20 centimeters depth, for every location that the non – polarizing electrodes is moved.

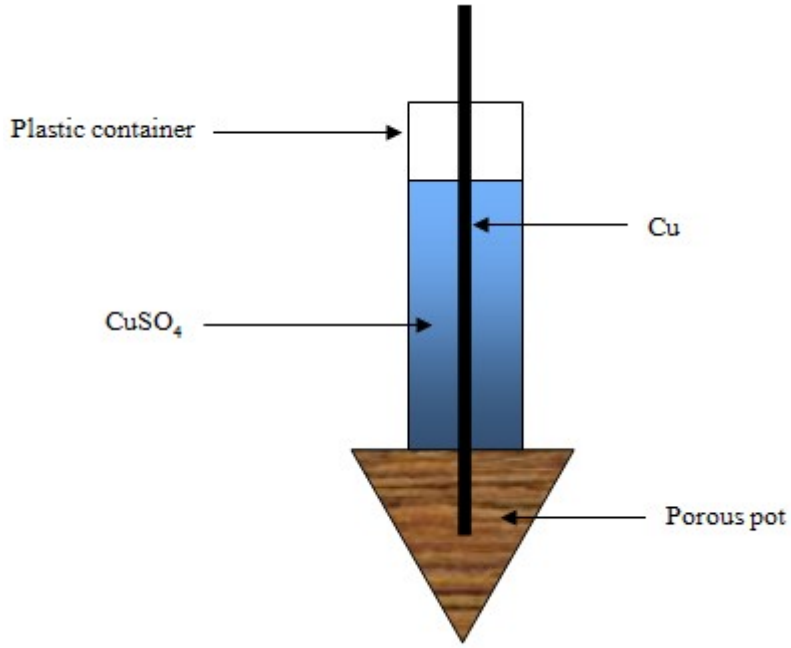

Figure 2.13 Non – polarizing electrode.

(Modified; Telford, 1990)

The induced polarization and resistivity measurement will do in the same time and the same electrode configuration. Thus, two data sets of an apparent resistivity and an apparent IP data will get from the measurement. The dipole – dipole configuration is used for the IP measurement in this study and the apparent resistivity over homogeneous ground is expressed by

$$\rho_a = \pi n a (n+1)(n+2)\frac{\Delta V}{I} \tag{2.20}$$

For some data sets in the induced polarization measurement, an observed IP values are over 1000 milliseconds (or less than -1000 milliseconds) almost certainly caused by noise due to a very weak IP signal. For checking whether high IP values are real, the apparent resistivity pseudo section is checked. If high and low value of the apparent resistivity pseudo section is shown due to vary in an erratic manner, the data is noisy and if the apparent IP values also show an erratic pattern, then the IP data is too noisy.

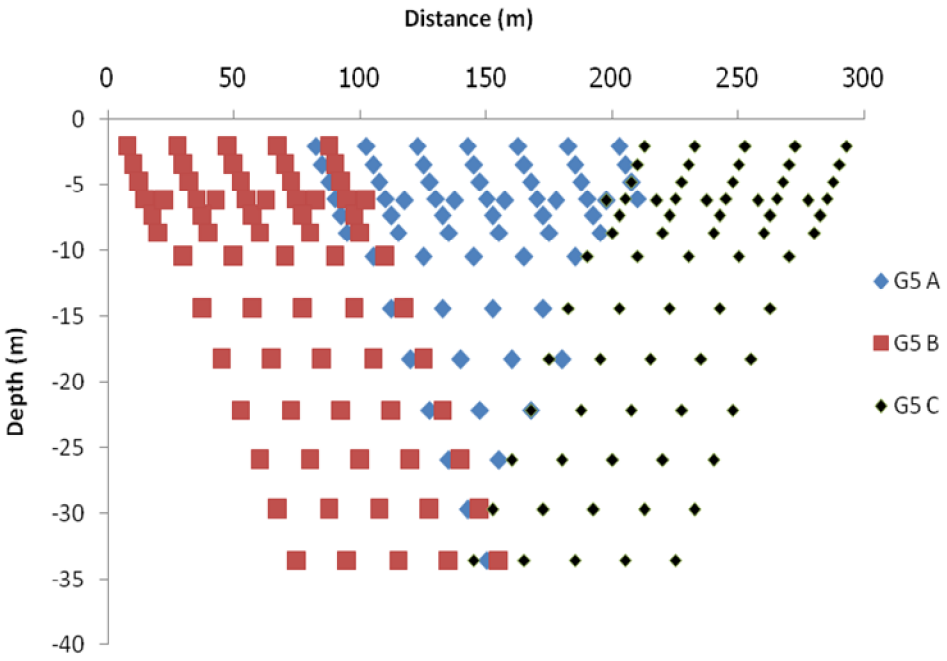

Figure 2.14 Datum point for resistivity and IP survey in G5 line

2.3.2.2 Data processing of 2D-IP & resistivity investigation

The resistivity and IP data are inverted by the RES2DINV program (Loke, 1999) to get the resistivity model section and the IP model section. This inversion program supports four different types of IP data; (I) Time domain chargeability measurement, (II) Frequency domain percent frequency effect measurements, (III) Phase angle measurement, and (IV) Metal factor IP values. File of the resistivity and IP data for inverting by the RES2DINV program is saved in DAT format. The pattern of data file format for the double – dipole (dipole - dipole) array is shown as below:

Table 2.3 The pattern of data file format for the IP measurement (Geotomo Software, 2009).

LINE 5.DAT File					Explanation
IP_Line5C site 2					Title
5.0					Smallest electrode spacing
3					Array type
59					Total number of data points
0					X-location (0 for first electrode and 1 for mid-point location)
1					1 for IP present and 0 for no IP
Chargeability					Type of IP data
msec					IP unit
0.01,1.0					Delay, integration time
0	5	1	649.52	1.85	x-location, a, n, apparent resistivity, apparent IP
0	5	2	277.44	1.59	2^{nd} data point
⋮	⋮	⋮	⋮	⋮	
0	0	0	0	0	Few zero's at the end

In this inversion program, the subsurface is divided into small rectangular blocks. Each block represents the data point of IP value and/ or apparent resistivity. The inversion program will create a model of resistivity and IP in a pseudo section and adjust this model to fit the measured data by applying a non – linear least squares optimization technique (deGroot-Hedlin and Constable 1990, Loke and Baker 1996a). The setting option, which is the most important to consider, is the increase of the layer thickness. The thickness and depth to each of the subsequent layer of the inversion model will be determined by this option.

In the optimization, the program basically tries to get the best fitting between the calculated IP and measured IP by adjusting the IP of the model blocks to minimize the root – mean square (RMS) error. So, models with small values of RMS error sometimes might not represent the best models of the geological features. Therefore, geological information in the area will have an important role for the choice of the best model. The inversion program gives models of the subsurface IP, it was not ready to be used for interpretation due to the different setting parameter of each model, such as color scale. Thus, the models files were saved and then the

Surfer9 program (Golden software, Inc. 1999) was used to do more sophisticated contouring before interpretation.

In addition, IP data and apparent resistivity will be inverted together by using the same inversion process. The inverted option, which is used in the inversion of IP, will be used for resistivity.

2.3.3 Self - potential survey

Self – potential (or spontaneous polarization) method is based on the surface measurement of natural potential differences resulting from electrochemical reactions in the subsurface (Kearey, 1984). The self – potential is an electrical method that measures naturally occurring electric potential differences between two locations in the ground surface. The electric potential difference, which is measured, is associated with non - artificial electric currents transmitted through the ground. The naturally generated electric potential differences range in magnitude from less than millivolts (mV) to over one volt (Reynolds, 1997). The magnitude and sign (positive and negative) of a delineated self – potential anomaly can provide indications as to the character of the subsurface feature producing the anomaly.

2.3.3.1 Source of SP

For flow generated SP there is a linear relationship between flows of fluid, electricity, chemical, heat and hydraulic, electrical, chemical and thermal gradients. This is expressed by e.g. Darcy's law showing the relation between hydraulic gradient (i_h) and fluid flow (q_i), Fick's law expressing the relation between concentration gradient (i_c) and chemical diffusion (f), Fourier's law demonstrating the relation between thermal gradient (i_t) and heat flow (q_t), and Ohm's law showing the relation between electrical gradient (E) and electrical current density (J). The flows, driven by the gradients, are known as direct flows, which can be general written as:

$$J_i = L_{ii} X_i \tag{2.21}$$

Where J_i is the flow per unit area of type i, X_i is the gradient or driving force of type i, and L_{ii} is the conductivity coefficient for type i flow. In the nature when these flows occur at the same time, they interfere with each other. The gradient of one type can drive a flow of

another, in what is called coupled flows. For example an electrical flow can be driven by a hydraulic gradient, the absorption of heat in the metals may result from the flow of an electrical current etc. Thus, the total flow of type i can be written as:

$$J_i = \sum_{j=1}^{n} L_{ij} X_j \tag{2.22}$$

Where i = 1, 2, …, n and L_{ij} is the couple coefficient relating flow of type i to force of type j, and X_j is the gradient or driving force of type j. If in the measured area no external electric field is present. Then an electric current density in the porous media will be driven by hydraulic, thermal or chemical gradient, which can be expressed by:

$$J = L_{EH} i_h + L_{ET} i_t + L_{EC} i_c \tag{2.23}$$

This equation shows that the SP on the surface is not only a result of the electrical current density of fluid flow but also result from the thermal or chemical flows. Therefore information of hydraulic, thermal and chemical gradient in the ground can be obtained by measuring the SP. The SP anomaly that results from groundwater flow has not been fully explained from observation it has become widely accepted that it produces an important part of the electrical potential, a so-called streaming potential. Thus, the study of the direction of groundwater flow is based on the phenomenon of the streaming potential.

a) Streaming potential

The streaming potentials, or electrofiltration, are result from an electrolyte that flows through a porous media. When an electrolyte is in contact with a solid surface that normally exhibits negative charges, e.g. clay minerals, then the positive charges from an electrolyte will be attracted and accumulated at the solid surface. This phenomenon is known as the electrical double layer. The result being a diffuse layer that has an excess of positive charges with respect to negative charge in the vicinity of the solid surface. When a pressure gradient forces the electrolyte to flow relative to the solid, the excess positive charges within the diffuse layer will be dragged along with the fluid flow, this process will produce a convection current (I_{conv}). This will result in an imbalance between the positive charges in the upstream part (the low pressure) and negative charges in the downstream part (the high pressure). This charge separation results in a streaming potential that will drive a conduction current (I_{cond}) back through the fluid.

At steady state equilibrium for a capillary or porous medium with a non-conducting matrix, I_{conv} is balanced by I_{cond}. According the Poisson's equation, a Gouy –Chapman diffuse layer and the parabolic velocity profile characteristic of Poiseuille's flow, the convection and the conduction current (Morgan et al., 1989; in Wattanasen, 2001) can be expressed by:

$$I_{conv} = -\pi\varepsilon \frac{\xi}{\eta} G\Delta P \tag{2.24}$$

$$I_{cond} = \pi\sigma_w G\Delta V \tag{2.25}$$

Where ΔV and ΔP are the potential difference (streaming potential) and the pressure difference driving the flow, σ_w is the fluid conductivity, ε is the dielectric permittivity of fluid, ξ is the zeta potential (the voltage a closest plane to the solid surface where charge movement occur), η is the viscosity of fluid, and G is the geometrical factor. From equation (2.24) and (2.25) will get:

$$\Delta V = -\frac{\varepsilon\xi}{\eta\sigma_w}\Delta P \tag{2.26}$$

This is the Helmholtz-Smoluchowski equation, the ratio $\Delta V/\Delta P$ is referred to as the streaming potential coefficient C. If equation (2.23) is considered together with an Ohm's law in case of no other gradient than hydraulic gradient (only electrolyte flow) is present, which will get the ratio $\Delta V/\Delta P$ as below:

$$\frac{\Delta V}{\Delta P} = \frac{L_{EH}}{\sigma_w} = C \tag{2.27}$$

It is seen that the streaming potential coefficient C depends upon the conductivity, the dielectric permittivity, the zeta potential, and the viscosity of an electrolyte along the flow path. So, this C value is referred to as the apparent streaming potential coefficient. However, in the field the porous media or matrixes around an electrolyte are not completely non-conducting. Thus, the value of an apparent streaming potential coefficient will be less than the value estimated in laboratory, which C = 1 – 15 mV/m. In case of a surface conductivity σ_s, equation (2.26) will be rewritten as below:

$$\Delta V = -\frac{\varepsilon\xi}{\eta\left(\sigma_w + 2\frac{\sigma_s}{r}\right)}\Delta P \tag{2.28}$$

Where r is the pore or capillary radius.

b) Diffusion potential

Concentration differences of ions in the groundwater will produce electrical potential difference, so-called diffusion potential. The ions will diffuse in the direction of increasing concentration gradient. A diffusion current density J_D will be created from the net flow of ions until it is balanced by the conduction current in the reverse direction to the steady state conditions. NaCl is one solute that usually exists in nature electrolytes, and the net diffusion current density J_D can be expressed below:

$$J_D = e^o \nabla C(D_{Na} - D_{Cl}) \tag{2.29}$$

Where e^o is the elementary electric charge and C is is the electrolyte concentration. D_{Na} and D_{Cl} are the diffusivity of cations and anions of Na and Cl, respectively. Normally in thr nature, there are several different species of solutes in an electrolyte, the situation is more complicated. If the concentration of electrolytes in the ground varies locally, the background SP anomalies will be in the order of fractions of millivolts to some ten of millivolts (Parasnis, 1997). Such background anomalies should disappear in the absence of concentration differences in the ground, since the flow of ions creates an equilibrium state, but in reality it seems that the concentration difference occurs of all time. The phenomenon is suggested that the concentration differences are regenerated by redox reactions involving oxygen from the atmosphere.

c) Other sources of SP

The influence of topography on the SP investigation is always corrected for in the interpretation procedure. This effect of topography can be observed in the SP data as an approximately linear trend, with SP values that become more positive going downhill. Ernstson and Scherer (1986) showed topographic effects of maximum 80 mV per 100 m different in elevation. Other sources of SP anomalies that can be involved in the measuring data are due to: 1) cultural activity: stray currents generated by power lines, well casings etc., 2) conductive mineral deposits that are related to negative potential over the top of the deposit,3) biological root activity.

2.3.3.2 SP measurements

A pair of non – polarizing electrodes is used for self – potential (SP) investigation. The non – polarizing electrodes are made by using the porous pot that contain metal immersed in saturated solution such as Copper in Copper sulphate (Cu-$CuSO_4$) or Silver in Silver chloride

(Ag-AgCl). The electrodes of SP survey will be similar to the potential electrodes of IP survey. The SP survey will only use a pair of potential electrodes, which are the non – polarizing electrodes, because of this method measure natural potential differences that occurred from natural current.

There are two common techniques in the self – potential investigation to perform the mapping. The first technique is the gradient configuration, which also called the dipole or leapfrog, that utilized two electrodes (P_1 and P_2) consecutively moving together along a line survey or a series of transects with constant distance electrodes separation, for each movement the pair of electrode, the new position of electrode P_1 corresponds with the previous position electrode P_2. The SP value is the midpoint between the two electrodes for each moving. The second one is the fixed – base configuration that used a stationary base electrode P_1 and measuring the moving electrode P_2 along a line survey or a series of transects (Figure 2.14). The fixed base configuration is used for SP measurement in this research. The reference electrode was buried approximate 20 centimeters depth to decrease temperature and polarization effects.

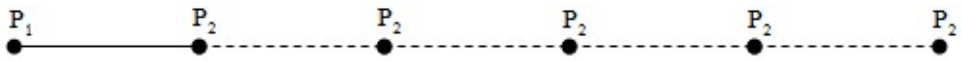

Figure 2.15 Fixed – base configuration for SP data collection.

(Modified: Allred, 2008)

At each measuring point, the moving electrode was set approximate 20 centimeters depth into the soil to decrease the SP effect from chemical and moisture variations in the topsoil. The base station, which is near the reference electrode, reading was re-measured at every hour for drift correction. The SP survey is measured in character of a loop. Theoretically, value of the first and the last measurement at the base station must be equal.

2.3.3.3 Data processing

The objective of data processing in this work is to get SP anomalies resulting from the streaming potential that is associated with groundwater flow in the area. The processing was

performed by drift-correction followed by removing the topographic effect from the drift-corrected SP data. Other noise anomalies were assumed to be very small and negligible.

2.3.4 Seismic refraction method

2.2.4.1 Elastic properties and wave velocity

Seismic survey is method that utilize the propagation of elastic wave through the subsurface in the earth because of differences in elastic properties of rocks cause the differences in the propagation in the subsurface. The elastic properties of subsurface are characterized by elastic constants. The main two elastic constants for studying elastic wave propagation are the bulk modulus (κ) and the shear modulus (μ). So, there are two groups of seismic waves, surface waves and body waves, which are utilized in seismic surveys. The velocity of body wave propagation can be determined as a function of the density (ρ) and the elastic constants. There are two types of body wave, Compressional waves and Shear waves, which are explained as follows. Compressional waves (also called P-wave, primary wave or longitudinal wave) propagate in the medium in the same direction with the direction of wave propagation. Its velocity is given as follows:

$$V_P = \sqrt{\frac{\kappa + \frac{4}{3}\mu}{\rho}} \tag{2.30}$$

Shear waves (also called S-wave, secondary or transverse wave) propagate in the medium in the direction perpendicular to the direction of wave propagation. Its velocity is given as below:

$$V_S = \sqrt{\frac{\mu}{\rho}} \tag{2.31}$$

The shear waves cannot propagate through the liquids and gases because liquids and gases offer no resistance to shear deformation ($\mu = 0$). And the shear waves always travel slower than the compressional waves in the same medium.

In addition, there are two types of surface wave, Rayleigh waves and Love waves, which are explained as follows. The Rayleigh waves, the particles in the medium move in elliptical paths in the vertical plane of the direction of wave propagation and particles at the surface move backward with respect to the direction of wave propagation. The velocity of

Rayleigh wave is about $0.9V_S$. For Love waves, the particles of the medium move parallel to the surface and oscillate perpendicular to the direction of the wave, which is similar to the shear wave where the particles move in the horizontal plane and transverse to the direction of the wave. In this case, the shear wave is called SH-waves and the velocity of them depends on the frequency. At high frequency (short wavelengths), their velocity is equal to V_S in the upper layer. And for low frequency (long wavelengths), their velocity is equal to V_S in the substratum layer.

For geophysical investigation by using seismic method, artificial energy sources are used to generate the seismic waves that are timed as waves travel through the subsurface from wave's source to the geophones, which respond to the incoming seismic wave amplitudes and the timed arrivals. The rocks, sediments or materials will have different velocity as shown in Table 2.4. Seismic geophysical investigation is separated into the two methods that are seismic refraction and seismic reflection. Because of this research work wants to investigate the shallow structure of the subsurface (approximately 30 meters depth). So, the seismic refraction method is used for this investigation.

Table 2.4 The compressional wave velocity of various materials (Reynolds, 1997).

Material	**V_P [m/s]**	**Material**	**V_P [m/s]**
Air	330	Granite	4600-6200
Water	1450-1530	Made ground (rubble etc.)	160-600
Soil	100-500	Landfill refuse	400-750
Sand (loose)	200-2000	Concrete	3000-3500
Sand (dry, loose)	200-1000	Disturbed soil	180-335
Sand (water saturated, loose)	1500-2000	Clay landfill cap	355-380
Sand & Gravel (near surface)	400-2300	(compacted)	
Sand & Gravel (at 2 km depth)	3000-3500	Weathered surface material	305-610
Clay	1000-2500	Limestone (hard)	2800-7000
Estuarine mud/clay	300-1800	Gypsum	2000-3500
Sandstone	1400-4500	Shale	2000-4100
Limestone (soft)	1700-4200		

2.3.4.2 Seismic refraction measurements

The seismic refraction investigating method utilizes seismic energy, which returns to the surface after traveling through the ground along refracted ray paths. This method is normally used to locate refracting interfaces (refractors) separating layers of different seismic velocity, but the method is also applicable in cases where velocity varies smoothly as a function of depth or laterally (Kearey, 1984).

Normally, the seismic survey is illustrated in the case of a flat interface that is between two horizontal layers (Figure 2.16). For this research, the seismic investigation is interested in the term of direct and refraction waves. Progressive position of the wave fronts associated with the direct and refracted ray path (Figure 2.17).

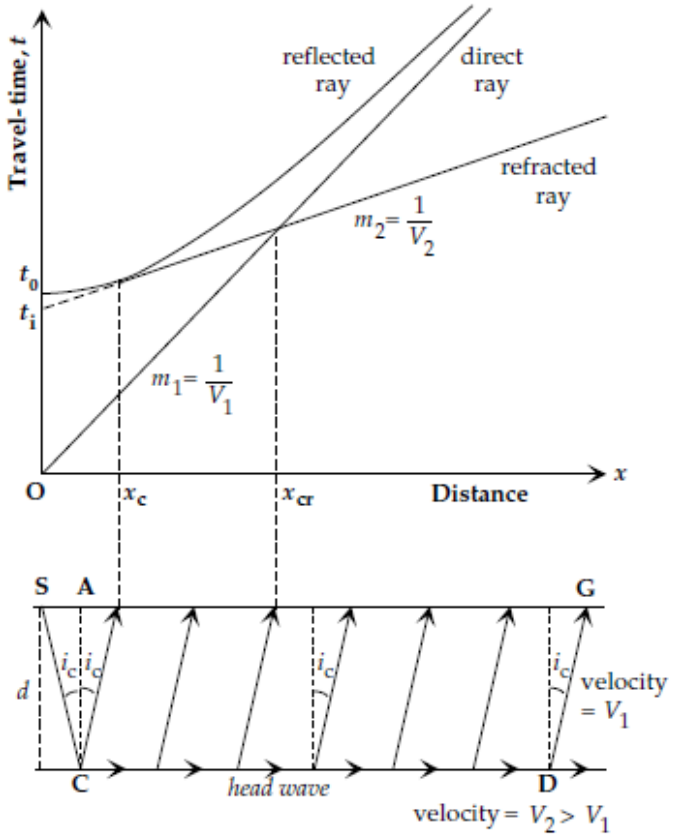

Figure 2.16 Travel-time versus distance curve for the direct, reflection and refraction waves at a horizontal interface between two layers with seismic velocities V_1 and V_2 ($V_2 > V_1$).

(Lowrie, 2007)

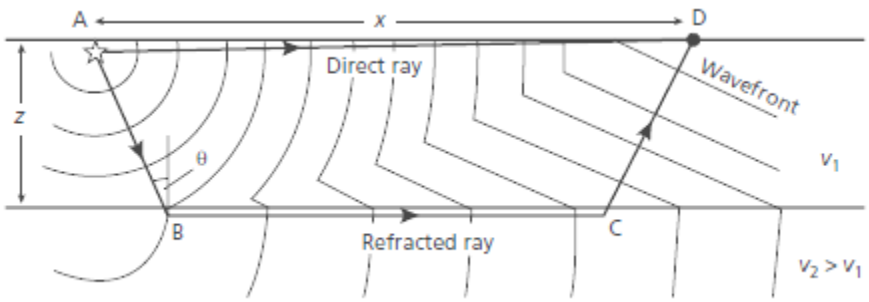

Figure 2.17 Position of wavefronts associated with the direct and refracted waves.

(Kearey, 1984)

From figure 2.17, the direct wave travels through the top of the upper layer from A to D with velocity V_1 which A is seismic source and D is the detector. The refracting interface is at depth z. The refracted ray travels down to the interface and back up to the surface at velocity V_1 along slant paths AB and CD that are inclined at the critical angle θ, and travels along the interface between B and C at the higher velocity V_2. The total travel time along the refracted wave through position of ABCD is given by

$$t = t_{AB} + t_{BC} + t_{CD}$$

$$= \frac{z}{V_1 \cos\theta} + \frac{x - 2z\tan\theta}{V_2} + \frac{z}{V_1 \cos\theta} \qquad (2.32)$$

From Snell's law, it shown that $\sin\theta = V_1 / V_2$ and $\cos\theta = (1 - V_1^2 / V_2^2)^{1/2}$. So, the travel time equation may be represented in different forms, a useful general form being

$$t = \frac{x\sin\theta}{V_1} + \frac{2z\cos\theta}{V_1} \qquad (2.33)$$

Alternatively

$$t = \frac{x}{V_2} + \frac{2z\left(V_2^2 - V_1^2\right)^{1/2}}{V_1 V_2} \qquad (2.34)$$

Or

$$t = \frac{x}{V_2} + t_i \tag{2.35}$$

That t_i is the intercept time on axis of a travel-time curve or time-distance curve that has a gradient of $1/V_2$. t_i is given as below

$$t_i = \frac{2z\left(V_2^2 - V_1^2\right)^{1/2}}{V_1 V_2} \tag{2.36}$$

So, refractor depth is expressed by

$$z = \frac{t_i V_1 V_2}{2\left(V_2^2 - V_1^2\right)^{1/2}} \tag{2.37}$$

The seismic refraction data is plotted between time (t) and distance (x) that are known as travel time curve or time – distance curve (see in Figure 2.18). The refraction data appearance on t-x graph with straight line by its slope is equal to $1/V$.

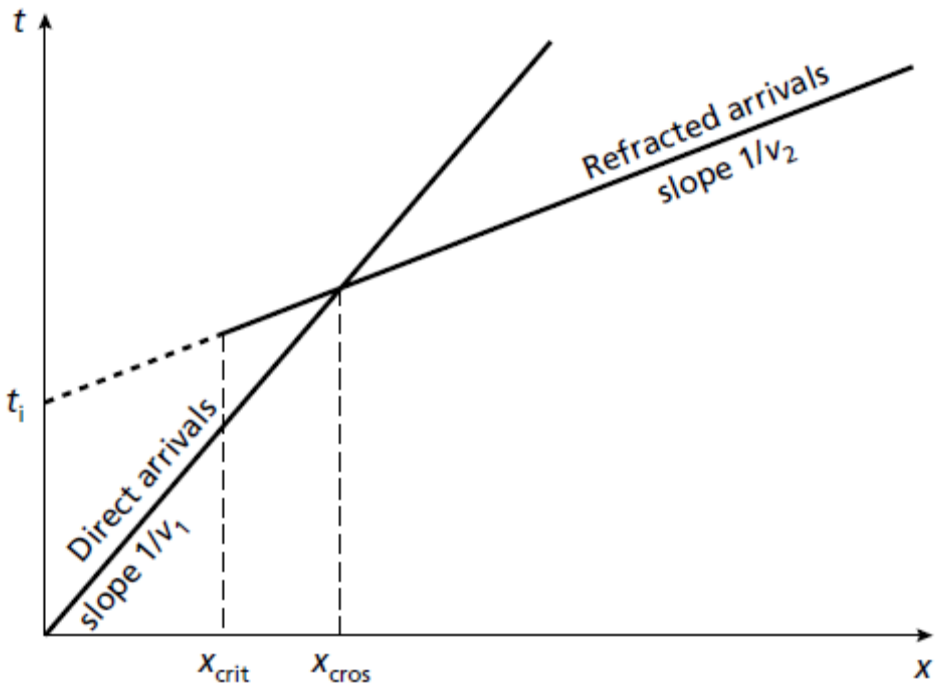

Figure 2.18 Travel-time curves for the direct wave and refracted wave.

(Kearey, 1984)

The crossover distance X_{cr} is the distance where the direct waves and refracted waves arrive at the same time as shown in the t-x graph (Figure 2.18). The crossover distance can be calculated as below

$$X_{cr} = 2z\left[\frac{V_2 + V_1}{V_2 - V_1}\right]^{1/2} \tag{2.38}$$

For the case of the horizontal multilayer with a flat interface, the travel time t_n of a ray critically refracted along the top surface of the nth layer is given as below

$$t_n = \frac{x \sin\theta}{V_1} + \sum_{i=1}^{n-1} \frac{2z_i \cos\theta_i}{V_i} \tag{2.39}$$

Where $\theta_i = \sin^{-1}\left(V_i / V_n\right)$

In the case of a dipping refractor (Figure 2.19 (a)), the forward and reverse travel time graphs for refracted waves is shown as Figure 2.19 (b).

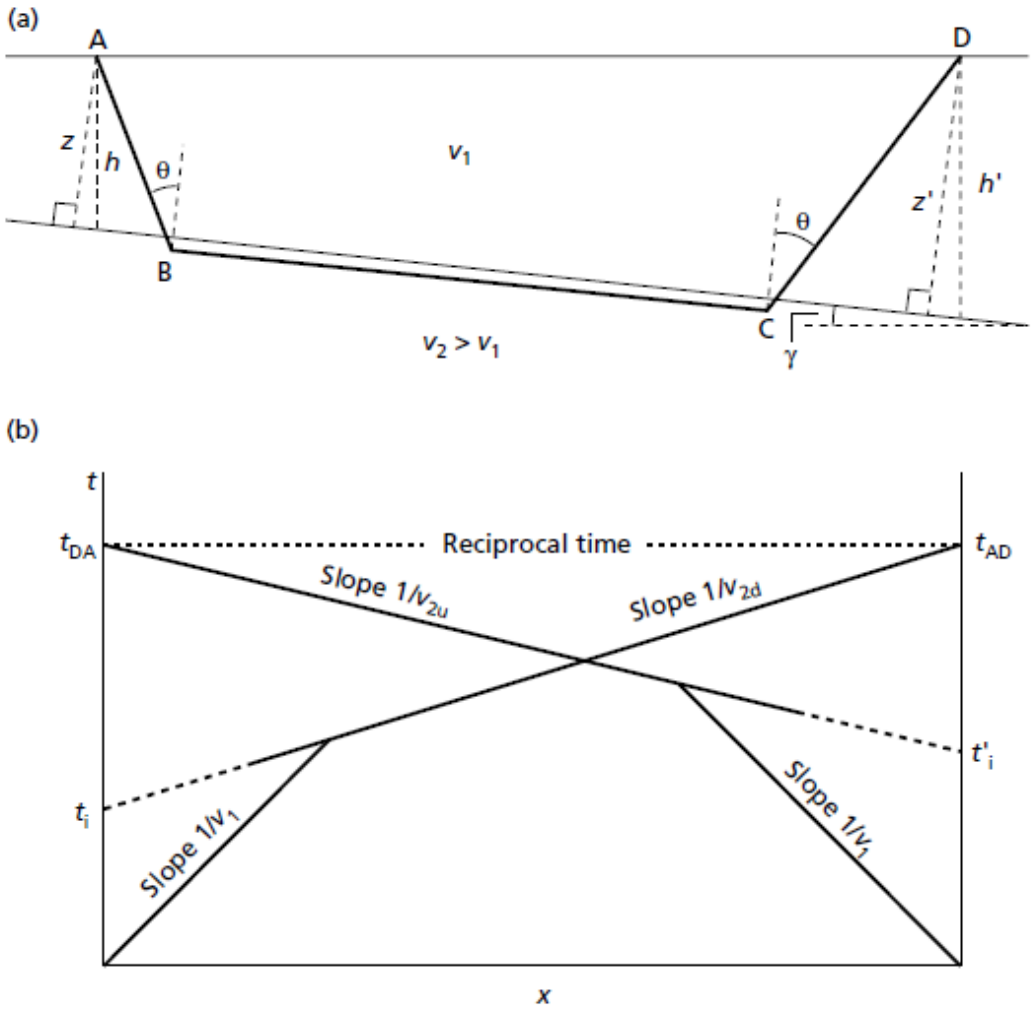

Figure 2.19 (a) Ray path geometry for dipping refractor and (b) Travel-time of refraction profile from dipping refractor in the forward and reverse directions.

(Kearey, 1984)

The travel time t_n of a ray critically refraction in the nth dipping refractor is shown as below

$$t_n = \frac{x \sin \beta_1}{V_1} + \sum_{i=1}^{n-1} \frac{h_i (\cos \alpha_i + \cos \beta_1)}{V_i} \tag{2.40}$$

By h_i is the vertical thickness of the ith layer beneath the shot.

V_i is the velocity of the ray in the ith layer.

α_i is the angle with respect to the vertical made by the downgoing ray in the ith layer which $\alpha_i = \theta_i - \gamma_i$.

β_i is the angle with respect to the vertical made by the upgoing ray in the ith layer which $\beta_i = \theta_i + \gamma_i$.

x is offset distance between source and detector.

Solving for θ and γ as below

$$\theta = \frac{1}{2}\left[\sin^{-1}\left(V_1 / V_{2d}\right) + \sin^{-1}\left(V_1 / V_{2u}\right)\right] \tag{2.41}$$

$$\gamma = \frac{1}{2}\left[\sin^{-1}\left(V_1 / V_{2d}\right) - \sin^{-1}\left(V_1 / V_{2u}\right)\right] \tag{2.42}$$

The perpendiculars distance z and z' to the interface under the two ends of profile are obtained from the intercept times t_i and t_i' of the travel times graph in the forward and reverse direction. The perpendicular distances are given by

$$z = \frac{V_1 t_i}{2 \cos \theta} \tag{2.43}$$

Similarly

$$z' = \frac{V_1 t_i'}{2 \cos \theta} \tag{2.44}$$

From equation (2.43) and (2.44) can be converted into vertical depth h and h' by using equation as below

$$h = \frac{z}{\cos \gamma} \tag{2.45}$$

And

$$h' = \frac{z'}{\cos \gamma} \tag{2.46}$$

In the case of irregular refractor, the plus-minus method will be used for refraction interpretation. The intercept time (t_i) can be considered to be composed of two delay time, which is shot point delay time and geophone delay time, as they are associated with the portion of the path down from the shot and up to the geophone.

2.3.4.3 Data processing

SIP software by a registered trademark of Rimrock Geophysics Inc has been used for data processing of seismic refraction data. An initial model was created based on the time-distance graph. The program calculated the velocity of each layer. The depth of each layer beneath each geophone was determined. These depths were then interpolated between adjacent geophone positions. The program assumed that each layer encountered was horizontally continuous and that there were no lateral changes in velocity within any layer (Kutrubes et al., 2002).

After the raw data had been collected and saved in digital format, they were transferred to a personal computer for processing using the SIP program. For more details of background theory that is related to this program sees Scott (1973). The general processing and interpretation procedure are as follows:

(1) Determine the first arrival time (picking the first break) of the seismic wave at each geophone for every geophone spread. This step is the most important one and will determine the reliability of the resulting model.

(2) Create the data files for the interpretation program by using the first arrival data together with the elevation of each source points and geophones. The T-X graph can be created. The program is limited to handle a maximum of 5 layers and 5 inline spreads with up to 7 shot points and 48 geophones per spread.

(3) Interpret the data using iterative ray-tracing techniques as an inversion program for modeling. The delay-time method (Parkiser and Black, 1957) is used to obtain a first-approximation depth model, which is tested for validity by a ray-tracing procedure. The program will simulate ray propagation through the model and adjust the model itself by using field-measured refraction arrival time.

The velocity of the top layer is computed by dividing the distance from each shot point to each geophone by the corresponding arrival times. These individual velocities are averaged for each shot point, and a weighted average is computed. The refraction velocities of all layers beneath the top layer are computed by two methods as below:

1) Regression, in which a straight line is fit by least squares to the arrival times, representing the velocity of the layer and average velocities are computed by taking the reciprocals of the weighted average of the slopes of the regression lines.

2) The Hobson-Overton method (Hobson – Overtone, 1968: in Scott, 1973), by which velocities can be computed if there are reciprocal arrivals from two opposing source points at two or more geophones. Final velocities used in the inversion process are computed by taking an average of the two methods. The inversion procedure normally requires only two iterations (Scott, 1973).

Analyzing the subsurface along profile, which composes many spreads of data coverage, every spreads are processed as a model. The image of the subsurface along the total profile is conducted by joining the adjacent models together.

CHAPTER 3

RESULTS AND DISCUSSION

3.1 Geophysical Results

All geophysical lines of the both study areas are in the area that is in the line of hydrogeological cross section, which it explained by Arun (2009). So, all geophysical results should be related to cross section explained by Arun (2009).

3.1.1. Resistivity imaging subsurface characterization

For study area at an active landfill of Hat Yai municipality (Kuan Lang area), the six profiles for investigation were shown in Figure 3.1. Measurement of G4, G5, and G6 profile is divided into three parts (Part A, B, and C) as shown in Figure 2.14. Part A and B are mixed for inversion together. After that inverted result of part A, B will be interpreted along with part C.

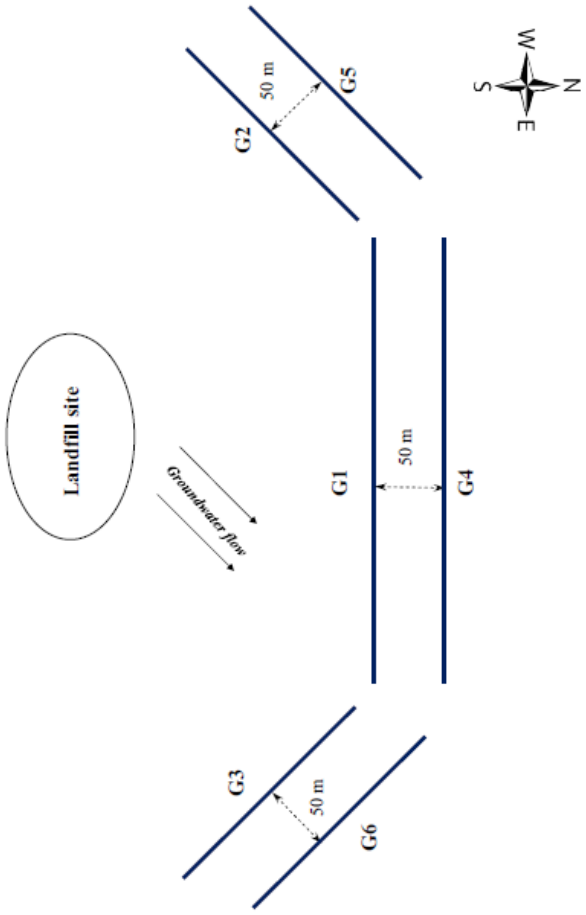

Figure 3.1 Study area at landfill site, Kuan Lang subdistrict

(a)

(b)

Figure 3.2 Example of study area; a) G1 profile of northern active landfill, b) Ban Na Wat Pho school site.

Figure 3.3 Preparing Cu-$CuSO_4$ electrodes for IP& resistivity and SP surveys

3.1.1.1 Resistivity pseudosection result

Site 1: the active landfill site

The inversion resistivity model sections of the six investigation profiles are presented in figure 3.2 to show the apparent resistivity variation along all the profiles. The display will partly help to understand the overall apparent resistivity variation in the area. All six model sections are shown that resistivity will decrease with the depth.

The inversion resistivity model of G1 profile is shown in Figure 3.4(a). The subsurface structure can be divided into two layers, a top soil layer (from surface down to green color) and a high conductivity layer (blue color). Top soil layer is presented by green color, which it has a resistivity of about 100 ohm-m with approximate 10 meters thickness. This layer, it may be represented by dry mud or sandy clay. The second layer is presented by blue color, which it has a resistivity of about 10-40 ohm-m; it may be unconsolidated wet clay and/or saturated some contents of clay layer.

The inversion resistivity model of G2 profile is shown in Figure 3.4(b). The subsurface structure can be divided into two layers, a top soil layer (from surface down to green color) and a

high conductivity layer (blue color). Top soil layer is presented by green color, which it has a resistivity of about 100 ohm-m with approximate 15 meters thickness; it may be dry mud or sandy clay. The second layer is presented by blue color, which it has a resistivity of about 15-20 ohm-m; it may be unconsolidated wet clay and/or saturated some contents of clay layer.

The inversion resistivity model of G3 profile is shown in Figure 3.4(c). The subsurface structure can be divided into two layers, a top soil layer (from surface down to green color) and a high conductivity layer (blue color). Top soil layer is presented by green color, which it has a resistivity of about 100 ohm-m with approximate 5-10 meters thickness; it may be dry mud or sandy clay. The second layer is presented by blue color, which it has a resistivity of about 1.6-20 ohm-m; it may be unconsolidated wet clay and/or saturated some contents of clay layer.

The inversion resistivity model of G4 profile is shown in Figure 3.4(d) and Figure 3.4 (e). The subsurface structure can be divided into two layers, a top soil layer (from surface down to green color) and a high conductivity layer (blue color). Top soil layer is presented by green color, which it has a resistivity of about 100 ohm-m with approximate 10 meters thickness; it may be dry mud or sandy clay. The second layer is presented by blue color, which it has a resistivity of about 15-40 ohm-m; it may be unconsolidated wet clay and/or saturated some contents of clay layer. Moreover, there are flooding zone, which be from distance 0 to 220 meters in Figure 3.2 (d). In addition, green color is seen at bottom in direction west of profile. It may mean clay layer in the bottom has more interconnected pore containing water.

The inversion resistivity model of G5 profile is shown in Figure 3.4(f) and Figure 3.4 (g). The subsurface structure can be divided into two layers, a top soil layer (from surface down to green color) and a high conductivity layer (blue color). Top soil layer is presented by green color, which it has a resistivity of about 100 ohm-m with approximate 15-18 meters thickness; it may be dry mud or sandy clay. The second layer is presented by blue color, which it has a resistivity of about 4-20 ohm-m; it may be unconsolidated wet clay and/or saturated some contents of clay layer.

The inversion resistivity model of G6 profile is shown in Figure 3.4(h) and Figure 3.4 (i). The subsurface structure can be divided into three layers, a top layer (from surface down to yellow color), a resistivity layer (green color) and a high conductivity layer (blue color). Top soil layer is presented by yellow color, which it has a resistivity of about 600-1600 ohm-m with

approximate 1-2 meters thickness; it may be top soil and/or sand layer. The second layer is presented by green color, which it has a resistivity of about 100 ohm-m with 12 meters thickness; it may be dry mud or sandy clay. The last layer is presented by blue color, which it has a resistivity of about 1.5-10 ohm-m; it may be unconsolidated wet clay and/or saturated some contents of clay layer. There are flooding zone in direction SE as Figure 3.4(i).

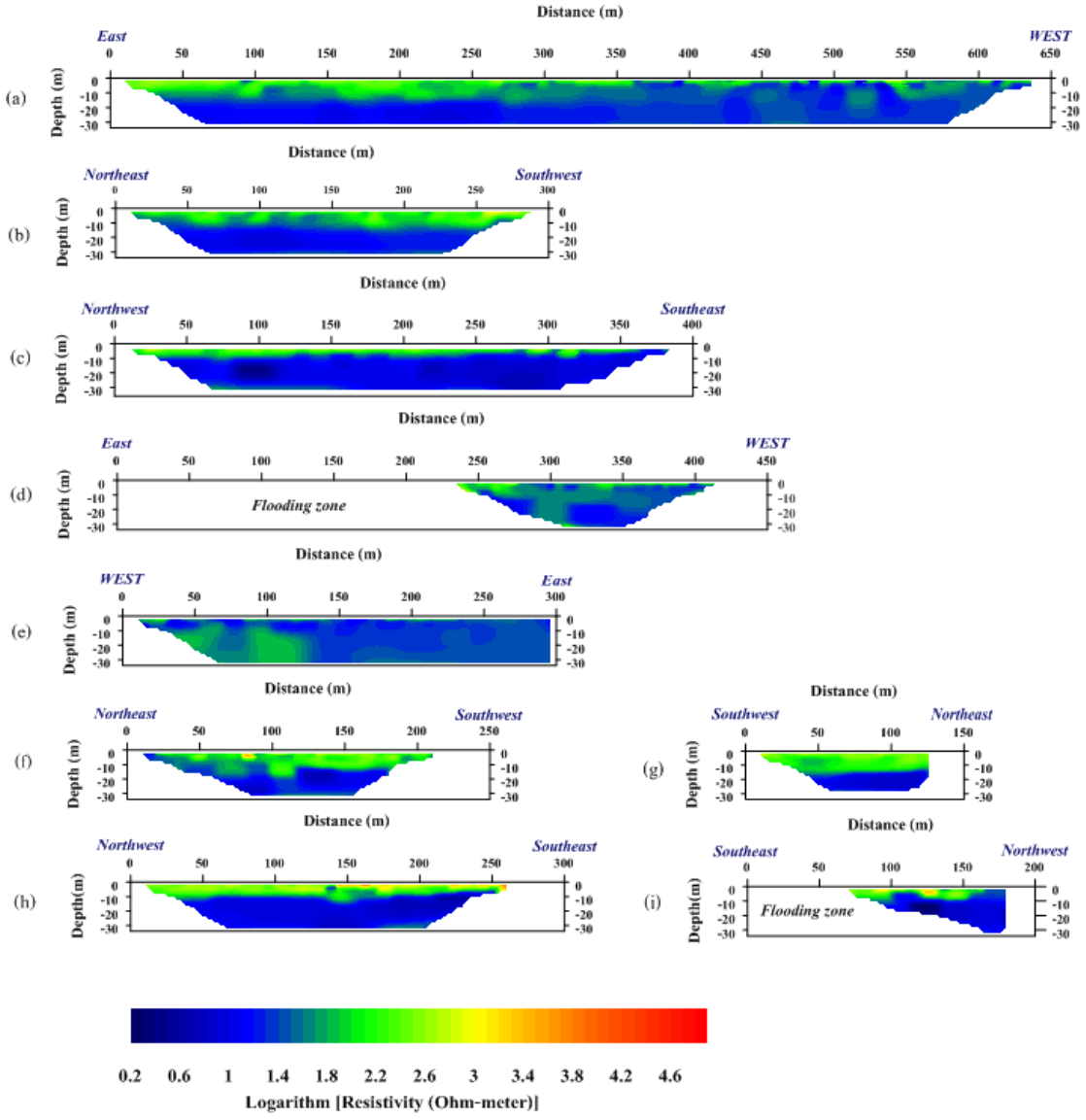

Figure 3.4 Inversion resistivity model section; a) G1 profile, b) G2 profile, c) G3 profile, d) G4(AB) profile, e) G4(C) profile, f) G5 (AB) profile, g) G5(C) profile, h) G6(AB) profile, and i) G6 (C) profile.

Site 2: Ban Na Wat Pho School

The inversion resistivity model section of investigation profiles is presented in figure 3.5 to show the apparent resistivity variation along all the profiles. The display will partly help to understand the overall apparent resistivity variation in the area. The subsurface structure is characterized by resistivity variation. The mostly subsurface structure is presented by green color, which it has a resistivity of about 100 ohm-m; it may be represented by dry mud or sandy clay. And this layer is permeated by blue color, which it has resistivity of about 4-25 ohm-m; it may be groundwater and it makes clay layer to become unconsolidated wet clay.

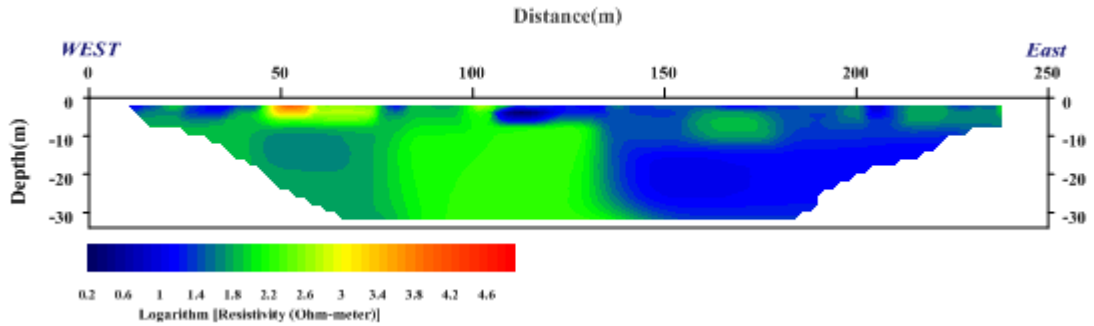

Figure 3.5 Inversion resistivity model section of KH01 profile.

3.1.1.2 VES result

Site 1: the active landfill site

The resistivity data interpretation resulted at borehole H0853SKL373 (Figure 3.6). The two upper layers have resistivity of about 80 – 200 Ohm-m with a thickness of 0.8-9.0 meters; they may be dry mud or sandy clay. The third layer has a resistivity of 4 ohm-m with 10 meters thickness; it may be unconsolidated wet clay and/or saturated some contents of clay layer because this layer will have more interconnected pore containing water, which will result in low resistivity values following Archie's law (Equation 2.2). The last layer has resistivity of 80 ohm-m, which has resistivity equal to resistivity of second layer, and it is likely to be dry mud or sandy clay. After comparison with borehole H0853SKL373 (Table 3.1), it is shown that the resistivity data interpretation resulted is according to geological information.

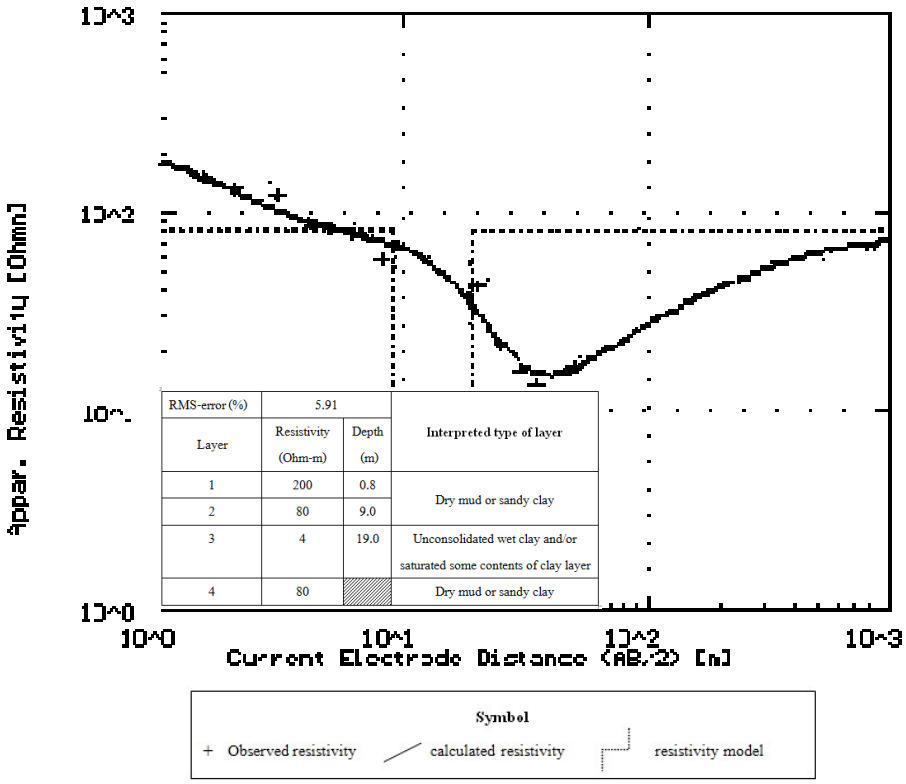

Figure 3.6 The sounding curve of measurement point borehole H0853SKL373

Table 3.1 Geological information of borehole H0853SKL372.

Depth (m) from-to	Type of layer	Description
0-5	Clay	Reddish brown and pinkish brown, gray mottied, silty, calcareous, compacted
5-12	Clay	Yellowish brown, gray mottied, silty, calcareous, compacted
12-18	Sand&Clay	Yellowish brown, calcareous, coarse sand, subangular, consists of 60% sand, 40% clay, plastic,compacted
18-33	Clay	Yellowish brown, gray mottied, silty, calcareous, composed of sand prsented at the upper parts, plastic, compacted
33-36	Sand&Clay	Yellowish brown, calcareous, coarse sand, subangular, consists of 60% sand, 40% clay, plastic,compacted
36-59	Clay	Yellowish brown, calcareous, plastic, compacted
59-60	Sand	Yellowish brown, clayey, coarse grainted, subangular, moderately sorted, slighly compacted
60-80	Clay	Yellowish brown, calcareous, plastic, compacted
80-86	Sand	Yellowish brown, coarse grained, subangular, well sorted
86-90	Gravel	Various colors, very fine grained, subangular, well sorted, composed of quartz, limestone, chert
90-105	Limestone	Light gray, limonitic, brittle, slightly weathered, moderately hard, highly weathered at the upper part.

For landfill site, the resistivity data interpretation resulted at each of the six measurement points in this site. The measurement point of G2 to G6 is in the middle of G2 to G6 profile respectively. G1 measurement point is located at 450 meters of G1 profile. Detail of resistivity interpretation resulted is shown as following;

The resistivity data interpretation resulted at G1 measurement point (Figure 3.7a), there are three layers. The upper layer has a resistivity of about 200 ohm-m with 0.96 meters thickness; it may be top soil layer. The second layer has a resistivity of 400 ohm-m with 0.9 meters thickness; it may be loose sand and/or clayey sand layer. The last layer has a resistivity of 24 ohm-m which may be unconsolidated wet clay and/or saturated some contents of clay layer.

The resistivity data interpretation resulted at G2 measurement point (Figure 3.7b), there are five layers. The upper layer has a resistivity of about 700 ohm-m with 1.36 meters thick; it may loose sand layer. The second layer has a resistivity of 80 ohm-m with 1.6 meters thick; it

may be dry mud or sandy clay. The third layer has a resistivity of 120 ohm-m with 10 meters thickness; it may be sandy clay layer. The fourth layer has a resistivity of 4 ohm-m with 10 meters thickness; it may be unconsolidated wet clay and/or saturated some contents of clay layer. The last layer has a resistivity of 80 ohm-m which may be dry mud or sandy clay layer.

The resistivity data interpretation resulted at G3 measurement point (Figure 3.8a), there are five layers. The upper layer has a resistivity of about 400 ohm-m with 0.9 meters thick; it is top soil. The second layer has a resistivity of 180 ohm-m with 1.08 meters thickness; it may be sandy clay layer. The third layer has a resistivity of 800 ohm-m with 2.43 meters thick; it may be loose sand layer. The fourth layer has a resistivity of 10 ohm-m with 60 meters thick; it may be unconsolidated wet clay and/or saturated some contents of clay layer. The last layer has a resistivity of 400 ohm-m which may be clayey sand layer.

The resistivity data interpretation resulted at G4 measurement point (Figure 3.8b), there are four layers. The upper layer has a resistivity of about 300 ohm-m with 0.79 meters thickness; it is top soil. The second layer has a resistivity of 140 ohm-m with 3.26 meters thick; it may be dry mud or sandy clay layer. The third layer has a resistivity of 32 ohm-m with 21 meters thickness; it may be wet clay. The last layer has a resistivity of 25 ohm-m which may be unconsolidated wet clay and/or saturated some contents of clay layer.

The resistivity data interpretation resulted at G5 measurement point (Figure 3.9a), there are four layers. The upper layer has a resistivity of about 700 ohm-m with 0.45 meters thickness; it is top soil and/or loose sand layer. The second layer has a resistivity of 2080 ohm-m with 0.91 meters thickness; it may be sand layer. The third layer has a resistivity of 260 ohm-m with 5.12 meters thickness; it may be sandy clay layer. The fourth layer has a resistivity of 64 ohm-m with 11.4 meters thickness; it may be clay layer. The last layer has a resistivity of 25 ohm-m which may be unconsolidated wet clay and/or saturated some contents of clay layer.

The resistivity data interpretation resulted at G6 measurement point (Figure 3.9b), there are four layers. The upper layer has a resistivity of about 1500 ohm-m with 1.25 meters thickness; it is sand layer. The second layer has a resistivity of 850 ohm-m with 4.53 meters thickness; it may be loose sand layer. The third layer has a resistivity of 8.5 ohm-m with 57 meters thickness; it may be unconsolidated wet clay layer and/or saturated some contents of clay layer. The last layer has a resistivity of 400 ohm-m which may be clayey sand layer.

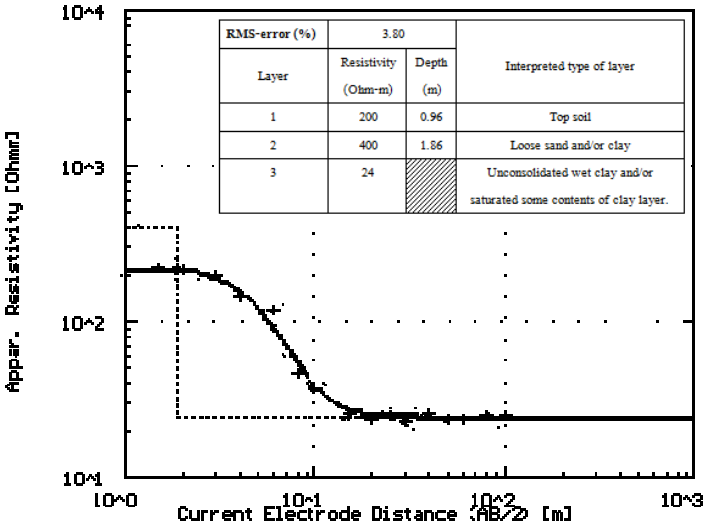

(a)

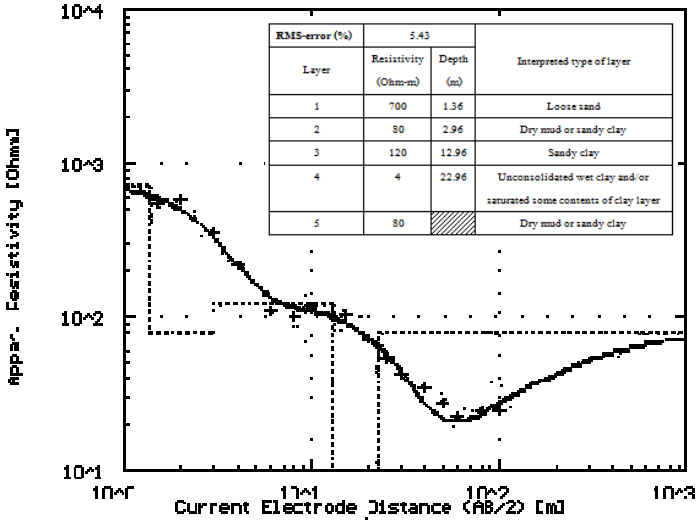

(b)

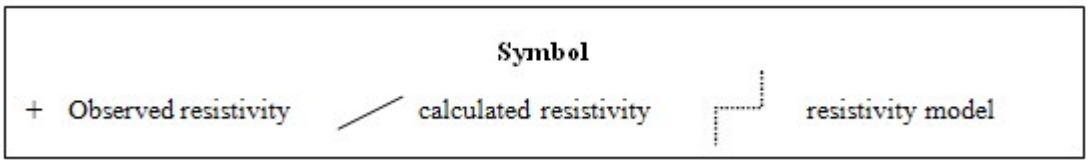

*Figure 3.*7 The sounding curve of measurement point; a) G1 point, b) G2 point

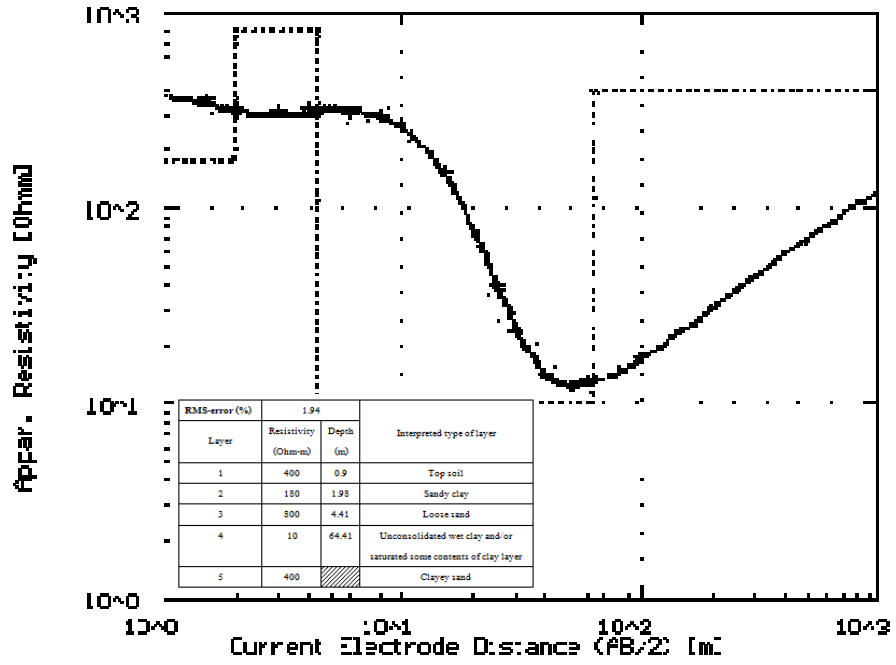

(a)

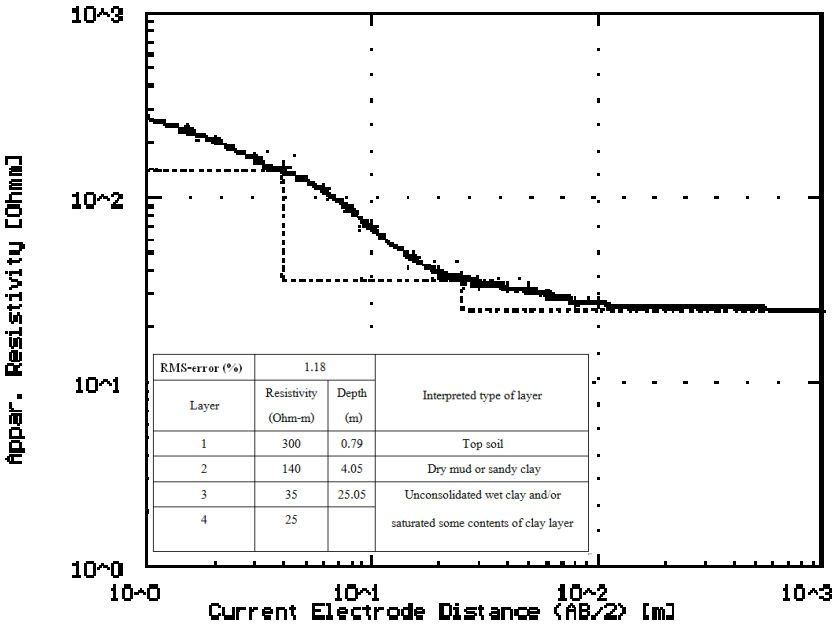

(b)

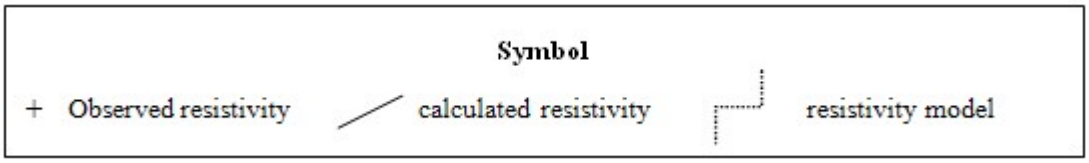

*Figure 3.*8 The sounding curve of measurement point; a) G3 point, b) G4 point

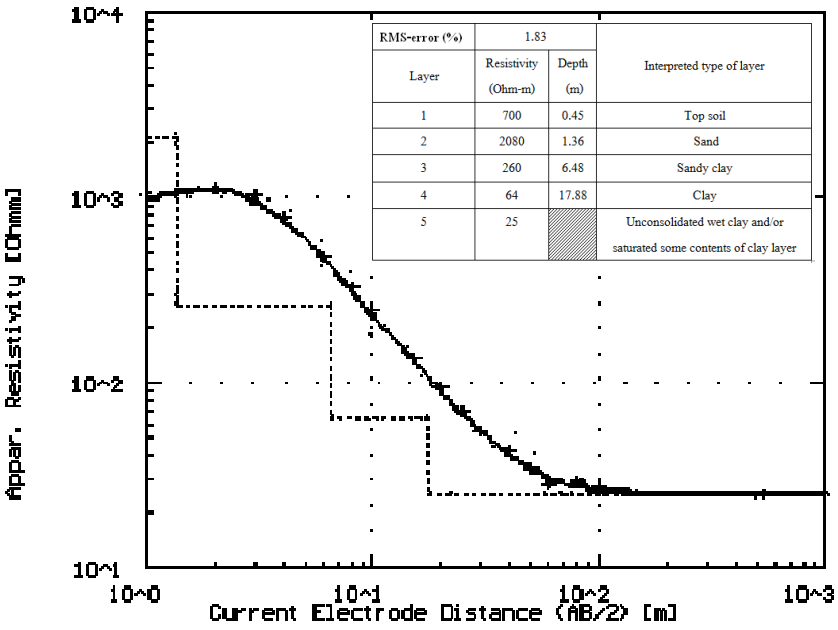

(a)

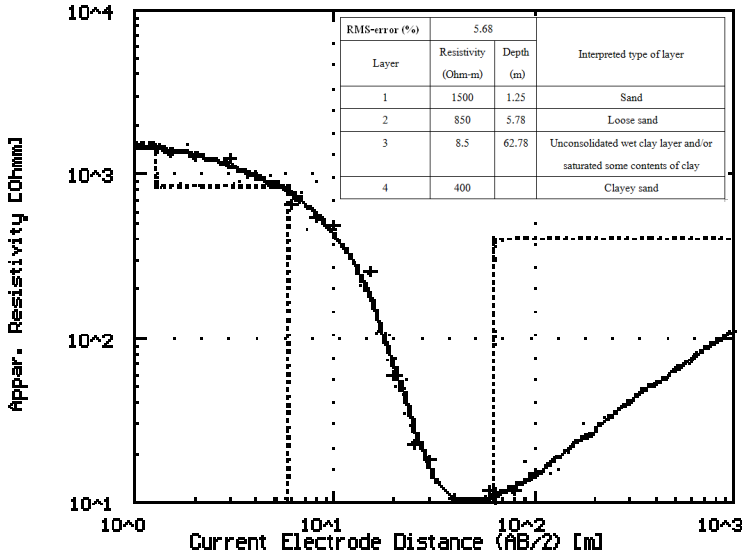

(b)

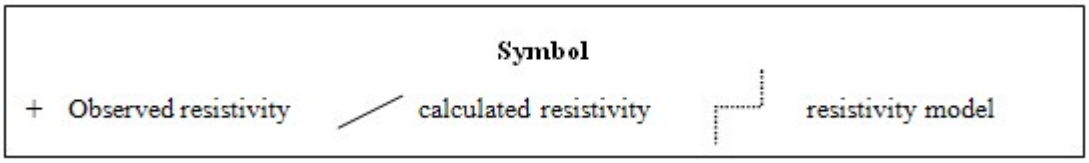

*Figure 3.*9 The sounding curve of measurement point; a) G5 point, and b) G6 point.

Site 2: Ban Na Wat Pho School

The interpretation resulted of resistivity data is shown in Figure 3.10. The measurement point is in the middle of KH01 profile. The resistivity data interpretation resulted at KH01 measurement point, there are three layers. The upper layer has a resistivity of about 100 ohm-m with 2.05 meters thickness; it may be dry mud or sandy clay. The second layer has a resistivity of 18 ohm-m with 64 meters thickness; it may be unconsolidated wet clay layer and/or saturated some contents of clay layer. The last layer has a resistivity of 0.2 ohm-m which may be much unconsolidated wet clay and/or saturated some contents of clay layer, which may have more interconnected pore containing water that will result in low resistivity values following Archie's law (Equation 2.2).

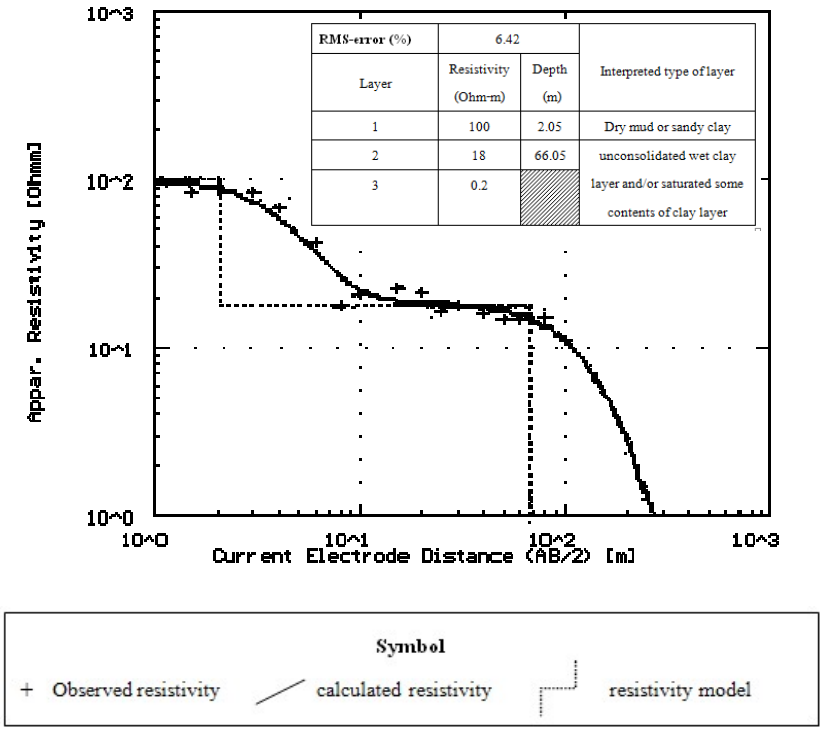

*Figure 3.*10 The sounding curve of measurement point KH01

3.1.2. IP imaging subsurface characterization

Site 1: the active landfill site

The inversion IP model sections of the six investigation profiles are presented in figure 3.7 to show the apparent IP variation along all the profiles. The display will partly help to understand the overall apparent resistivity variation in the area. IP models of G1 and G2 profiles are shown in Figure 3.11 (a) and Figure 3.11 (b). Subsurface structure of G1 and G2 profiles is presented by blue color, which it has chargeability of less than 100 msec; it may be clay layer. G3 profile can be divided into two zones (Figure 3.11(c)), low chargeability (blue color), and high chargeability (green-yellow color at the bottom). The first zone is presented by blue color, which it has chargeability of less than 100 msec; it may be clay layer. Second zone is presented by green-yellow color, which it is the bottom of profile and it has chargeability of 350-500 msec. G4 profile (Figure 3.11(d) and Figure3.11 (e)) is presented by blue color, which it has chargeability of less than 100 msec; it may be clay layer. G5 profile can be divided into two zones (Figure 3.11(f) and Figure 3.11(g)), low chargeability (blue color), and high chargeability (green-red color at the bottom). The first zone is presented by blue color, which it has chargeability of less than 100 msec; it may be clay layer. Second zone is presented by green-red color, which it is the bottom of throughout profile and it has chargeability of more than 350 msec. G6 profile can be divided into two zones (Figure 3.11(h) and Figure 3.11 (i)), low chargeability (blue color), and high chargeability (green-red color at the bottom). The first zone is presented by blue color, which it has chargeability of less than 100 msec; it may be clay layer. Second zone is presented by green-red color, which it is the bottom of profile and it has chargeability of more than 300 msec. The high chargeability area, which it appears in chargebility pseudosection, has a few of datum point. So, high chargeability should be bad datum or error value that it's not real value in the nature.

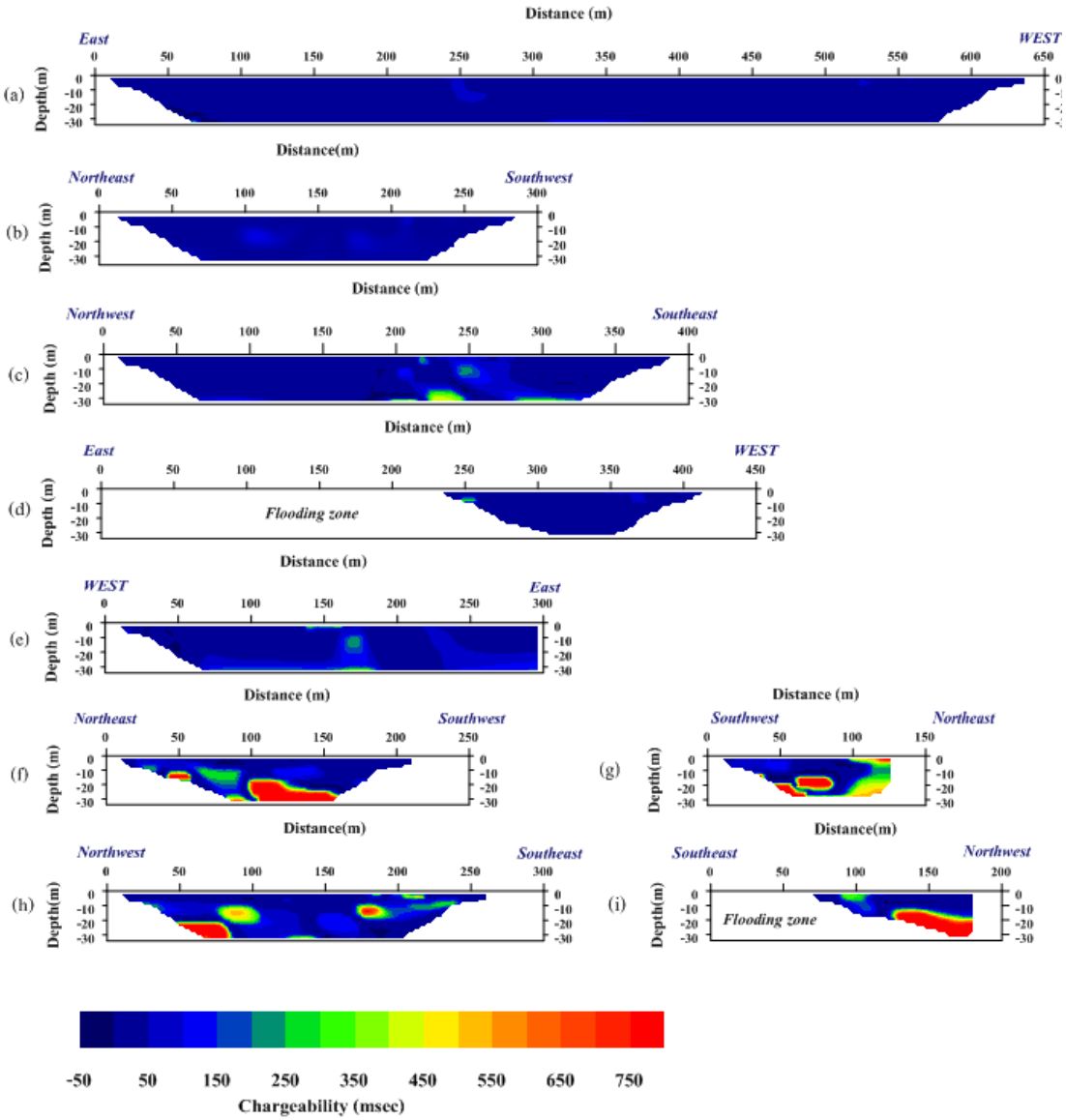

*Figure 3.*11 Inversion IP model section; a) G1 profile, b) G2 profile, c) G3 profile, d) G4(AB) profile, e) G4(C) profile, f) G5 (AB) profile, g) G5(C) profile, h) G6(AB) profile, and i) G6 (C) profile.

Site 2: Ban Na Wat Pho School

The inversion IP model sections of the six investigation profiles are presented in figure 3.12 to show the apparent IP variation along all the profiles. The display will partly help to understand the overall apparent resistivity variation in the area. IP model of KH01 profile is shown in Figure 3.12. KH01 profile is presented by blue color, which it has chargeability of less than 100 msec; it may be clay layer.

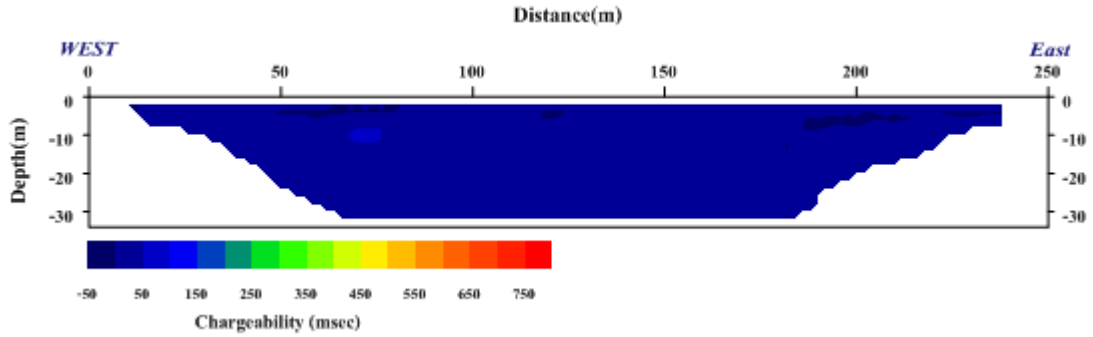

*Figure 3.*12 Inversion IP model section of KH01 profile.

3.1.3. Seismic refraction

Site 1: the active landfill site

The result of the seismic refraction investigation along G1 profile is shown as model section in Figure 3.13. Two layers in the subsurface are indicated. The first layer is layer, which it has a thickness that ranges between 2.0 and 5.0 meters. The P-waves velocities vary between 305 and 1375 meters per second as shown in Figure 3.13(a), with an average of about 640 m/s as shown in Figure 3.13 (b). This range of velocities may represent the velocity of soil or weathered surface material (see table 2.5). The first layer is underlain by a layer, which a P-wave velocity ranges from 1,809 to 1,993 m/s (computation by regression method), and range from 1,829 to 2,018 m/s (computation by Hobson-Overton method), with an average of about 1,946 m/s, which may be velocity of clay layer (see table 2.5).

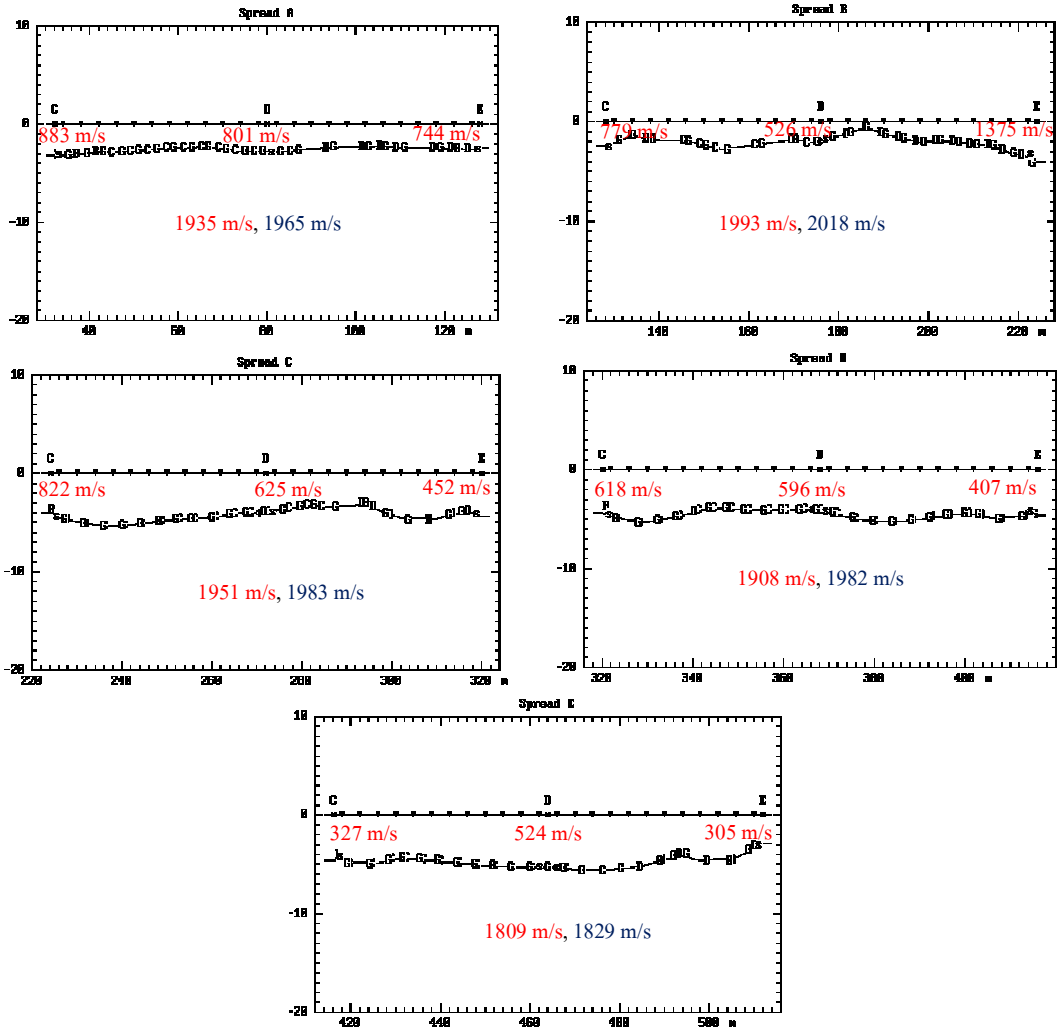

(a)

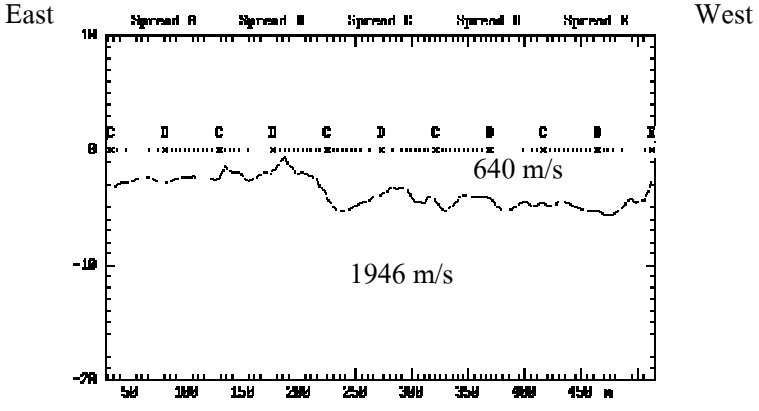

(b)

*Figure 3.*13 Subsurface structure from refraction interpretation of G1 profile; Velocity computation in layer 2 by regression and the Hobson-Overton method is represented by red and blue number, respectively. And Weighted average of velocity is represented by black number.

The result of the seismic refraction investigation along G2 profile is shown as model section in Figure 3.14. Two layers in the subsurface are indicated. The first layer is layer, which it has a thickness that ranges between 2.0 and 4.0 meters and the P-waves velocities vary between 327 and 583 meters per second as shown in Figure 3.14(a), with an average of about 468 m/s as shown in Figure 3.14 (b). This range of velocities may represent the velocity of soil or weathered surface material (see table 2.5). The first layer is underlain by a layer, which a P-wave velocity ranges from 1,750 to 2,009 m/s (computation by regression method), and range from 1,770 to 2,017 m/s (computation by Hobson-Overton method), with an average of about 1,895 m/s, which may be velocity of clay layer (see table 2.5).

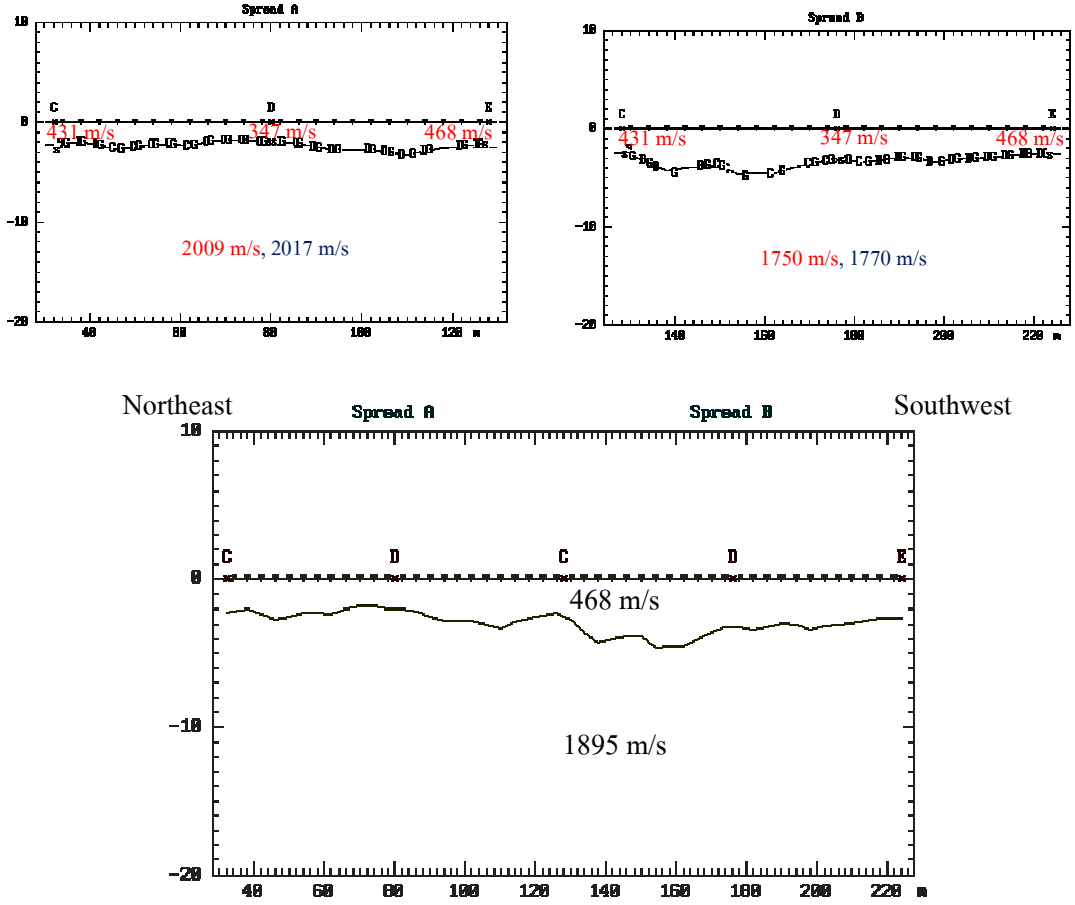

Figure 3.14 Subsurface structure from refraction interpretation of G2 profile; Velocity computation in layer 2 by regression and the Hobson-Overton method is represented by red and blue number, respectively. And Weighted average of velocity is represented by black number.

The result of the seismic refraction investigation along G3 profile is shown as model section in Figure 3.15. Two layers in the subsurface are indicated. The first layer is layer, which it has a thickness that ranges between 4.0 and 7.0 meters and the P-waves velocities vary between 365 and 1,417 meters per second as shown in Figure 3.15(a), with an average of about 895 m/s as shown in Figure 3.15 (b). This range of velocities may represent the velocity of sand. The first layer is underlain by a layer, which a P-wave velocity ranges from 1,761 to 1,947 m/s (computation by regression method), and range from 1,813 to 1,945 m/s (computation by Hobson-Overton method), with an average of about 1,873 m/s, which may be velocity of clay layer.

The seismic refraction result along G4 profile is shown as model section in Figure 3.16. Two layers in the subsurface are indicated. The first layer is layer, which it has a thickness that ranges between 2.0 and 6.0 meters and the P-waves velocities vary between 331 and 952 meters per second as shown in Figure 3.16(a), with an average of about 619 m/s as shown in Figure 3.16 (b). This range of velocities may represent the velocity of weathered surface material. Second layer is a layer, which a P-wave velocity ranges from 1,882 to 1,943 m/s (computation by regression method), and range from 1,889 to 1,891 m/s (computation by Hobson-Overton method), with an average of about 1,895 m/s, which may be velocity of clay layer.

The result of the seismic refraction investigation along G5 profile is shown as model section in Figure 3.17. Two layers in the subsurface are indicated. The first layer is layer, which it has a thickness that ranges between 2.0 and 5.0 meters and the P-waves velocities vary between 383 and 983 meters per second as shown in Figure 3.17(a), with an average of about 767 m/s as shown in Figure 3.17 (b). This range of velocities may represent the velocity of sand. Second layer is a layer, which a P-wave velocity ranges from 1,763 to 1,863 m/s (computation by regression method), and range from 1,764 to 1,847 m/s (computation by Hobson-Overton method), with an average of about 1,805 m/s, which may be velocity of clay layer.

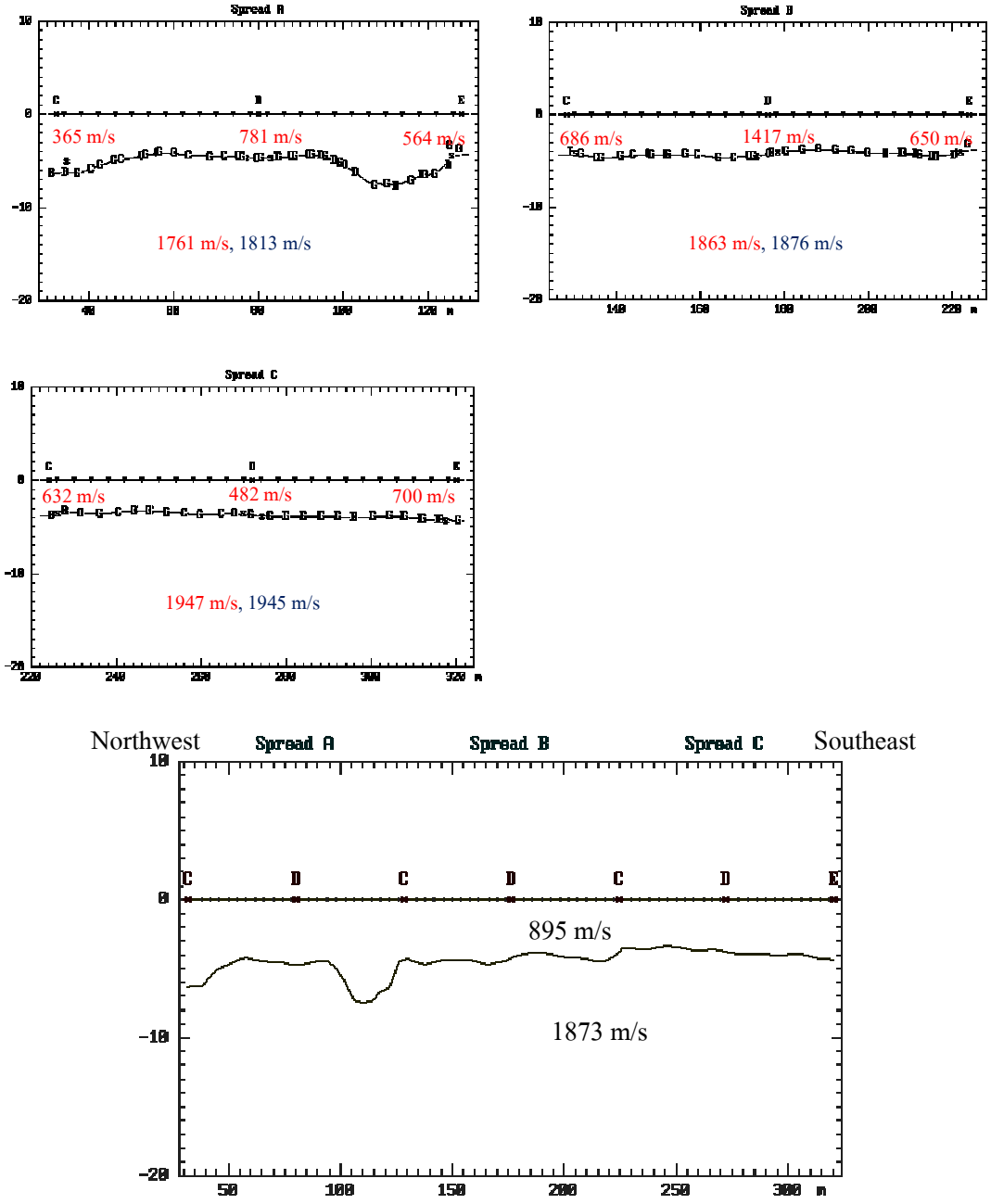

Figure 3.15 Subsurface structure from refraction interpretation of G3 profile; Velocity computation in layer 2 by regression and the Hobson-Overton method is represented by red and blue number, respectively. And Weighted average of velocity is represented by black number.

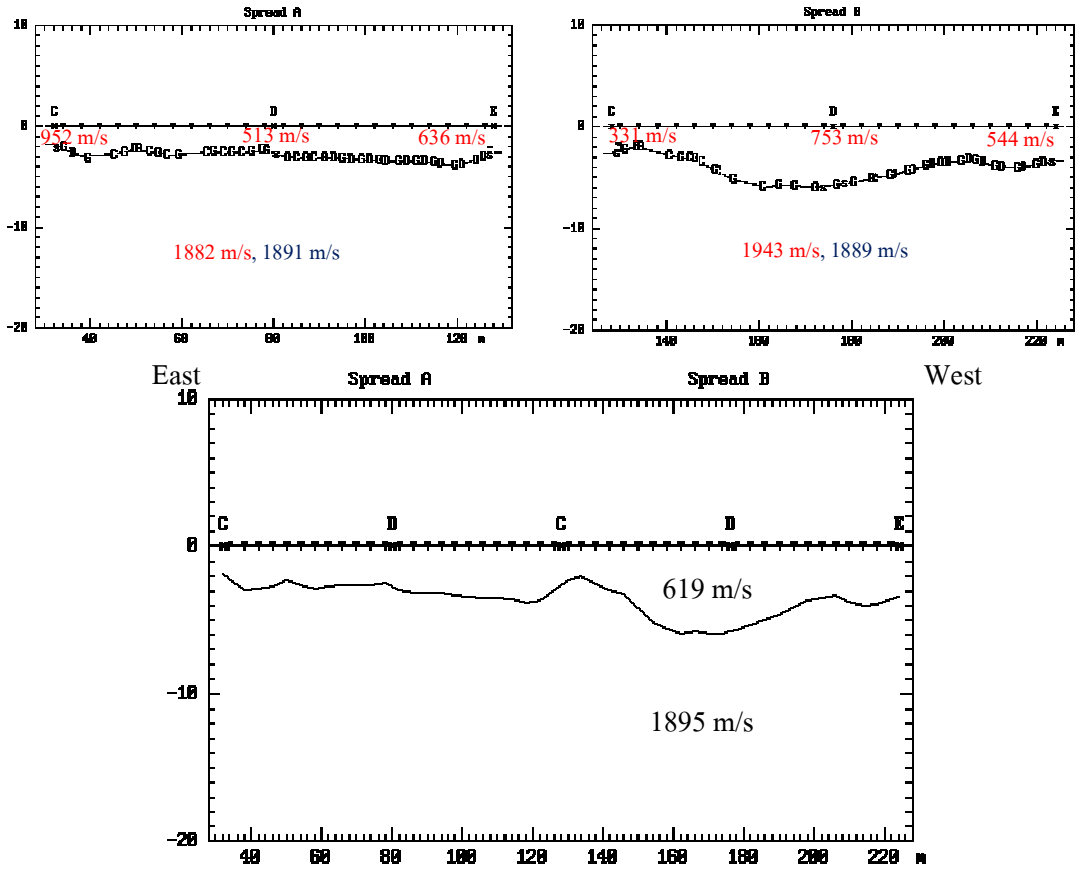

Figure 3.16 Subsurface structure from refraction interpretation of G4 profile; Velocity computation in layer 2 by regression and the Hobson-Overton method is represented by red and blue number, respectively. And Weighted average of velocity is represented by black number.

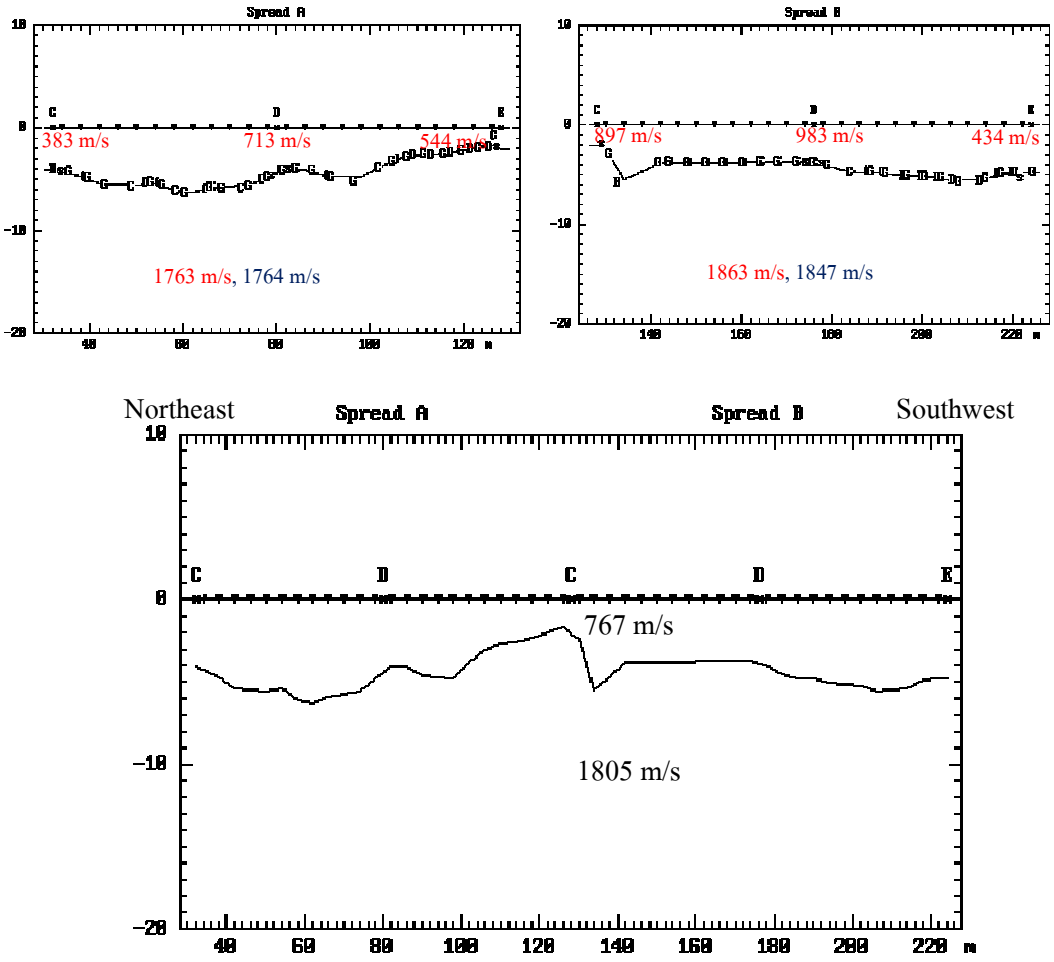

Figure 3.17 Subsurface structure from refraction interpretation of G5 profile; Velocity computation in layer 2 by regression and the Hobson-Overton method is represented by red and blue number, respectively. And Weighted average of velocity is represented by black number.

The result of the seismic refraction investigation along G6 profile is shown as model section in Figure 3.18. Two layers in the subsurface are indicated. The first layer is layer, which it has a thickness that ranges between 4.0 and 6.0 meters and the P-waves velocities vary between 467 and 1,343 meters per second as shown in Figure 3.18(a), with an average of about 890 m/s as shown in Figure 3.18 (b). This range of velocities may represent the velocity of sand. The first layer is underlain by a layer, which a P-wave velocity ranges from 1,764 to 1,962 m/s (computation by regression method), and range from 1,791 to 1,985 m/s (computation by Hobson-Overton method), with an average of about 1,898 m/s, which may be velocity of clay layer.

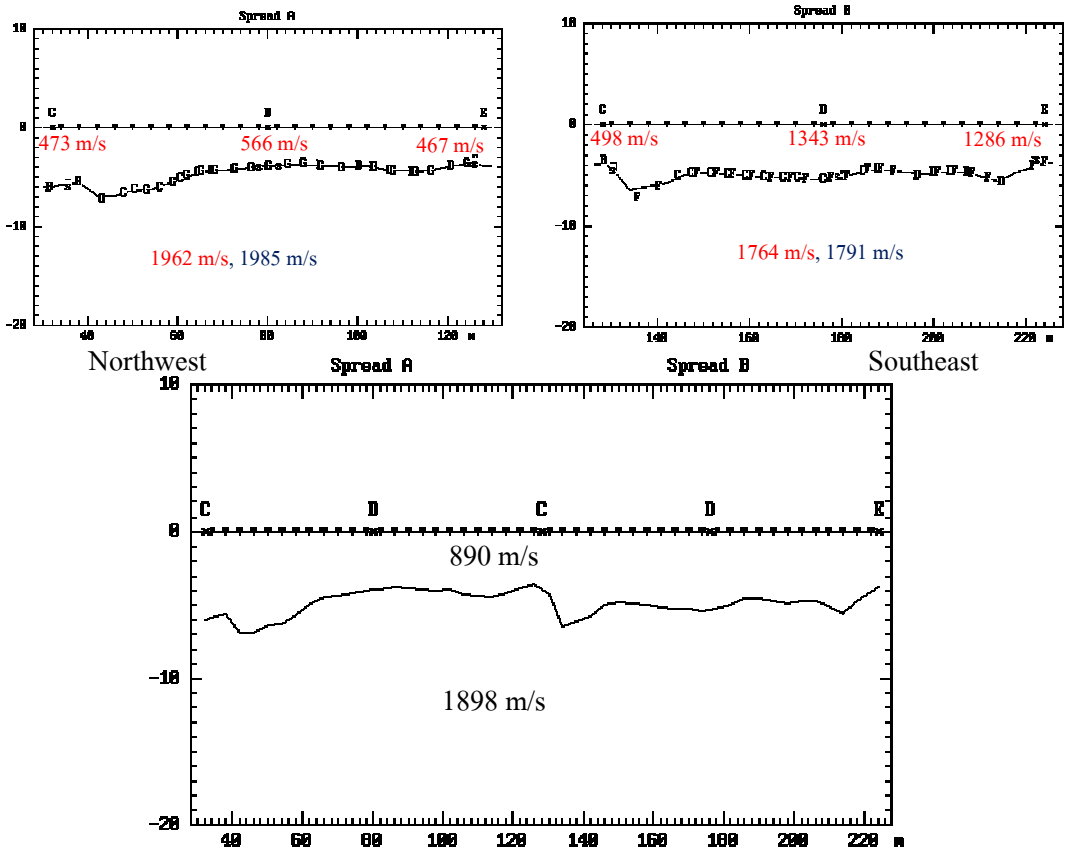

Figure 3.18 Subsurface structure from refraction interpretation of G6 profile; Velocity computation in layer 2 by regression and the Hobson-Overton method is represented by red and blue number, respectively. And Weighted average of velocity is represented by black number.

Site 2: Ban Na Wat Pho School

The seismic refraction investigation result along KH01 profile is shown as model section in Figure 3.19. Two layers in the subsurface are indicated. The first layer is layer, which it has a thickness that ranges between 4.0 and 6.0 meters and the P-waves velocities vary between 462 and 754 meters per second as shown in Figure 3.19(a), with an average of about 596 m/s as shown in Figure 3.19 (b). This range of velocities may represent the velocity of soil or weathered surface material. The first layer is underlain by a layer, which a P-wave velocity ranges from 1,951 to 1,962 m/s (computation by regression method), and range from 1,956 to 1,976 m/s (computation by Hobson-Overton method), with an average of about 1,963 m/s, which may be velocity of clay layer.

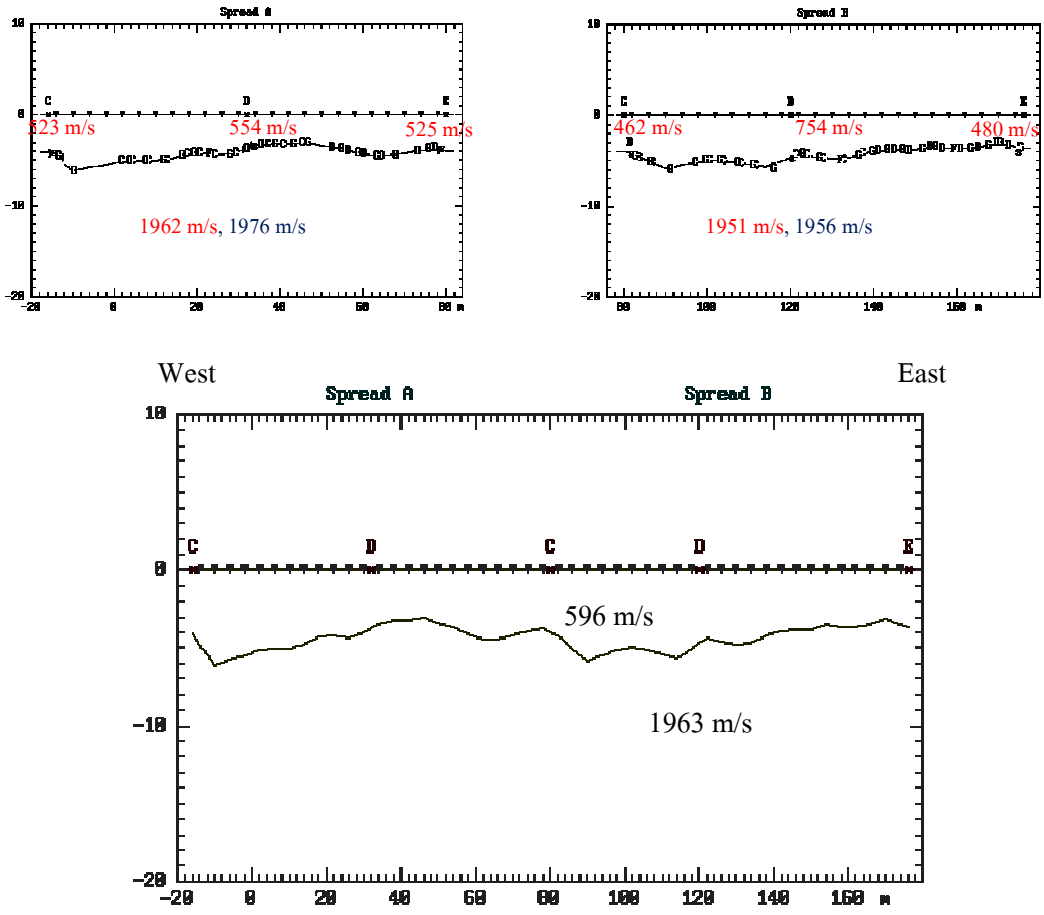

Figure 3.19 Subsurface structure from refraction interpretation of KH01 profile; Velocity computation in layer 2 by regression and the Hobson-Overton method is represented by red and blue number, respectively. And Weighted average of velocity is represented by black number.

3.1.4. SP interpretation

Site 1: the active landfill site

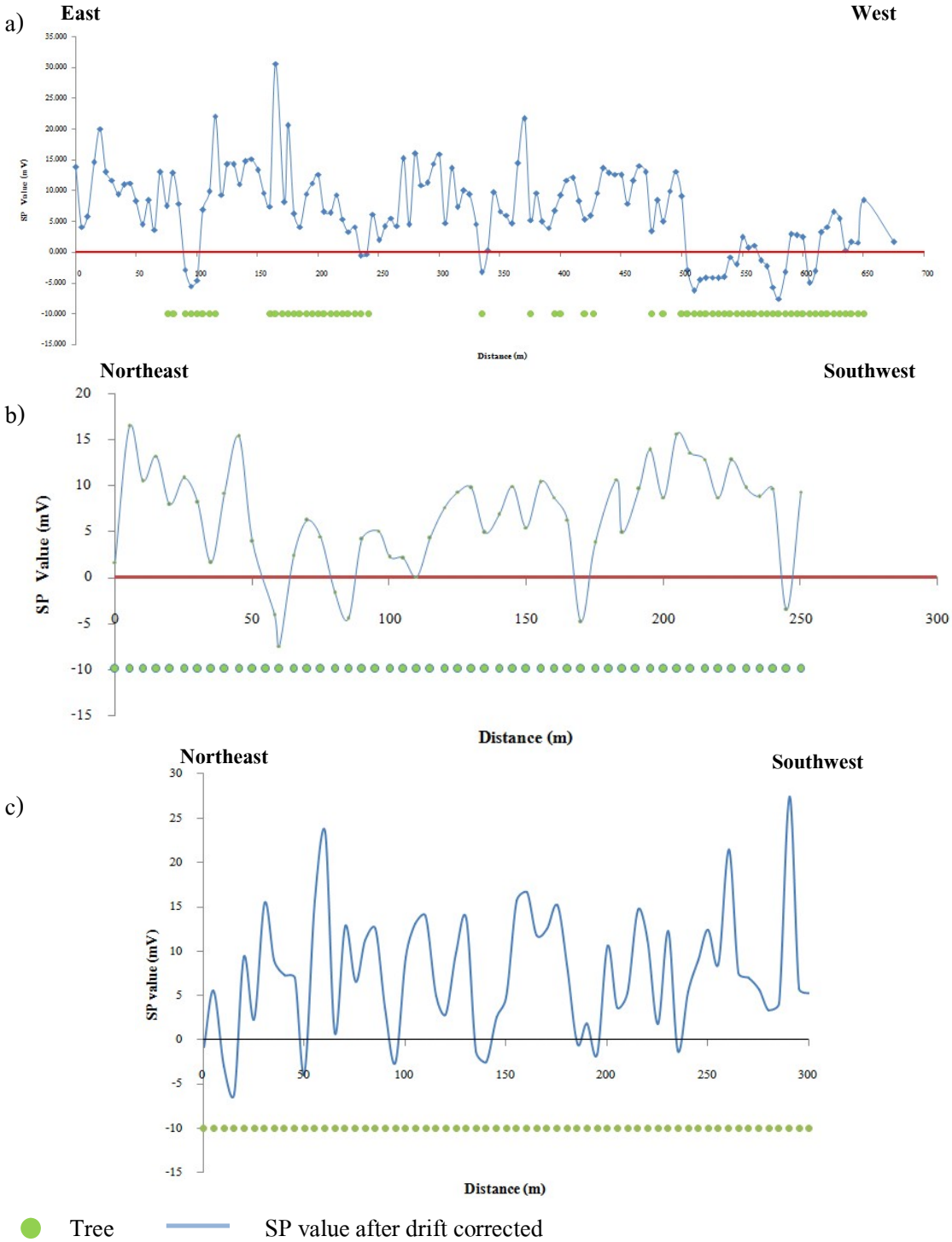

Figure 3.20 SP value after drift corrected of measurement profile; (a) G1 profile, (b) G2 profile , and (c) G5 profile.

SP value after drift corrected of measurement profile is shown in Figure 3.20. All the SP data indicate different zones with positive and negative SP value. The negative SP values are possible the result of root activity of rubber tree and the result of the water flowing from surrounding area. The mostly investigation profile is perpendicular with direction of groundwater flowing. All investigation profile is located in rubber plantation, which it means SP measurement will always indicate different zones with positive and negative SP value. And negative SP is always the result of root activity of rubber tree. For this site, the result of SP value cannot explain subsurface structure because the biological root activity, which is one source of SP, is presence.

Positive SP is normally associated with clay layer or low resistive layer (Wattanasen, 2007), in flow of groundwater from surrounding area. Negative SP is basically related to conductive minerals deposits such as pyrite, pyrhotite, magnetite etc., biological root activity (Wattanasen, 2007), high resistive medium.

In this site, there are some others sources of SP that created the fuctuation of SP values shown in Figure 3.20. Thus, the SP results here have no significant for any interpretation.

Site 2: Ban Na Wat Pho School

SP value after drift corrected of measurement profile is shown in Figure 3.21. All the SP data indicate different zones with positive and negative SP value. The negative SP values are the result of root activity of tree and electricity post. The investigation profile is almost perpendicular with direction of groundwater flowing. For this site, the result of SP value cannot explain subsurface structure because the biological root activity, which is one source of SP, is presence.

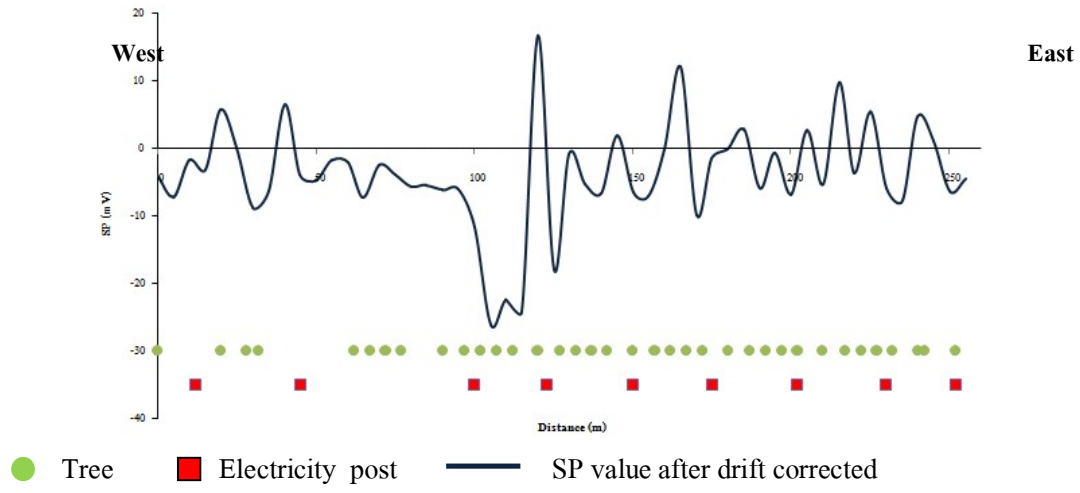

Figure 3.21 SP value after drift corrected of measurement KH01 profile

3.2 Integrated interpretation of geophysical results

The ambiguity in the interpretation of geophysical data can be reduced by combining data from several methods since there is often a correlation between the physical properties reflected by each method. In this research, an integrated interpretation is possible along all profiles.

Site 1: the active landfill site

Combining of IP and resistivity investigation is shown that there is a zone, which is possibly contaminated by leakage from landfill. The zones of high chargeability (more than 300 msec) may be contaminated by leachate were found in the bottom of G3, G5, and G6 profiles. The zone of uncontaminated area has a chargeability of less than 100 msec, which may be interpreted as sandy clay layer.

Combining of VES and resistivity pseudo section is shown that their interpretation result accord together. Subsurface structure of resistivity variation is divided into two main layers. First layer has resistivity of about 100 ohm-m with an average thickness of about 10 meters, which it may be dry mud or sandy clay. Second layer has resistivity of about less than 40 ohm-m, which it may be unconsolidated wet clay and/or saturated some contents of clay layer. Moreover, it accord with hydrogeological section (Figure 2.4). Thus, the second layer is probably an aquifer, which it may be Hat Yai aquifer with reference to a hydrogeological section (Figure 2.4). The first layer is probably clay layer. From result of VES, it shown that unconsolidated wet clay and/or saturated some contents of clay layer may be underlain by clay or clayey sand layer.

Combining of resistivity and seismic refraction investigation is shown subsurface structure of resistivity according to subsuface structure of seismic refraction investigation. All six investigation profiles can indicate subsurface structure to be divided into two layers. First layer is a layer, which it has P-wave velocities that ranges between 468 and 895 m/s with an average of 3.0-5.0 meters thickness, and it has resistivity of about 300 ohm-m; it may be soil or weathered surface material. The first layer is underlain by the second layer, which it has P-wave velocities that ranges between 1,805 and 1946 m/s and it has the resistivity of about 100 ohm-m. This layer may be dry mud or sandy clay.

Site 2: Ban Na Wat Pho School

Combining of IP and resistivity investigation is shown that there is a zone of low chargeability (less than 100 msec) which it may be represented by clay layer.

Combining of VES and resistivity pseudosection is shown that their model results are good agreement. Subsurface structure of resistivity variation is divided into two main zones. First zone is mostly area that has resistivity of about 100 ohm-m, which it may be sandy clay layer. Second zone has resistivity of about less than 40 ohm-m, which it may be unconsolidated wet clay and/or saturated some contents of clay layer. The first zone is permeated by second zone, which it may probably be groundwater. Moreover, it accord to hydrogeological section (Figure 2.4). Thus, the subsurface structure is presented by resistivity of about 100 ohm-m, which it is probably sandy clay layer.

Combining of resistivity and seismic refraction investigation is shown that the model of subsurface structure are in good agreement. The subsurface structure can be divided into two layers. First layer is a layer, which has P-wave velocities of about 596 m/s with an average of 5.0 meters thickness, and it has resistivity of about 300 ohm-m. This layer may be soil or weathered surface material. The first layer is underlain by a second layer, which it has P-wave velocities of about 1,963 m/s, and it has resistivity of about 100 ohm-m. This layer may be dry mud or sandy clay.

3.3 Discussion

For active landfill site, the subsurface structure can be divided in two layers, top soil (P-wave velocities of about 600 m/s, and resistivity of about 300 ohm-m), and sandy clay layer (P-wave velocities of about 1900 m/s , and resistivity of about 100 ohm-m). Moreover, aquifer is seen by resistivity investigation. The aquifer has an average of 10 meters thickness. And the aquifer may probably be Hat Yai aquifer with reference to a hydrogeological section. In addition, high IP zones (chargeability > 300 msec) appeared in the bottom of G3, G5, and G6 profiles. These profiles located in the north of the landfill, whereas the direction of groundwater flow in the area is in SE to NE direction. It is thus possible for the high IP zones at G3 and G6 that may be the contaminated areas that caused by the wastes leaked from landfill and have been transported by groundwater through the channel of discontinuous clay layer. For high IP zone at

G5 profile the cause of this result is difficult to explain. However, to confirm these possible contaminated areas, water and soil samples around surrounding area of landfill (between the G3, G5, and G6 profiles and landfill) have to be taken for chemical analyzing for further understanding the distribution of the chemical composition in the groundwater correlated to an occurrence of contamination are recommended.

For Ban Na Wat Pho School, the subsurface structure can be divided in two layers, top soil (P-wave velocities of about 596 m/s, and resistivity of about 300 ohm-m), and sandy clay layer (P-wave velocities of about 1963 m/s, and resistivity of about 100 ohm-m). This P-wave velocities value of this layer, it seem to be sandy clay layer saturated with some of water content. The subsurface model showed that this site is covered by thick clay layer. However, the result from resistivity pseudo-section showed that there is a lateral resistivity variation in the subsurface clay layer. This indicate that the clay layer might not be homogeneous, there should have difference in composition of subsurface layer. Therefore only the GIS method cannot provide more information of the subsurface geological barrier for selecting landfill site.

CHAPTER 4

CONCLUSIONS AND RECOMMENDATION

This work shows an application of geophysical methods in characterizing the subsurface structures of an active solid waste disposal landfill of HatYai municipality, Kuanlang sub-district, HatYai district and a high potential area for selected solid waste disposal sites at Ban Na Wat Pho School, Klong Hoi Khong sub-district, Klong Hoi Khong district, Songkhla province. The study results in the first area, Kuanlang active landfill site found that the model of subsurface geological structure consists of top soil layer (weathered surface material or soil) underlain by a layer of about 100 ohm-m, low IP, and P-wave velocity about 1,900 m/s, interpreted as dry mud or sandy clay with a thickness of about 10 meters. The third layer of low resistivity (< 40 ohm-m) is possibly wet clay or saturated some contents of clay found at a depth of >10 meters. The high IP zones (chargeability > 300 msec) may be the contaminated areas that caused by the wastes leaked from landfill and have been transported by groundwater through the channel of discontinuous clay layer were found. The results from the second area, Ban Na Wat Pho School site, the geophysics data showed mainly 2 layers of top soil layer and a underlain thick layer (> 20 m) of low IP, P-wave velocity about 1,960 m/s, and low resistivity of 4 -100 ohm-m interpreted as dry mud, sandy clay, wet clay and/or some contents of clay layer. The resistivity pseudo-section here showed lateral resistivity variation indicated the difference in materials or environmental conditions.

With according to the standard criteria for the subsurface geological structure of landfill site, the subsurface geological barrier (e.g. clay layer) can be obtained by 2D – IP & resistivity imaging and seismic refraction data. In addition, the contaminated area in the ground can probably be provided by high IP (high chargeability) and low resistivity data. IP and resistivity measurement is thus suitability geophysical methods for detection and evaluation contamination. For SP measurement in this study, SP data showed no significant to correlate with subsurface structure, contaminated areas or direction of groundwater flow in the area due to a complex effect of sources related to SP such as biological root activity of rubber tree, soil moisture content etc. SP measurement may be providing a good result in the area without the trees. The subsurface

geological structure in Kuanlang landfill site is mostly agree well to the standard criteria of subsurface structure for selecting landfill site. However there is a point to be concerned that the geophysical results showed possible contaminated areas. To clarify this result, water and soil samples around surrounding area of landfill (between the G3, G5, and G6 profiles and landfill) should be taken for chemical analyzing for further understanding the distribution of the chemical composition in the groundwater correlated to an occurrence of contamination are recommended. For Ban Na Wat Pho School site, The subsurface geological structure in Kuanlang landfill site showed that there is a thick clay layer, which is mostly agree well to the standard criteria of subsurface structure for selecting landfill site. However, the result from resistivity pseudo-section showed that there is a lateral resistivity variation in the subsurface clay layer. This indicates that the clay layer might not be homogeneous, there should have difference in composition of subsurface layer. Therefore, only the GIS method cannot provide more information of the subsurface geological barrier for selecting landfill site.

This study also showed that geophysical methods can be an importance tools for characterizing the subsurface geological structure of selected landfill site after roughly selected by e.g. GIS method, which it cannot be possible to give a detail image of subsurface geological structure.

BIBLIOGRAPHY

Aristodemou,E. & Thomas-Betts,A., 2000. DC resistivity and induced polarization investigations at a waste disposal site and its environments, *Journal of Applied Geophysics*, 44,275-302.

Arora, T., et al., 2007. Non-intrusive characterization of the redox potential of landfill leachate plumes from self- potential data, *Journal of Applied Geophysics*, 92, 274-292.

Arun Lookjan, 2009. Study of seawater intrusion into aquifer in Hat Yai basin using a mathematical model. Master's thesis, Faculty of Engineering, Prince of Songkla University.

Class,A., et al., 2008. Assessing aquifer vulnerability to pollutants by electrical resistivity tomography (ERT) at a nitrate vulnerable zone in NE Spain, Journal *of Environmental Geology*, 54, 515-520.

Chalermyanont, T., et al., 2008. *Aquifer Characteristic and Quality of Groundwater in the vicinity area of the Songkhla lake, Hat Yai basin*, research report,Prince of Songkla University.

Chandra, S., et al., 2010. Geophysical model of geological discontinuities in a granite aquifer:Analyzing small scale variability of electrical resistivity for groundwater occurrences, *Journal of Applied Geophysics*, 71, 137-148.

C.N. Nwankwo et al. (2012). Geophysical Method of Investigating Groundwater and Sub-Soil Contamination-A Case Study, *American Journal of Environmental Engineering*, 2(3),49-53.

Dahlin,T.& Leroux,V.& Nissen,J., 2002. Measuring techniques in induced polarization imaging,*Journal of applied geophysics* ,50, 279-298.

Edet,A.E.,et al., 2002. Delineation of shallow groundwater aquifers in the coastal plain sands of Calabar area using surface resistivity and hydrogeological data, *Journal of Applied Geophysics*, 35, 433-443.

Edwards, L.S., 1977. A modified pseudosection of resistivity and IP, Geophysics, Vol. 42, No. 5, p. 1020-1036.

Ehlrim, C.N. & Ofor,W, 2011. Assessing aquifer vulnerability to contaminants near solid waste landfill sites in a coastal environment,Port Harcourt,Nigeria, *Trends in Applied Sciences Research*, 6 , 165-173.

Ernstson, K. and Scherer, H.U., 1986. Self-potential variations time and their relation to hydrogeologic and meteorological parameters, Geophysics, Vol. 51, No. 10, p. 1967-1977.

Fanny Genelle et al., 2012. Monitoring landfill cover by electrical resistivity tomography on an experimental site, *Journal of Engineering Geology*, 145-146, 18-29.

Gemail, Kh.S. et al., 2011. Assessment of aquifer vulnerability to industrial waste water using resistivity measurements. A case study, along El-Gharbyia main drain, Nile Delta, Egypt, *Journal of Applied Geophysics*, 75, 140-150.

Georgaki,I., et al., 2008. Evaluating the use of electrical resistivity imaging technique for improving CH_4 and CO_2 emission rate estimations in landfills, *Journal of Science of the Total Environment*, 389, 522-531.

Geotomo Software, 2009. RES2DINV version 3.58. Rapid 2-D Resistivity& IP inversion using the least-squares method.

Loke, M.H., 1999. *Electrical imaging surveys for environmental and engineering studies*, A practical guide to 2-D and 3-D surveys, Dr. M.H.Loke, 57p.

Loke, M.H., 1999. *RES2DINV version 3.4 Rapid 2-D Resistivity & IP inversion using the least squares method,* ABEM Instrument AB, user manual.

Lowrie, W., 2007. *Fundamentals of geophysics*, 2nd Ed. Cambridge University Press. Cambridge, UK. 381 pp.

Meesin,W., 1996. *The contamination of some pollutants in groundwater, Amphoe Hat Yai, Changwat Songkhla*, Master's thesis, Prince of Songkhla University.

Milsom,J., 2003. *Field Geophysics*, 3rd Ed. John Wiley & Sons. UK. 88 pp.

Morgan, F.D., Williams, E.R., and Madden, T.R., 1989. Streaming potential properties of westerly granite with applications, Journal of Geophysical Research, Vol. 94, No. B9, p. 12,449-12,461

Mota,R., et al., 2004. Granite fracturing and incipient pollution beneath a recent landfill facility as detected by geoelectrical surveys, *Journal of Applied Geophysics*, 57, 11-22.

Pakiser, L.C., and Black, R.A., 1957. Exploring for ancient channels with the refraction seismograph. Geophysics, Vol. 22, No. 1, p. 32-47.

Parasnis, D.S., 1997. *Principles of Applied Geophysics*, 5th Ed. Chapman & Hall. London, UK. 429 pp.

Pollution Control Department, 2009. *Sanitary Landfill*, Pollution Control Department.

Reinhard K. Frohlich, et al., 2008. Investigating changes of electrical characteristics of the saturated zone affected by hazardous organic waste, *Journal of Applied Geophysics*, 64, 25-36.

Robinson, Edwin S., 1988. *Basic Exploration Geophysics*, John Wiley & Sons, 562 pp.

Rottana Ladachart, 2002. *Area* University *selection for solid waste disposal at changwat Songkhla*, Master's thesis, Faculty of Science, Chulalongkorn University.

Schmutz,M., et al., 2006. Azimuthal resistivity soundings over a steeply dipping anisotropic formation: A case history in central Tunisia, *Journal of Applied Geophysics*, 60, 213-224

Scott, J., 1973. Seismic refraction modeling by computer. Geophysics, Vol. 38, No.2.

Sharma, P. Vallabh, 1997. Environmental and engineering geophysics. Cambridge University Press. Cambridge, UK. 477 pp.

Telford, W.M., Geldart, L.P. and Sheriff, R.E., 1990. *Applied Geophysics*, 2nd Ed. Cambridge University Press. Cambridge, UK. 770 pp.

Thongnark,Kh., 1998. *Solid waste management of municipalities and sanitary districts in Southern Thailand*, Master's thesis, Prince of Songkla University.

UGWU,S.A. et al., 2009. Effect of Waste Dumps on Groundwater in Choba using Geophysical Method, *Journal of Applied Sciences Environmental Manage*, 13(1), 85-89.

Vivienne Ruth Smith, 1992. The Paparua Landfill: hydrogeological, geophysical and hydrogeochemical investigations of groundwater contamination by leachate, Christchurch, New Zealand. Doctor of Philosophy's thesis, University of Canterbury.

Wattanathum, A., 2006. *Numerical Simulation of Groundwater Flow in Hat Yai Basin, Changwat Songkhla*, Master's thesis, Prince of Songkhla University.

William, M., Fordyce, F., Paijitprapapon, A., Chsroenchaisri P., 1996. Arsenic contamination in surface drainage and groundwater in part of the southeast Asian tin belt, Na Khon Si Thammarat province, Southern Thailand. Environmental Geology, Vol. 27 Issue 1,16-33.

VITAE

Name Mr. Thirat Sommai

Student ID 5310220134

Educational Attainment

Degree	Name of Institution	Year of Graduation
B.Sc. (Physics)	Prince of Songkla University	2010

Scholarship Awards during Enrolment

Research Assistant relationship (RA)	November 2010-October 2012
Teacher Assistant relationship (TA)	November 2012- February 2013
Teacher Assistant relationship (TA)	June 2013 – September 2013
Teacher Assistant relationship (TA)	November 2013 – February 2014

List of Publication and Proceeding

Sommai, T., Wattanasen, K. and Yodkayhun, S. 2012. Application of geophysical methods for characterizing a selected solid waste disposal site in Songkhla province. In proceedings of the 6th International Conference on Applied Geophysics : Applied Geophysics, 15-17 November 2012, Kanchanaburi, Thailand.